12-15-2017

Modeling Iron Oxide Reactivity in the Environment

Nefeli Maria Bompoti
University of Connecticut - Storrs, nefeli.bompoti@uconn.edu

Modeling Iron Oxide Reactivity in the Environment

Nefeli Maria Bompoti, Ph.D.

University of Connecticut, 2017

Abstract

Iron oxides and hydroxides are highly reactive mineral phases in natural systems since they interact with pollutants, controlling their fate and transport in the environment. Goethite (GH) and hematite (HT) are the most abundant iron minerals in nature, while ferrihydrite (FH) is a nanomineral with high surface reactivity. Subsurface transport modeling has usually represented the adsorption processes by empirical relationships, such as distribution coefficients (K_d) or isotherm equations. However, empirical approaches cannot account for variable geochemical conditions. These effects can be addressed by the mechanistic surface complexation models (SCMs). So far, the application of SCMs has been limited mostly to the description of laboratory experiments, resulting in highly variable parameters even when a pure sorbent–ligand system is described. This limits their usefulness and transferability in reactive transport models.

This study is an attempt to bridge the gap between laboratory and field studies, but keep the predictive power of SCMs. The latter is achieved by analyzing several adsorption datasets systematically to extract unified parameters, and understand the driving forces leading to parameter variability. The optimization process is a problem itself that may lead to non-unique parameters. With this in mind, a hybridized optimization approach (MUSE algorithm), based on

a multi–start algorithm combined with a local optimizer, has been developed to allow the simultaneous optimization of SCM parameters. A unified model for surface charge was developed to simulate the variable charging behavior of FH. The model was able to capture differences in both surface charge magnitude and points of zero net proton charge (PZNPCs). Finally, the ultimate purpose of this work was to study the adsorption of one ligand (i.e. chromate) on a group of iron oxides (FH, HT, and GH), and examine whether the complexation parameters can be represented by a unified framework. The results of this analysis showed that thermodynamic constants are highly dependent on the surface properties, an effect that can be quantified by the model calculations, while differences in adsorption energetics are also present under different surface coverages. The latter is reflected in thermodynamic parameters and added to the complexity of the model.

Modeling Iron Oxide Reactivity in the Environment

Nefeli Maria Bompoti

M.S. Water Resources Science and Technology, National Technical University of Athens, 2014

B.S. Civil Engineering, National Technical University of Athens, 2012

A Dissertation

Submitted in Partial Fulfillment of the

Requirements for the Degree of

Doctor of Philosophy

at the

University of Connecticut

2017

APPROVAL PAGE

Doctor of Philosophy Dissertation

Modeling Iron Oxide Reactivity in the Environment

Presented by

Nefeli Maria Bompoti, B.A., M.A.

Major Advisor _____
Maria Chrysochoou

Associate Advisor _____
Nadine Kabengi

Associate Advisor _____
Michael Machesky

Associate Advisor _____
Mario Villalobos

Associate Advisor _____
Alexander Agrios

Associate Advisor _____
Cristian Schulthess

University of Connecticut
[2017]

“The scientist is motivated primarily by curiosity and a desire for truth.”

Irving Langmuir

AKNOWLEDGEMENTS

I would like to thank all my teachers who put their faith in me and urged me to do better. The Ph.D. path, circuitous and challenging as is, required constant effort by many individuals who supported me along the way.

First and foremost, I would like to express my gratitude for the unlimited help and support of my advisor, Maria Chrysochoou, who introduced me to the amazing world of science and academia. Without her constant effort none of this work would be achievable. I am grateful for her invaluable guidance and mentorship that shaped my way of thinking and put my messy thoughts into perspective. A role model in every single aspect, her innovative thinking will always accompany me for the rest of my life.

I also would like to thank Dr. Michael Machesky for introducing me to the art of surface complexation modeling. I will never forget the week we spent together in May of 2015, discussing surface complexation modeling, and trying every single Asiatic restaurant in Urbana-Champaign. I am grateful he passed me down all this knowledge, entitling me as one of the few people that understand those models.

I cannot express my gratitude for Dr. Nadine Kabengi, for her support and collegial guidance in every single step of this journey. Being present to every single conference presentation, I always had a friendly face to look at. I will never forget discussing those finicky ferrihydrite nanoparticles on skype calls, and she always enlightened me with her deep scientific knowledge.

I am highly indebted to Dr. Mario Villalobos for spending his time and effort to help develop the CO_2 experimental set-up. His endless knowledge of geochemistry and excellence in experimental techniques made me a better scientist in many ways.

Finally, I am thankful to Dr. Alexander Agrios and Dr. Cristian Schulthess for being excellent teachers, and teaching me the fundamentals of environmental science. I appreciate their time and effort in being on my committee and contribute to my research.

I would also like to thank my husband, Konstantinos Zarboutis, for his unlimited love and support during my graduate years. Keeping me connected to the real world and putting up with my roller-coaster mood every time something did not work in the lab. I also thank my mother, Yvonne Nikolaou, for her unconditional love and effort to make me a better person and shape my personality through all these years. I also thank my close friends Alexandra Trampeli and Angelika Niarhou for being next to me in every single step of my life, even the ones that did not make sense. Special thanks to Mike Kastelorizios and Athina for being always there to share my thoughts over coffee and lunch breaks. I also thank my lab mate, Yaguang Du, or Kevin, for having a friendly face to say good morning, and of course, for introducing me to Chinese culture.

Finally I would like to thank the financial aid of the National Science Foundation, the Gerondelis Foundation, and the FEI Center of Excellence in Microscopy. I would also like to thank the Department of Civil and Environmental Engineering at the University of Connecticut for being a center of academic excellence and a friendly environment that fosters new scientists and engineers.

TABLE OF CONTENTS

LIST OF FIGURES

LIST OF TABLES

CHAPTER 1 Introduction

Iron oxides and hydroxides are critical phases in geochemical cycling, and thus are important components for the fate and transport of many chemical substances in the environment (Hochella et al., 2008). They are abundant in the environment and provide a host surface for many chemical ions. Thus, understanding their microscopic behavior and interaction with ions is essential for the understanding of the macroscopic behavior of chemicals in the natural environment.

Along with experimental observations of adsorption phenomena, various modeling efforts have been used to represent adsorption within reactive transport modeling. In the field, the modeling of adsorption processes is usually represented by empirical relationships, such as distribution coefficients (K_d) and Freundlich isotherms (Goldberg et al., 2007), or by the simplest mechanistic model of Langmuir isotherm. However, sorption phenomena are strongly dependent on chemical conditions, such as pH, ionic strength, and the presence of competitive ions. Therefore, empirical approaches are extremely limited on this aspect, since they do not account for variable environmental conditions. Thus, they are field – specific and restricted to the system for which they were obtained. On the contrary, surface complexation models (SCMs) simulate surface reactions similar to solute equilibria described by mass law, mass action, and charge balance equations. Since the publication of the surface complexation approach by Schindler, Stumm, and co-authors (Huang and Stumm, 1973; Schindler, 1981; Schindler and Stumm, 1987; Stumm et al., 1970, 1980), a number of different surface complexation models have been proposed. Several formulations arise from combinations of different pK models (1-pK or 2-pK), single or multisite expressions (charge distribution multisite complexation (CD – MUSIC)

(Hiemstra and Van Riemsdijk, 1996a)), and various electrostatic models (constant capacitance (CCM) (Stumm et al., 1980), basic Stern, diffuse layer model (DLM) (Huang and Stumm, 1973; Stumm et al., 1970), and triple layer model (TLM) (Davis et al., 1978; Yates et al., 1974)).

The surface complexation modeling approach can be divided into two major types: (a) the component additivity, and (b) the generalized composite approach. In the component additivity (CA) approach the adsorption is described as the summation of each contributing mineral phase present in the soil matrix (Davis et al., 1998; Goldberg et al., 2007; Landry et al., 2009). To apply this approach, a database with surface properties and surface complexation parameters for each individual solid phase is required to build a model for a complex mineral assemblage. The seminal work of Dzombak and Morel (1990) for hydrous ferric oxide and Karamalidis and Dzombak (2011) for gibbsite built upon this approach by providing self-consistent surface complexation constants for numerous binding ions. On the other hand, the generalized composite (GC) approach assumes that the soil constituents are too complex to be represented by individual components, and therefore "generic" surface functional groups are used to simulate adsorption. This approach is most commonly adopted due to difficulties in determining speciation, mineral surface areas, and complexation parameters in heterogeneous soils and sediments.

The major difference between the two approaches is the predictive capability of the surface complexation model. Although both require the calibration of the model on adsorption data, the CA approach is based on adding the individual parameters acquired for each phase, while the GC approach requires calibration of the model for every situation (Davis et al., 1998; Goldberg et al., 2007; Kent et al., 2000). Theoretically speaking, once the surface complexation parameters are obtained from experimental observations, no additional calibration is needed to predict adsorption by mineral assemblages in the field.

To build a surface complexation model, a significant number of parameters is required. The type and number of surface sites must be determined, usually based on crystallographic estimations in order to yield physically realistic values. Experimentally obtained surface speciation has to be incorporated into the model, if possible in a quantitative manner, to describe the distribution of surface species using spectroscopic and/or molecular modeling information (Machesky et al., 2008). Besides a well–characterized surface and surface speciation, a thermodynamic framework is also required to link surface complexation to chemical equilibrium. The corresponding thermodynamic equilibrium constants are however far from constants; both in terms of electrostatics and surface activity. The variable electrostatic charge of the surface is corrected by applying a coulombic factor as described by the electric double–layer (EDL) theory (Dzombak and Morel, 1990; Grahame, 1947; Overbeek, 1952). The surface activity is highly dependent on surface properties (solid concentration, surface area, and site densities), and thus further increases the uncertainty of those parameters. Sverjensky (2003) proposed standard states for surface species by including the surface area and solid concentration, enabling the comparison of equilibrium constants for different minerals and different surface areas.

Following the CA approach to adequately describe sorption processes with surface complexation modeling, three steps are required:

1. Understanding and predicting the surface charge behavior. Describing the surface charge behavior is always a prerequisite to ion adsorption modeling.
2. Description of specific ion binding for each ligand.
3. Understanding the competitive ion binding mechanisms. The presence of other competitive ligands in the natural systems affects sorption processes. Carbonate is one of the most pervasive species in natural systems and sorbs strongly to minerals (van Geen et al., 1994;

Villalobos and Leckie, 2000). Carbonate sorbs strongly on iron oxides affecting the mineral surface charge, by increasing the adsorption of protons (Hiemstra et al., 2004), and decreasing (or enhancing) sorptive capacity (Wijnja and Schulthess, 2001).

Each of aforementioned steps is an optimization problem that involves collection of different experimental data and elucidation of specific surface complexation parameters. Specifically, the common experimental techniques involved:

1. The acid-base properties of oxide minerals, and consequently the surface charge, are usually elucidated by performing potentiometric acid-base titrations (Parks and De Bruyn, 1962; Dzombak and Morel, 1990). A strong acid or base is added to the iron oxide suspension, while pH is constantly monitored. Then, the consumption of H+ or OH- is calculated based on the expression: $\Gamma_{H^+} - \Gamma_{OH^-} = \frac{C_{acid} - C_{base} - (H^+) + (OH^-)}{SSA \times Gs}$, where C_{acid} and C_{base} is the molar concentration of the added acid and base respectively, H^+ and OH^- are calculated form the pH measurements, SSA is the specific surface area (m^2/g), and Gs is the solid concentration (g/L). This expression however assumes that the hydrous oxide is insoluble, and the uptake of H^+ by dissolved metal species is negligible. The backtitration technique can account for the surface characteristics of soluble species by backtitrating the supernatant samples to pH 7, and then correcting the titration curves (Schulthess and Sparks, 1986). In this study, we assume that the solid phase dissolution is minimal and, therefore, the above expression can be used without adjustments. The acid base titration data reveal how the surface charge varies with pH, including the pH at which the net proton charge is zero, and hence the term point of zero net proton charge (PZNPC). When other adsorbing ions are present into the system, the pH at which the net total particle charge is equal to zero is called zero point of charge (PZC) (Sposito, 2008). In the following chapter,

the term PZNPC will be used since the surface charge calculations are based on the potentiometric titration data which refer to H^+ adsorption. The proton equilibrium constants can be then determined by fitting potentiometric titration data.

2. Spectroscopic or molecular modeling data are usually employed to understand the speciation of the surface complexes. The common techniques involve spectroscopy (infrared spectroscopy (IR), Extended X-Ray Absorption Fine Structure (EXAFS)), density functional modeling (DFT), and adsorption calorimetry.
3. Batch adsorption data. The adsorption of ions on oxides and hydroxides are most commonly determined by measuring the change in solute concentration in presence of a solid phase. Since the adsorption of ion on oxides is strongly dependent on pH, the ion adsorption data are usually presented in plots of adsorbed ion with respect to pH, named as pH envelopes or edges. Adsorption isotherms are also used, representing the quantity of adsorbate on the surface against the equilibrium concertation of the adsorbate at fixed temperature and pressure. The specific ion equilibrium constants can be determined by fitting adsorption data.

Due to the complexity of surface complexation modeling, SCMs have been used to describe mostly laboratory experiments, while their application to the field is quite limited, with a few exceptions that attempted to apply SCMs to more complex systems (Davis et al., 1998, 2004; Dong and Wan, 2014). Even when a pure sorbent–ligand system is described, the large number of parameters required, and the heterogeneous nature of oxides, results in variations in surface reactivity, and consequently, to significant differences in parameters fit by a SCM. Over the past decade, the RES^{3}T (Rossendorf Expert System for Surface and Sorption Thermodynamics) has provided a digitized version of a thermodynamic sorption database, reporting detailed surface

complexation parameters from different studies (Brendler et al., 2003). Although the purpose of this database is to facilitate sorption modeling, and substitute for distribution coefficients (K_d values) in geochemical modelling with the surface complexation approach, the high variability of the parameters reported precludes that purpose. To bridge the gap between the laboratory and field studies, we should, or at least attempt, to unify the model parameters to maintain the predictive power of SCMs.

The present work is devoted to this purpose, by analyzing several datasets from different studies systematically to extract unified parameters, when that is achievable, and to understand the driving forces leading to parameter variability. The majority of this work focuses on ferrihydrite due to its high reactivity that is attributed to the high available surface area (Schwertmann and Cornell, 2008). However, the proposed approach can be applied to other surfaces as well. A unified model for ferrihydrite reactivity was developed to capture FH's variable surface charging behavior. Finally, the ultimate purpose of this work is to study the adsorption of one ligand (i.e. chromate) on a group of iron oxides (FH, HT, and GH), and examine whether the thermodynamic parameters can be represented by a unified framework. The latter is achieved by integrating the experimental work that was published over several decades into a unified surface complexation model. The predictive relationships developed in this research enable the description of a variety of experimental data and can be incorporated to reactive transport models to enhance their predictive capability.

The following three chapters include three manuscripts addressing the aforementioned mission: one published in the Journal of Chemical Geology (Bompoti et al., 2017), one under revision for Environmental Science and Technology, and one under preparation. Specifically, Chapter 2 includes the first publication which proposes a unified model for ferrihydrite surface

charge using the charge distribution multisite ion complexation (CD-MUSIC) framework (Hiemstra and Van Riemsdijk, 1996b). This study is the first attempt to build a surface complexation model using the recently proposed surface structure that incorporates tetrahedrally coordinated Fe atoms (Hiemstra, 2013). The unified model for ferrihydrite reactivity was developed to capture the surface charge differences both on mass and surface area basis, and differences in the point of zero net proton charge (PZNPC), which ranges between 8.0 and 8.7. Chapter 3 describes the development of the MUlti–start optimization algorithm for Surface complexation parameter Estimation (MUSE). The MUSE algorithm facilitates the process of simultaneous optimization of SCM parameters by determining a global optimum based on the minimization of the mean squared error between the simulated and observed data. The MUSE is applied to a spectroscopic dataset, as well as to a macroscopic adsorption dataset for chromate on ferrihydrite. Chapter 4 includes the MUSE application on a large dataset for chromate adsorption on three iron oxides (FH, HT, and GH).

References

Bompoti, N., Chrysochoou, M., Machesky, M., 2017. Surface structure of ferrihydrite: Insights from modeling surface charge. Chem. Geol., Adsorption of metals by geomedia III: Fundamentals and implications of metal adsorption 464, 34–45. https://doi.org/10.1016/j.chemgeo.2016.12.018

Brendler, V., Vahle, A., Arnold, T., Bernhard, G., Fanghänel, T., 2003. RES3T-Rossendorf expert system for surface and sorption thermodynamics. J. Contam. Hydrol., 8th Internation Conference on Chemistry and Migration Behaviour of Actinides and Fission Products in the Geosphere - Migration 01 61, 281–291. https://doi.org/10.1016/S0169-7722(02)00129-8

Davis, J.A., Coston, J.A., Kent, D.B., Fuller, C.C., 1998. Application of the Surface Complexation Concept to Complex Mineral Assemblages. Environ. Sci. Technol. 32, 2820–2828. https://doi.org/10.1021/es980312q

Davis, J.A., James, R.O., Leckie, J.O., 1978. Surface ionization and complexation at the oxide/water interface. J. Colloid Interface Sci. 63, 480–499. https://doi.org/10.1016/S0021-9797(78)80009-5

Davis, J.A., Meece, D.E., Kohler, M., Curtis, G.P., 2004. Approaches to surface complexation modeling of Uranium(VI) adsorption on aquifer sediments1. Geochim. Cosmochim. Acta 68, 3621–3641. https://doi.org/10.1016/j.gca.2004.03.003

Dong, W., Wan, J., 2014. Additive Surface Complexation Modeling of Uranium(VI) Adsorption onto Quartz-Sand Dominated Sediments. Environ. Sci. Technol. 48, 6569–6577. https://doi.org/10.1021/es501782g

Dzombak, D.A., Morel, F.M.M., 1990. Surface Complexation Modeling: Hydrous Ferric Oxide. John Wiley & Sons.

Goldberg, S., Criscenti, L.J., Turner, D.R., Davis, J.A., Cantrell, K.J., 2007. Adsorption–Desorption Processes in Subsurface Reactive Transport Modeling. Vadose Zone J. 6, 407. https://doi.org/10.2136/vzj2006.0085

Grahame, D.C., 1947. The Electrical Double Layer and the Theory of Electrocapillarity. Chem. Rev. 41, 441–501. https://doi.org/10.1021/cr60130a002

Hiemstra, T., 2013. Surface and mineral structure of ferrihydrite. Geochim. Cosmochim. Acta 105, 316–325. https://doi.org/10.1016/j.gca.2012.12.002

Hiemstra, T., Rahnemaie, R., van Riemsdijk, W.H., 2004. Surface complexation of carbonate on goethite: IR spectroscopy, structure and charge distribution. J. Colloid Interface Sci. 278, 282–290. https://doi.org/10.1016/j.jcis.2004.06.014

Hiemstra, T., Van Riemsdijk, W.H., 1996a. A Surface Structural Approach to Ion Adsorption: The Charge Distribution (CD) Model. J. Colloid Interface Sci. 179, 488–508. https://doi.org/10.1006/jcis.1996.0242

Hiemstra, T., Van Riemsdijk, W.H., 1996b. A Surface Structural Approach to Ion Adsorption: The Charge Distribution (CD) Model. J. Colloid Interface Sci. 179, 488–508. https://doi.org/10.1006/jcis.1996.0242

Hochella, M.F., Lower, S.K., Maurice, P.A., Penn, R.L., Sahai, N., Sparks, D.L., Twining, B.S., 2008. Nanominerals, Mineral Nanoparticles, and Earth Systems. Science 319, 1631–1635. https://doi.org/10.1126/science.1141134

Huang, C.-P., Stumm, W., 1973. Specific adsorption of cations on hydrous γ-Al2O3. J. Colloid Interface Sci., Kendall Award Symposium 163rd American Chemical Society Meeting 43, 409–420. https://doi.org/10.1016/0021-9797(73)90387-1

Karamalidis, A.K., Dzombak, D.A., 2011. Surface Complexation Modeling: Gibbsite. John Wiley & Sons.

Kent, D.B., Abrams, R.H., Davis, J.A., Coston, J.A., LeBlanc, D.R., 2000. Modeling the influence of variable pH on the transport of zinc in a contaminated aquifer using semiempirical surface complexation models. Water Resour. Res. 36, 3411–3425. https://doi.org/10.1029/2000WR900244

Landry, C.J., Koretsky, C.M., Lund, T.J., Schaller, M., Das, S., 2009. Surface complexation modeling of Co(II) adsorption on mixtures of hydrous ferric oxide, quartz and kaolinite. Geochim. Cosmochim. Acta 73, 3723–3737. https://doi.org/10.1016/j.gca.2009.03.028

Machesky, M.L., Předota, M., Wesolowski, D.J., Vlcek, L., Cummings, P.T., Rosenqvist, J., Ridley, M.K., Kubicki, J.D., Bandura, A.V., Kumar, N., Sofo, J.O., 2008. Surface Protonation at the Rutile (110) Interface: Explicit Incorporation of Solvation Structure within the Refined MUSIC Model Framework. Langmuir 24, 12331–12339. https://doi.org/10.1021/la801356m

Overbeek, J.T.G., 1952. Electrochemistry of the double layer. Colloid Sci. 1, 115–193.

Parks, G.A., Bruyn, P.L. de, 1962. The zero point of charge of oxides. J. Phys. Chem. 66, 967–973. doi:10.1021/j100812a002

Schindler, P.W., 1981. Surface Complexes at Oxide-Water Interfaces. Adsorpt. Inorg. Solid-Liq. Interfaces 1.

Schindler, P.W., Stumm, W., 1987. The surface chemistry of oxides, hydroxides, and oxide minerals. Aquat. Surf. Chem. Chem. Process. Part.-Water Interface John Wiley Sons N. Y. 1987 P 83-110 13 Fig 7 Tab 49 Ref.

Schulthess, C.P., Sparks, D.L., 1986. Backtitration Technique for Proton Isotherm Modeling of Oxide Surfaces. Soil Sci. Soc. Am. J. 50, 1406–1411.

Schwertmann, U., Cornell, R.M., 2008. Iron Oxides in the Laboratory: Preparation and Characterization. John Wiley & Sons.

Sposito, G., 2008. The Chemistry of Soils. Oxford University Press, USA.

Stumm, W., Huang, C.P., Jenkins, S.R., 1970. Specific chemical interaction affecting stability of dispersed systems. Croat. Chem. Acta 42, 223.

Stumm, W., Kummert, R., Sigg, L., 1980. A ligand-exchange model for the adsorption of inorganic and organic-ligands at hydrous oxide interfaces. Croat. Chem. Acta 53, 291–312.

Sverjensky, D.A., 2003. Standard states for the activities of mineral surface sites and species. Geochim. Cosmochim. Acta 67, 17–28. https://doi.org/10.1016/S0016-7037(02)01074-8

van Geen, A., Robertson, A.P., Leckie, J.O., 1994. Complexation of carbonate species at the goethite surface: Implications for adsorption of metal ions in natural waters. Geochim. Cosmochim. Acta 58, 2073–2086. https://doi.org/10.1016/0016-7037(94)90286-0

Villalobos, M., Leckie, J.O., 2000. Carbonate adsorption on goethite under closed and open CO2 conditions. Geochim. Cosmochim. Acta 64, 3787–3802. https://doi.org/10.1016/S0016-7037(00)00465-8

Wijnja, H., Schulthess, C.P., 2001. Carbonate adsorption mechanism on goethite studied with ATR–FTIR, DRIFT, and proton coadsorption measurements. Soil Sci. Soc. Am. J. 65, 324–330.

Yates, D.E., Levine, S., Healy, T.W., 1974. Site-binding model of the electrical double layer at the oxide/water interface. J. Chem. Soc. Faraday Trans. 1 Phys. Chem. Condens. Phases 70, 1807. https://doi.org/10.1039/f19747001807

CHAPTER 2 Surface structure of ferrihydrite: Insights from modeling surface charge

Nefeli Bompoti, Maria Chrysochoou, and Michael Machesky

Published in Journal of Chemical Geology

Special Issue: Adsorption of metals by geomedia III: Fundamentals and implications of metal adsorption, Volume 464, Pages 34–45, August 5, 2017

Abstract

Ferrihydrite (FH) plays an important role in controlling the fate and transport of many compounds in nature due to its large surface area and high reactivity. This study is the first attempt to build a surface complexation model using the recently proposed surface structure that incorporates tetrahedrally coordinated Fe atoms (Hiemstra, 2013). The ability of the model to describe the surface charge curves of FH with different preparation methods and Points of Zero Net Proton Charge (PZNPC) is tested. In general, FH particles that have been subject to aging are larger and have lower specific surface area (SSA) and higher PZNPCs. The structural model includes 2 types of singly coordinated (SC) oxygens that are present only on the $(1\bar{1}1)$ and $(1\bar{1}0)$ faces and 5 types of triply coordinated (TC) oxygens that are also present on the basal planes (001) and $(00\bar{1})$, for a total of 11 sites. The 11 - site model was able to simulate fresh FH datasets with PZNPC lower than 8.5, but could only simulate higher PZNPCs when the contribution of the more acidic basal planes was minimized. The available microscopic observations do not support this condition, which suggests TC groups on the basal planes likely have log K values higher than the macroscopic PZNPC. We attempted to test this hypothesis through three versions of simplified 3-site models, using SC and one TC on $(1\bar{1}0)$ and $(1\bar{1}1)$, with log K 8.0 (equal to fresh FH PZNPC) and one TC group on the basal planes with log K 9.5. This enables fitting of the PZNPC of aged FH datasets by adjusting the face contributions. An unresolved issue is whether this model accurately describes the relative contribution of SC and TC sites to the overall charge, which has implications for accurate description of specific ion adsorption.

Introduction

Ferrihydrite (FH) is one of the most common iron oxyhydroxides in soils and sediments, where it occurs both naturally and as result of human activities such as acid mine drainage. It has also been observed in Martian soils and several meteorites. In addition to its importance in geologic systems, its structure is also important in biological applications due to its resemblance to ferritin, an iron-storing protein. Finally, FH is a precursor phase in several materials that have technological and catalytic uses (Cornell and Schwertmann, 2003). FH possesses a high surface reactivity because it typically forms nanoparticles of very high surface area, for which theoretical values as high as ~1250 m^2/g have been reported (Villalobos and Antelo, 2012). Thus, understanding surface reactions of FH is critical in describing the geochemical cycling and behavior of iron in many natural and engineered systems, as well as predicting the fate and transport of the wide variety of chemical compounds that interact with iron oxides.

Such understanding has been complicated by the small diameter of FH nanoparticles (2-6 nm) and by its disordered structure, which prohibits the application of traditional structural analysis methods, such as X-ray Diffraction. The low degree of crystallinity of FH was thought to be linked to the high number of vacant Fe sites in the structure and the replacement of bulk oxygens with water or hydroxyl molecules (Cornell and Schwertmann, 2003). Until relatively recently, FH was considered to comprise three intermingled phases; the defect-free f-phase, the defect-rich d-phase and hematite-like crystallites (Drits et al., 1993). All three phases consisted of octahedrally-coordinated Fe with variable stacking sequences of the iron octahedra. In 2007, this model was overturned by Michel et al. (2007), who utilized synchrotron X-ray Pair Distribution Function analysis to propose a new structure based on a single phase, the isostructural mineral akdalaite ($Al_{10}O_{14}(OH)_2$); this structure contains ~20% of tetrahedrally coordinated Fe with a δ-Keggin-like local structure (Michel et al., 2007). This new structure stirred controversy in the geochemical

community and several follow up studies to elucidate the structure (Cismasu et al., 2011; Maillot et al., 2011; Manceau, 2011, 2010; Michel et al., 2010; Peak and Regier, 2012; Pinney et al., 2009; Rancourt and Meunier, 2008; Xu et al., 2011). Currently there is experimental evidence supporting the new structure of FH.

All of the aforementioned studies focused on the bulk FH structure and there was little discussion on the implication of the structure for surface properties. Surface complexation models that took surface structure into account continued to rely on the goethite structure to derive FH surface properties such as site density and proton affinities (Antelo et al., 2010; Gustafsson et al., 2011; Hiemstra et al., 2009a; Hiemstra and Van Riemsdijk, 2009; Tiberg et al., 2013; Villalobos and Antelo, 2012). Hiemstra (2013) recently published the first study that discussed the implications of the new structure for FH surface properties, and which also proposed a variation in the accepted structure. Surface depletion of two types of Fe polyhedra is postulated to be the controlling factor for various FH properties. The mineral core is considered to be hydrogen poor; however, the contribution of the surface is dominant for the macroscopic properties of FH. Based on this model, Hiemstra (2013) identified 12 different types of surface oxygens and calculated site densities and proton affinities for each. There is currently no experimental evidence that these calculated values are correct, or surface complexation models based on this new structure. Given the complexity of the proposed structure and the high number of reactive oxygen sites, experimentally verifying the surface structure is no easy task. Previous attempts to characterize goethite surface properties, which has four types of surface O atoms, relied on fitting titration curves (Hiemstra et al., 1996). However, the analysis indicated that titration curves may be fitted adequately using only two surface sites, although whether the log K's for those sites were equal or 4 log units apart resulted

in similar fits to the titration curves. Thus, determining the proton affinities and site densities of surface O atoms is ambiguous when fitting individual titration curves.

An additional complication with modeling surface charge is the variable nature of FH; different methods of preparation, including initial iron concentration, rate of precipitation, and time of aging result in different particles sizes and degrees of crystallinity (Wang et al., 2013). The majority of studies report potentiometric titration results for freshly precipitated FH (Ching-kuo Daniel Hsi and Langmuir, 1985; Davis, 1977; Fukushi et al., 2013; D. C. Girvin et al., 1991; Nagata et al., 2009) and some for aged FH (Antelo et al., 2010; Hofmann et al., 2005; Jain et al., 1999; Wang et al., 2013). As a result, substantial differences arise in the charging behavior, both in terms of magnitude and the point of zero net proton charge (PZNPC).

Modeling surface charge requires a significant number of parameters, including the available specific surface area (SSA), the number of proton reactive sites (Ns) and the equilibrium constants for proton (Log K_{H+}) and electrolyte binding (Log K_{C+}), (Log K_{A-}). In addition, the choice of the electrostatic (e.g., diffuse layer, Basic Stern, Triple Layer) and pK models (e.g., generic 2-pK, 1-pK, multisite complexation (MUSIC) (Hiemstra and Van Riemsdijk, 1996b)) further increases the number of parameters to be entered or fitted by the model and different authors typically make different assumptions. Several attempts in unifying modeling approaches have been made. The seminal work of Dzombak and Morel (1990) utilized the generic 2-pK protonation model in combination with the Guoy-Chapman diffuse layer model to describe FH surface charge and ion sorption data. Sahai and Sverjensky (1997) and Sverjensky and Sahai (1996) developed a triple layer model for titration data on iron oxides by predicting the protonation constants with electrostatic and Born solvation theory. Ponthieu et al. (2006) employed the charge distribution (CD)-MUSIC approach to describe ion sorption and surface charge of goethite and amorphous

iron oxyhydroxide based on the goethite surface structure using a single set of parameters. Although this approach provided good results for ion sorption, it could not capture the lower PZNPC of FH. Other attempts to model the FH surface behavior also relied on the goethite surface structure, but the log Ks (for singly- and triply- coordinated surface groups) used were much different in each study, including 8.06 (Hiemstra and Van Riemsdijk, 2009), 8.1 (Tiberg et al., 2013) 8.1-8.5 (Gustafsson, 2001; Gustafsson et al., 2009) and 8.7 (Antelo et al., 2010). In each case, the log Ks reflect the PZNPC of the particular dataset that was modeled.

Villalobos and Antelo (2012) also proposed a unified 2-pK model for FH using the goethite structure as a proxy. Based on their approach, they were able to simulate titration data by optimizing the SSA and shifting the PZNPC of all datasets to 8.7. Their justification of this approach was based on the following premises: a) that SSA is a highly uncertain parameter and thus should be adjusted; and, b) that poor CO_2 exclusion during acid/ base titration experiments caused the lower PZNPC values (Villalobos and Leckie, 2000; Zeltner and Anderson, 1988).

To the knowledge of the authors there is no modeling study considering the recently postulated surface structure for FH. Accordingly, this study is the first attempt to model several sets of titration data with a unified surface complexation model, using the surface structure for ferrihydrite provided by Hiemstra (2013) and the CD-MUSIC formulation. Ultimately, the modeling exercise serves as indirect evidence to test the validity of the proposed structure and its applicability to the variable sizes and crystallinities of FH particles.

Experimental data and model description

FH surface charge datasets

Several FH titration data sets have been reported in the literature, for a wide range of ionic strengths and electrolytes. Table 2-1 lists the nine data sets used in this study and summarizes the reported

preparation methods and titration parameters. Titration data for three electrolytes were included: $NaNO_3$, NaCl and KNO_3. The surface charge data sets are shown in Figure 2-1a, plotted in C/g with respect to pH minus the PZNPC values shown in Table 2-1.

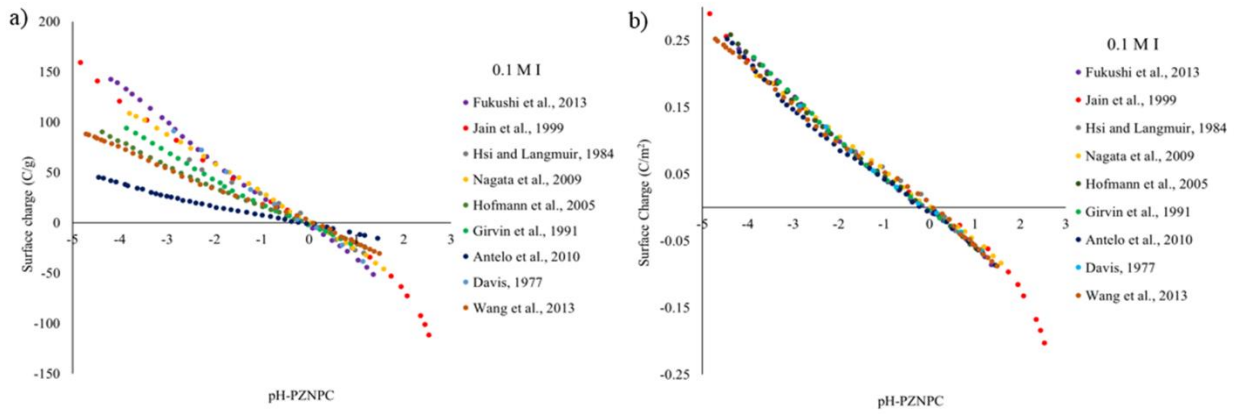

Figure 2-1. FH surface Charge at ionic strength 0.1 M, as given by nine studies (Table 1), in a) C/g and b) C/m^2.

The first issue when evaluating surface charge data is the choice of SSA to normalize the data from C/g to C/m^2 that are then used as input to the model. Surface area is difficult to measure for reactive solids such as FH. Various techniques have been used to estimate surface area, with the BET method being the most popular (Brunauer et al., 1938; Gregg et al., 1967a). Although the BET method provides self-consistent results, it has significant limitations as both the pre-drying and the N_2 drying during the test cause particle agglomeration and reduction in the accessible SSA (Antelo et al., 2010; Dzombak and Morel, 1990). Most studies shown in Table 2-1 adopted the value of 600 m^2/g as originally reported by (Davis et al., 1978), which relies on an empirical estimate. Although the theoretical estimation of surface area based on spherical particles of 20 Å and density of 3.57 g/cm^3 is 840 m^2/g, Davis et al. (1978) suggested 600 m^2/g in order to simulate their surface charge data. To overcome this uncertainty, SSA was treated as a fitting parameter in some modelling studies (Antelo et al., 2010; Villalobos and Antelo, 2012).

Table 2-1a. Preparation methods and characterization parameters of ferrihydrite surface charge data used.

Study	Preparation Method	Aging	After preparation	CO_2 exclusion
(Hsi and Langmuir, 1985)	Davis and Leckie 1978	4 h	Freeze dried	yes, based on the Davis and Leckie (1978) method
(Girvin et al., 1991)	Benjamin 1979	24 h	Suspension	yes
(Nagata et al., 2009)	Davis and Leckie 1978	4 h	Suspension	yes
(Davis, 1977)		4 h	Suspension	yes, from Dzombak and Morel (1990)
(Hofmann et al., 2005)	Schwertmann and Cornell 1991	At least 10 days	Freeze dried	yes
(Jain et al., 1999)	Schwertmann and Cornell 1991	Within 10 days	Suspension	yes
(Fukushi et al., 2013)	Davis et al., 1978	4 h	Suspension	yes
(Antelo et al., 2010)	Schwertmann and Cornell 1996	48 h	Freeze dried	yes
Wang et al. (2013)	Schwertmann and Cornell 2003	4 days	Heated and freeze dried	yes

Table 2-2b. Preparation methods and characterization parameters of ferrihydrite surface charge data used.

Study	SSA	Electrolyte	PZNPC
(Hsi and Langmuir, 1985)	306[a], 480[c]	$NaNO_3$	8.2
(Girvin et al., 1991)	600[b], 420[c]	$NaNO_3$	8.1
(Nagata et al., 2009)	600[b], 550[c]	$NaNO_3$	7.9
(Davis, 1977)	600[c]	$NaNO_3$	7.9
(Hofmann et al., 2005)	600[b], 350[c]	$NaNO_3$	8.7
(Jain et al., 1999)	not given, considered 600, 530[c]	NaCl	8.4
(Fukushi et al., 2013)	600[b, c]	NaCl	8.2
(Antelo et al., 2010)	229[a], 180[c], 350[d]	KNO_3	8.7
Wang et al. (2013)	427[a], 350[c]	KCl	8.7

[a] SSA measured with BET, [b] SSA theoretical as given by (Davis et al., 1978) and [c] optimized to obtain congruent curves, [d] SSA as modeling parameter.

Plotting the surface charge curves in C/g clearly shows that studies with aged FH reported lower charging values compared to fresh FH. This is reasonable, given that aged suspensions are likely to have larger or agglomerated particles with lower SSA. Villalobos and Antelo (2012) showed that it is possible to come up with fitted SSA values for a variety of datasets, and using these fitted values, the different charging curves fall on top of each other when plotted in C/m^2 instead of C/g. This was also the case for the datasets shown in Figure 2-1b when normalizing with SSA values reported in Table 2-1. These SSA values are considerably lower compared to the fitted values obtained by Villalobos and Antelo (2012); as will be discussed later, the high SSA values reported by these authors are necessitated by the low site density values used in their modeling approach, which were obtained from the goethite structural model. In addition, Villalobos and Antelo (2012)

fixed the capacitance values, which is also not the preferred approach in this study. These issues will be further discussed in Section 3.2.

The differences among the datasets are attributed mainly to: a) preparation methods, b) aging times and experimental conditions after precipitation, c) titration method and, d) estimation of SSA. Specifically, the precipitation rate affects FH crystallinity (Cismasu et al., 2012), while freeze drying and time of aging could lead to particle aggregation and induce a more crystalline phase (Fuller et al., 1993; Greffié et al., 2001). In addition, different charging values are apparent in data sets obtained by titration with different electrolytes. Fukushi et al. (2013) and Nagata et al. (2009) performed potentiometric titrations using 0.1, 0.05, and 0.01 M NaCl and $NaNO_3$, respectively. The results showed a difference of 34.65 ± 1.67 C/g at pH 4 - 4.5 for all ionic strengths. The higher charging in NaCl is driven by the higher affinity of Cl^- rather than NO_3^- (Villalobos and Antelo, 2012; Villalobos and Leckie, 2000). Finally, the titration rate may affect the surface charge as slower titrations could cause dissolution/reprecipitation of the mineral (Girvin et al. 1991).

The differences in charging behavior between fresh and aged FH are apparent when the titration curves are plotted in C/g and pH-PZNPC axes (Figure 2-1a), with the data of (Don C Girvin et al., 1991) exhibiting higher values than Antelo et al. (2010) for the same ionic strength. In both studies, the authors performed the titration experiments rapidly and with CO_2 exclusion. Although the titrations were performed in different background electrolytes, the binding of cation electrolyte (Na^+ or K^+) influences only the higher values of pH (> PZNPC) (Rahnemaie et al., 2006). The different charging behaviors of the two FH suspensions could be attributed to the different crystal morphologies resulting from varying aging stages of FH. Villalobos and Antelo (2012) postulated that the low PZNPC values could be attributed to CO_2 acidification in the freshly precipitated FH, while Hiemstra and Van Riemsdijk (2009) attributed the same phenomenon to a higher fraction of

singly coordinated oxygens in FH compared to goethite. Since the lower PZNPC values are accompanied by higher surface charge values, poor CO_2 exclusion alone cannot explain both differences. Instead, the different surface charge behaviors may be attributed to different crystal face distributions, which influences the amount of surface hydroxyls and their protonation constants. In recent work, Villacís-García et al. (2015) showed that different aging stages of FH result in different particle sizes and reactivity. Hiemstra and Van Riemsdijk (2009) also reported FH aging results in an alignment of particles, reducing the number of sites available for adsorption, and thus reducing the surface charge. The effect of FH crystallite size was studied by Wang et al. (2013), where the charging absolute values were higher for more crystalline FH suspensions, but there was no particular difference in PZNPC values. Studies of the effect of surface area and crystallinity on goethite showed that goethites with higher surface area and different crystallinity had much lower site densities, lower surface charge and a slight difference in PZNPC (Salazar-Camacho and Villalobos, 2010; Villalobos et al., 2009). Gaboriaud and Ehrhardt (2003) also investigated the effect of different crystallinities for goethite. They found a slight difference in PZNPC values and surface charge, with aged goethite exhibiting a higher PZNPC (9.1) and lower surface charge compared to fresher goethite (9.0). These differences were attributed to variable contribution of the (001) face.

In the nine datasets chosen in this study, the reported PZNZC values are in the range of 7.9 to 8.7. Most values are around 8.0 ± 0.2 with the exception of one value at 8.4 (Jain et al., 1999) and three values at 8.7 (Antelo et al., 2010; Hofmann et al., 2005; Wang et al., 2013). In order to test the FH surface structure proposed by Hiemstra (2013), two datasets are analyzed first, one with a low PZNPC and high surface charge (Girvin et al., 1991) and one with a higher PZNPC and lower

surface charge (Antelo et al., 2010). The approach was then refined using the findings for these two extreme datasets to develop a model that can be applied to all nine datasets.

Model description and parameterization

Surface complexation models require a high degree of parametrization to describe the solid surface, the reactions with the protons and other ions in solution and the electrostatics of the near-surface region. Given that the Hiemstra (2013) surface structure for FH is tested in this study, the CD-MUSIC formulation is used by default. This includes the calculated site densities for various types of oxygens (singly, doubly and triply coordinated) and the proposed log K values for protonation of the different oxygen types. From the 20 reactive sites proposed, only the 11 sites of singly- (SC) and triply- coordinated (TC) surface oxygens have proton affinities in the commonly accessible pH range. The pK values of doubly–coordinated surface groups are out of the normal environmental pH range and therefore are considered non-reactive (Hiemstra and Van Riemsdijk, 2009). Surface sites (Si_i) and site densities (Ns) shown in Table 2-2 are calculated given that the major crystal faces $(1\bar{1}0)$ and $(1\bar{1}1)$ account for 75% of the surface area. For the 11- site model, the charge of all singly- coordinated sites is -0.5 (si_1, si_2, si_6, si_7 while the charge of triply-coordinated sites is either -0.5 (si_3, si_4, si_8, si_{10}, si_{11}) or -0.25 (si_5 and si_9). Overall, there are two types of SC and 5 types of TC oxygens with different protonation constants according to this model. The first model utilizes all sites assuming that the Ns and log Ks provided are correct. A variation using different contributions of the dominant crystal faces is also tested.

Table 2-3. Ferrihydrite surface characteristics for 11- and 3- site models.

Designation	Face	Face distribution (%)	Type	Ns (nm^{-2})	Ns (nm^{-2}) accounting for the face contribution	Charge	log K
11 - site model							
si_1			FeOH	1.9	0.7125	-0.5	10.4
si_2			FeOH	7.4	2.775	-0.5	8
si_3	$1\bar{1}0$	37.5	Fe_3O	3.7	1.3875	-0.5	10.4
si_4			Fe_3O	1.9	0.7125	-0.5	5.5
si_5			Fe_3O	3.7	1.3875	-0.25	3.3
si_6			FeOH	1.6	0.6	-0.5	10.4
si_7	$1\bar{1}1$	37.5	FeOH	6.5	2.4375	-0.5	8
si_8			Fe_3O	3.3	1.2375	-0.5	10.4
si_9			Fe_3O	3.3	1.2375	-0.25	3.3
si_{10}	001	12.5	Fe_3O	3.3	0.4125	-0.5	5.5
si_{11}	$00\bar{1}$	12.5	Fe_3O	3.3	0.4125	-0.5	7.5
3 - site model (a+b)							
si_1	$1\bar{1}0$ and $1\bar{1}1$		FeOH		1.31	-0.5	10.4
si_2	$1\bar{1}0$ and $1\bar{1}01$		FeOH		5.21	-0.5	8
si_3	$1\bar{1}0$, $1\bar{1}1$, 001, $00\bar{1}$		Fe_3O		6.79	-0.5	Fitted (a) or 8.10 (b)
3 - site model (c) - Fresh FH							
si_1	$1\bar{1}0$ and $1\bar{1}1$		FeOH		6.53	-0.5	8
si_2	$1\bar{1}0$ and $1\bar{1}1$		Fe_3O		5.96	-0.5	8
si_3	001 and $00\bar{1}$		Fe_3O		0.83	-0.5	9.50
3 - site model (c) - Aged FH							
si_1	$1\bar{1}0$ and $1\bar{1}1$		FeOH		2.61	-0.5	8
si_2	$1\bar{1}0$ and $1\bar{1}1$		Fe_3O		2.39	-0.5	8
si_3	001 and $00\bar{1}$		Fe_3O		2.31	-0.5	9.50

Table 2-3 presents the protonation and surface complexation reactions, together with the CD factors considered in all three models. Specifically, protons are placed on the 0- plane and electrolyte ions on the 1- plane.

Table 2-4. Surface protonation reactions and electrolyte surface reactions.

Protonation reaction	**Log K**	**ΔZ_0**	**ΔZ_1**
$\equiv FeOH_i^{-0.5} + H^+ \leftrightarrow \equiv FeOH_{2i}^{+0.5}$	Log K_i	1	
$\equiv Fe_3O_j^{-0.5} + H^+ \leftrightarrow \equiv Fe_3OH_j^{+0.5}$	Log Kj	1	
$\equiv Fe_3O_k^{-0.25} + H^+ \leftrightarrow \equiv Fe_3OH_k^{+0.75}$	Log Kk	1	
Electrolytes – surface reactions	**Log K**	**ΔZ_0**	**ΔZ_1**
$\equiv FeOH_i^{-0.5} + M^+ \leftrightarrow [\equiv FeOH^{-0.5}\text{-}M^+]^{+0.5}$	Log K_M^+		1
$\equiv FeOH_i^{-0.5} + A^- + H^+ \leftrightarrow [\equiv FeOH_{2i}^{+0.5}\text{-}A^-]^{-0.5}$	Log K_A^-		-1
$\equiv Fe_3O_j^{-0.5} + M^+ \leftrightarrow [\equiv Fe_3O_j^{-0.5}\text{-}M^+]^{+0.5}$	Log K_M^+		1
$\equiv Fe_3O_k^{-0.25} + M^+ \leftrightarrow [\equiv Fe_3O_k^{-0.25}\text{-}M^+]^{+0.75}$	Log K_M^+		1
$\equiv Fe_3O_j^{-0.5} + A^- + H^+ \leftrightarrow [\equiv Fe_3OH_j^{+0.5}\text{-}A^-]^{-0.5}$	Log K_A^-		-1
$\equiv Fe_3O_k^{-0.25} + A^- + H^+ \leftrightarrow [\equiv Fe_3OH_k^{+0.75}\text{-}A^-]^{-0.25}$	Log K_A^-		-1

To help keep the number of parameters low, we have chosen a Basic Stern layer to describe interfacial electrostatics. The surface charge is calculated by the equation:

$$\sigma_0 = C_{stern}(\psi_0 - \psi_1)$$

$$= F\left(\left[\equiv \mathrm{FeOH}_i^{-0.5}\right](z_a) + \left[\equiv \mathrm{Fe_3O}_j^{-0.5}\right](z_a) + \left[\equiv \mathrm{Fe_3O}_k^{-0.25}\right](z_b)\right.$$

$$+ \left[\equiv \mathrm{FeOH}_{2i}^{+0.5}\right](z_a + z_H) + \left[\equiv \mathrm{Fe_3OH}_j^{+0.5}\right](z_a + z_H)$$

$$+ \left[\equiv \mathrm{Fe_3OH}_k^{+0.75}\right](z_b + z_H) + \left[\left[\equiv \mathrm{FeOH}_i^{-0.5} - \mathrm{M}^+\right]^{+0.5}\right](z_a)$$

$$+ \left[\left[\equiv \mathrm{Fe_3O}_j^{-0.5} - \mathrm{M}^+\right]^{+0.5}\right](z_a) + \left[\left[\equiv \mathrm{Fe_3O}_k^{-0.25} - \mathrm{M}^+\right]^{+0.75}\right](z_b)$$

$$+ \left[\ [\equiv \mathrm{FeOH}_i^{-0.5} - \mathrm{A}^+]^{-0.5}\right](z_a + z_H) + \left[\ [\equiv \mathrm{Fe_3OH}_j^{+0.5} - \mathrm{A}^+]^{-0.5}\right](z_a + z_H)$$

$$+ \left[\ [\equiv \mathrm{Fe_3OH}_k^{+0.75} - \mathrm{A}^+]^{-0.5}\right](z_b + z_H)$$

Where C_{stern} is the capacitance value for the Basic Stern layer, $z_a = -0.5$, $z_b = -0.25$ are the charges of singly and triply- coordinated groups as defined in Table 2, and $z_H = 1$ is the charge of protons. Custom-made Mathematica™ notebooks were used to build the model and obtain the best fit to the data sets, with two variations: one with set parameter values that minimizes the non-linear least squares problem and shows the best fit between model and the data, and one minimizing the mean square error in order to obtain the best value for the desired fitted parameter (capacitance or log K value). The goodness of fit was deduced by the Model Selection Criterion (MSC). This goodness of fit measure has been used previously (Machesky et al., 1998; Wesolowski et al., 2000), and larger MSC values indicate a better fit. In addition to the mean squares error, MSC depends on the number of parameters optimized and the length of the dataset.

As discussed before, reactive surface area (SSA) is highly dependent on the FH preparation method in each study. For that reason, SSA and solid concentration were first considered as given in each study, while the second attempt was to model the SSA-normalized titration curves as shown in Figure 2-1b. The electrolytes ($NaNO_3$, KNO_3 and NaCl) and ionic strength from each titration experiment were taken into account. Bulk solution activity coefficients were calculated from the Davies equation (for I = 0.5 M assuming the Davies equation is marginally valid).

The electrolyte binding constants typically lie within a narrow range in most modeling studies. Initially, we attempted to fit these. The equilibrium constant values for electrolytes used for SCM modeling on ferrihydrite (Antelo et al., 2010; Hiemstra and Van Riemsdijk, 2009; Tiberg et al., 2013) and goethite (Hiemstra et al., 2004b, 2007a, 2007a; Hiemstra and Van Riemsdijk, 2006), are shown in Table A4 in the SI. Using different pairs of values essentially led to equivalent fits that vary only with the optimal capacitance value (in inverse fashion). Thus, there is little added benefit from treating electrolyte binding constants as variables, and instead we adopted the most

common values used in the literature for CD-MUSIC modeling on iron oxides. These were Log K_{Na+} (-0.6), Log K_{K+} (-1.61), Log K_{NO3}- (-0.68) and Log K_{Cl-} (-0.45). Additionally, these binding constants were assumed to be equal for all sites.

Results and Discussion

11–site model

Figure 2-2 shows the results of the 11- site model approach for the fresh (Girvin) and aged (Antelo) FH datasets and Table 4 summarizes the model parameters. The original model proposed by Hiemstra (2013) can adequately simulate the titration data with the lower PZNPC. For the higher PZNPC data set, the charging behavior was underestimated above pH 8, predicting a lower PZNPC (8.45). In general, the proposed surface structure model with a 75 % contribution of $(1\bar{1}0)$ and $(1\bar{1}1)$ crystal faces can simulate FH titration data with a PZNPC between 7.8 and ~ 8.5. The PZNPC of $(1\bar{1}0)$ and $(1\bar{1}1)$ is 8.1 and 8.2, respectively, while the faces (001) and $(00\bar{1})$ contribute with lower PZNPC values of 7.5 and 5.5, respectively (Hiemstra, 2013). Increasing the relative contribution of the (001) and $(00\bar{1})$ faces thus results in a decrease of the overall PZNPC. This is important when considering the influence of morphology on surface charge.

To simulate FH titration datasets with higher PZNPC (8.7), a potential approach is to change the distribution of crystal faces needed to account for the different morphology, as done by Villalobos et al. (2009) for goethite. To the knowledge of the authors, there is no discussion in the literature specifically on the relationship between FH crystallite size and morphology. Wang et al. (2013) show TEM images of FH particles with different size and degree of crystallinity, along with surface charge and phosphate adsorption data. They found that both surface charge and phosphate

adsorption capacities were unchanged with crystallinity and size on a surface area basis, which suggests that larger FH particles essentially have the same morphology as smaller ones. In addition, their FH suspensions had a PZNPC of 8.7, which is very high for fresh FH. This may be a result of the specific preparation methods used, and is not typical of the majority of data found in literature. Recently, Villacis-Garcia et al. (2015) observed that chromate adsorption on fresh FH was lower on a surface area basis compared to aged FH, indicating that larger particles are more reactive.

Based on the surface structural model of Hiemstra (2013), basal planes have none of the SC groups that are required for inner sphere adsorption, and the existing TC groups on these planes are relatively acidic. Thus, increased reactivity towards inner sphere complexes such as chromate (Johnston and Chrysochoou, 2012) and higher PZNPC both require an increased contribution of the $(1\bar{1}0)$ and $(1\bar{1}1)$ faces. To incorporate this effect in the model, the face contribution was changed to 100% for the $(1\bar{1}0)$ and $(1\bar{1}1)$ faces, to test the extreme scenario where the basal faces are not expressed in the crystal. While TEM images by Wang et al. (2013) clearly show hexagonal particles (i.e., the basal planes) for both small and large FH particles, thus not supporting this scenario, we chose to test it from the modelling perspective alone. The results of this model are shown in Figure 2-2b and in Table 2-4.

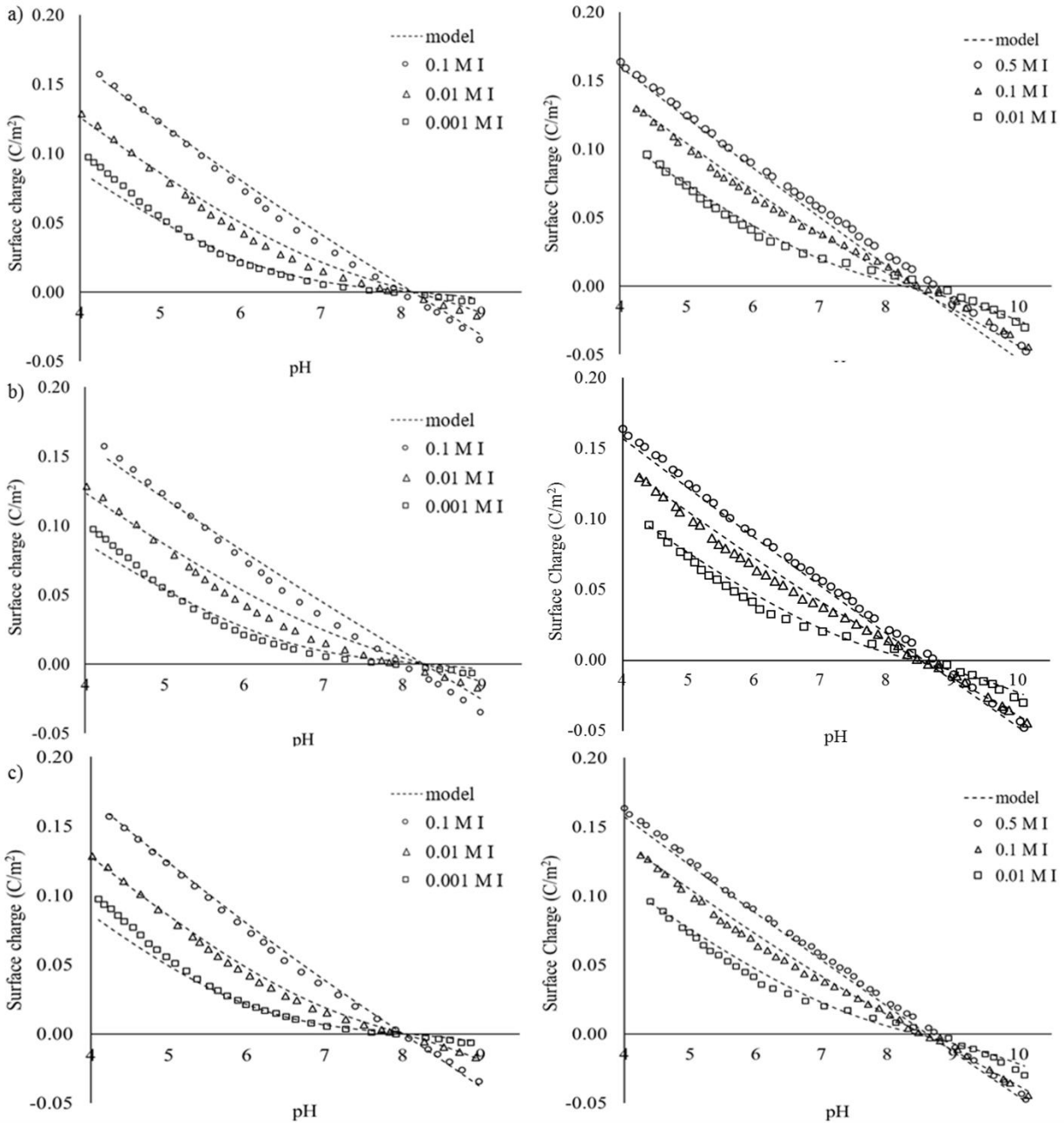

Figure 2-2. Surface charge modeling of Girvin et al. (1991) (1st column) and Antelo et al. (2010) (2nd column) datasets. Experimental data (symbols) and model simulations (lines) for a) the 11 - site model with 75% contribution of $(1\bar{1}0)$ and $(1\bar{1}1)$ faces b) for the 11-site model with 100 % contribution of the $(1\bar{1}0)$ and $(1\bar{1}1)$ faces and c) 3-site model 3a.

Table 2-5. Modeling results for Girvin et al. (1991) and Antelo et al. (2010) based on the 11-site model with two different face contributions.

		Contribution of faces (%) $1\bar{1}0$, $1\bar{1}1$	Contribution of faces (%) 001, $00\bar{1}$	C [F/m^2]	MSC
11 - site model	Girvin et al. (1991)	75	25	0.916	4.22
		100	0	0.813	3.74
	Antelo et al. (2010)	75	25	0.746	4.49
		100	0	0.68	4.92

The model yielded improved results for the Antelo dataset with the higher PZNPC (MSC: 4.92), but could not simulate the charging behavior of the fresh FH dataset from Girvin et al. (1991) as well (MSC: 3.74). The PZNPC for the fresh FH is predicted at 8.3, which is higher than the actual value, while the PZNPC of the aged FH agrees with the experimental value of 8.7. The fitted capacitance value was lower for the 11- site "aged" model to attain a higher value of PZNPC. In all model fits, the capacitance value was inversely related to the proton affinities and the PZNPC as previously observed (Hiemstra et al., 1996), however the capacitance has a limited ability to capture PZNPC values that are far from the protonation log Ks. This exercise indicates that this is possible to capture higher PZNPCs by increasing the contribution of the $(1\bar{1}0)$ and $(1\bar{1}1)$ planes and theoretically, this should also increase the contribution of the amount of SC groups. Conversely, increasing the contribution of the basal planes would result in a decrease in the overall PZNPC.

Based on this analysis, it is concluded that the surface structure proposed by Hiemstra (2013) can be used to model surface charge of fresh FH with PZNPC values lower than 8.4. For any FH with a higher PZNPC, either due to aging or other reasons, only a model with increased contribution of the $(1\bar{1}0)$ and $(1\bar{1}1)$ planes can provide an adequate fit.

3–site model

The first attempt to simplify the model was to calculate the log K of a single TC site as an average (6.56) or weighted average (7.55) of individual log Ks for all TC sites using the sum of their site densities. Neither protonation constant yielded a reasonable fit for both fresh and aged FH (Figure A2-14, A2-15 in Appendix), thus this approach is not appropriate for model simplification. In model 3a, both the proton affinity and capacitance were optimized for each dataset individually (Figure 2-2c and Table 2-5), resulting in log K_{Fe3O} of 7.89 and 8.43 for fresh and aged FH, respectively. This approach was able to describe the data very well, but it does not lead to a unified model that can describe different types of FH with a single set of thermodynamic constants. Again, changing crystal morphology emerges as a necessity to describe data exhibiting different PZNPCs. In our attempt towards a more unified model with one set of protonation constants, the protonation constant for the triply coordinated sites was optimized to provide an acceptable fit for both datasets (model 3b). The optimized log K_{Fe3O} was determined to be 8.1 and that provided an acceptable fit for the fresh FH, but it was not able to capture the PZNPC for the aged one (Figure A2-16). Comparing the MSCs for the 11-site and 3-site models thus far (Tables 2-4 and 2-5), the 3-site model provided superior fits for the fresh FH, and the 3a model provided optimal results for both fresh and aged FH. For aged FH, the 11-site model with the alternate face distribution was almost equivalent to 3-site model with a fitted log K for TC groups. These observations indicate that having a variable face distribution is necessary to describe different FHs with the same set of log Ks and also that simplifying the model to fewer sites is likely to yield improved results. Model 3c is an attempt to satisfy both these requirements.

Table 2-6. Modeling results for Girvin et al. (1991) and Antelo et al. (2010) based on the 3-site models (a) and (b).

		$LogK_{FeOHa}$	$LogK_{FeOHb}$	$LogK_{Fe3O}$	C [F/m^2]	MSC
3 - site model (a)	Girvin et al. (1991)	10.4	8	7.89	0.935	4.51
	Antelo et al. (2010)			8.43	0.67	5.02
3 - site model (b)	Girvin et al. (1991)	10.4	8	8.1	0.875	4.30
	Antelo et al. (2010)				0.71	4.33

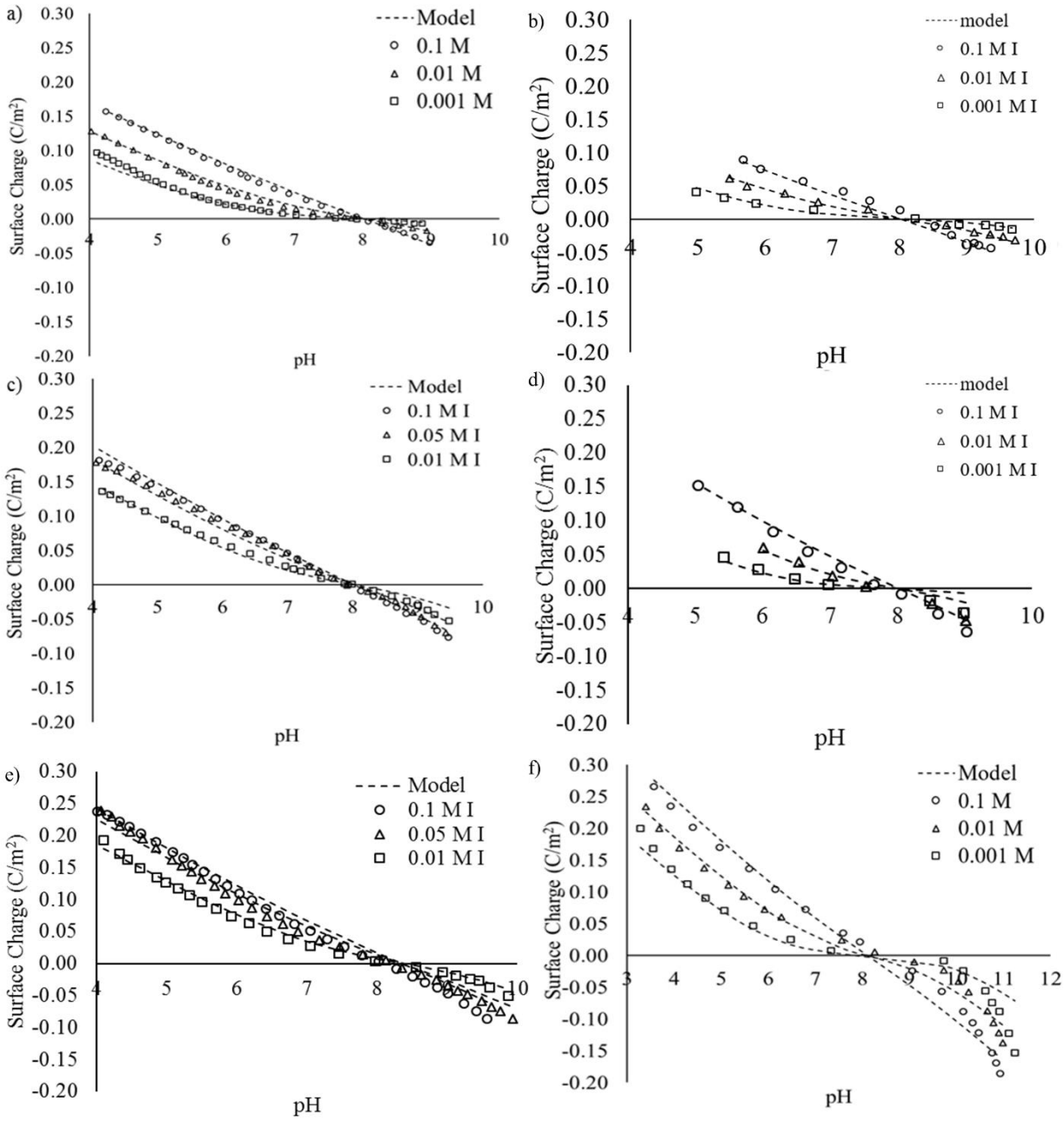

Figure 2-3. Surface charge modeling for the 3c - site model (fresh FH). Experimental data (symbols) and model simulations (lines) for a) Girvin et al. (1991), b) Hsi and Langmuir (1985), c) Nagata et al. (2009), d) Davis (1977), e) Fukushi et al. (2013) and f) Jain et al. (1999).

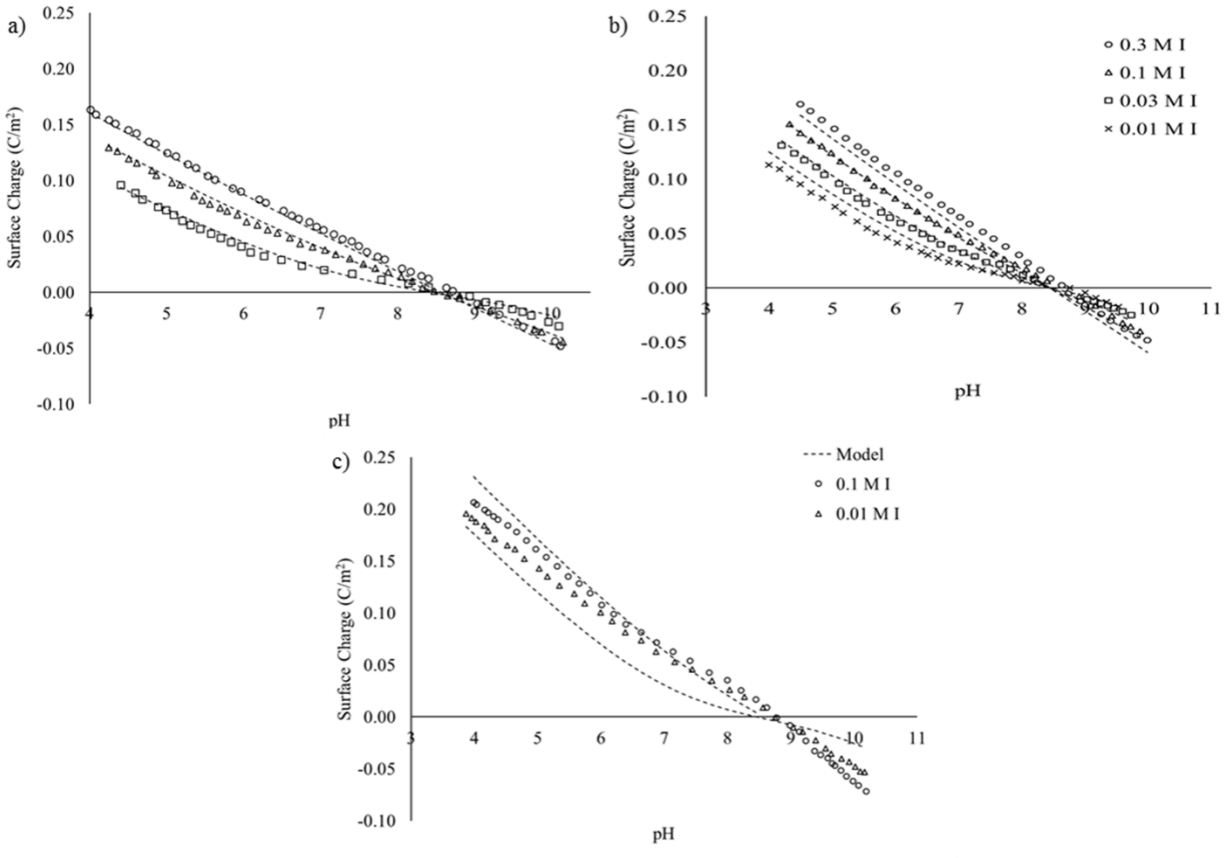

Figure 2-4. Surface charge modeling for the 3c - site model (aged FH). Experimental data (symbols) and model simulations (lines) for a) Antelo et al. (201), b) Hofmann et al. (2005), c) Wang et al. (2013).

Figure 2-3 shows the results of model 3c for fresh FH datasets, Figure 4 for aged FH datasets and Table 6 summarizes the relevant parameters for all datasets. The crystal faces are considered 75% $(1\bar{1}0)$ and $(1\bar{1}1)$ and 25 % (001) and $(00\bar{1})$ for the fresh FH. For the aged FH, assuming that the basal faces are becoming more evident while aging, the faces considered 30 % $(1\bar{1}0)$ and $(1\bar{1}1)$ and 70 % (001) and $(00\bar{1})$. This approach described very well the majority of both the fresh and aged FH datasets. For the Hoffman data set, since the FH was aged for 10 days, and is more aged than the Antelo (2010) FH that aged for 48 h, we assumed that the basal faces are slightly larger

(75 %). The model fit for the highest and lowest ionic strengths was still poor, and this may be related to the titration method that utilized the same suspension to conduct all four titrations. In the case of the Wang et al. (2013) charging curves, although the model was able to capture the PZNPC, none of the models was able to adequately simulate the charging behavior. The curves for different ionic strengths were more closely spaced and followed different slopes compared to the other studies.

Table 2-7. Modeling results for all studies based on the 3-site model (c).

		$LogK_{FeOHa}$	$LogK_{FeOHb}$	$LogK_{Fe3O}$	C [F/m^2]	MSC
3 - site model (fresh FH)	Girvin et al. (1991)	8	8	9.5	0.922	4.5
	Hsi and Langmuir (1985)				0.822	3.81
	Nagata et al. (2009)				1.105	4.64
	Davis (1977)				1.22	2.89
	Fukushi et al. (2013)				1.36	5.9
	Jain et al. (1999)				1.35	3.53
3 - site model (Aged FH)	Antelo et al. (2010)	8	8	9.5	0.74	5.20
	Hofmann et al. (2005)				0.898	4.11
	Wang et al. (2013)				1.3	3.39

The capacitance values were different for all datasets and ranged between 0.74 and 1.36 F/m^2, which are within a typical range of capacitances for a Basic Stern model. The capacitance value is also highly influenced by the choice of SSA used to convert the dataset from C/g to C/m^2 and the two have an inverse relationship, as has been established previously in the literature (Hwang and Lenhart, 2008; Sverjensky, 2005a). We also attempted a similar approach as followed by Villalobos and Antelo (2012), i.e. all data were normalized using the SSAs shown in Table 2-1.

The highest used value was 600 m^2/g for the Fukushi et al. (2013) dataset with the highest C/g values and all other curves were normalized to that dataset, thus the model used is equivalent to the Fukushi model with C_1= 1.36 F/m^2. While this is clearly an arbitrary choice, it works as well as modeling datasets individually and fitting capacitance values. The results of this exercise are shown in Figure 2-5. The only two datasets that are poorly described by this approach are Wang et al. (2013) and some by Hoffman et al. (2005), i.e. the same ones that are poorly described by any approach considered thus far.

Comparing the results of this model vs. the model developed by Villalobos and Antelo (2012), who utilized several of the same datasets, it is apparent that the fits are quite similar, even though the SSA values used to normalize the data are much lower. This is partially because Villalobos and Antelo (2012) used fixed capacitance values (C_1=0.74 and C_2=0.93 F/m^2) for all datasets and also because their overall site density was lower (max 8.8 sites/nm^2) compared to the site densities used here (13.3 sites/nm^2 for fresh FH), because they utilized the goethite structure as a basis to construct the model.

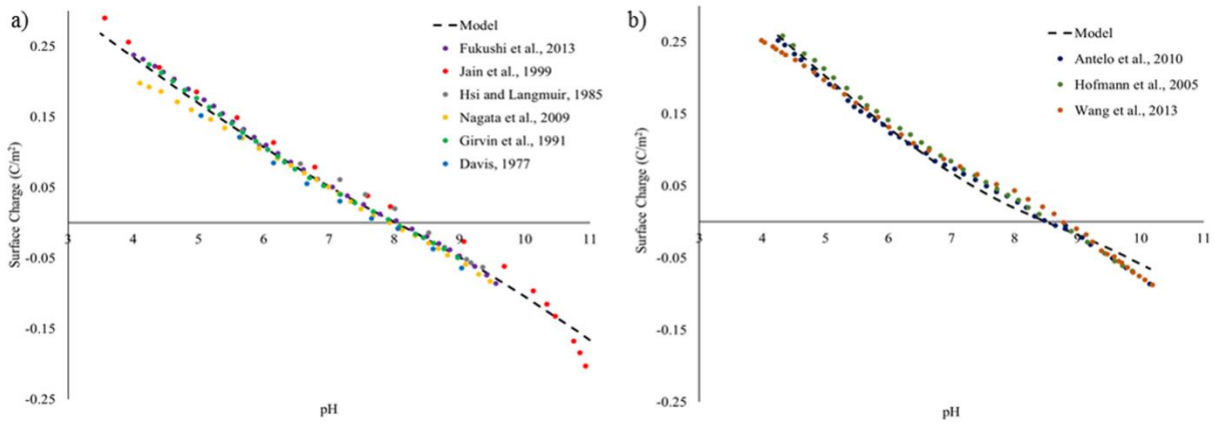

Figure 2-5. Surface charge modeling for model 3c on SSA-normalized data in 0.1 M for a) fresh FH and b) aged FH.

Site contribution to surface charge

An important question to address when simplifying surface structural models is whether the two models are truly equivalent. For example, Hiemstra et al. (1996) discuss the choice of the number of sites and log Ks for the goethite structure and consider the contribution of individual sites to the overall surface charge. While two models may be identical in terms of the overall fit to titration curves, the individual site contributions to the overall pH dependent charging behavior can be radically different. Assuming that SC groups contribute to both charge and inner sphere ion complexation and TC groups to charge and outer sphere complexation, it follows that using models with different site contributions will have implications on how successful these models will be in describing specific adsorption, as well as ion exchange reactions.

To investigate this question, the contribution of each site to the overall charge was investigated for the fresh FH data set (Girvin et al., 1991) for the 11-site and the 3-site 3c model with the 75-25 % face contribution. The contribution of each of the 11 sites to charge is shown in Figure 2-6, while Figure 2-6 shows the sum of the SC and TC groups. In the 11-site model, the SC sites with log K 10.4 (si_1 and si_6) are 99% protonated in the pH range 4 to 9, thus contributing a permanent positive charge. The SC sites with log K 8.0 (si_2 and si_7) are 45% to 38% protonated in pH range 4 to 9 and are thus overall negatively charged. The TC sites si_3 and si_8 with proton affinities 10.4, are 99 % protonated and contribute a positive charge to the overall charge. The remainder of the TC sites (si_4, si_5, si_9, si_{10}, and si_{11}) are mostly unprotonated and negatively charged in the common pH range. Collectively, the SC sites are predicted to be positively charged even above the PZNPC and account for the majority of surface charge (Figure 2-6a). The TC sites are contributing a smaller negative charge in the entire pH range. Considering that the site density of the TC surface groups

(6.76 nm^{-2}) is comparable to the SC surface groups (6.5 nm^{-2}), the combination of both site densities and proton affinities allow most of the SC groups to become protonated.

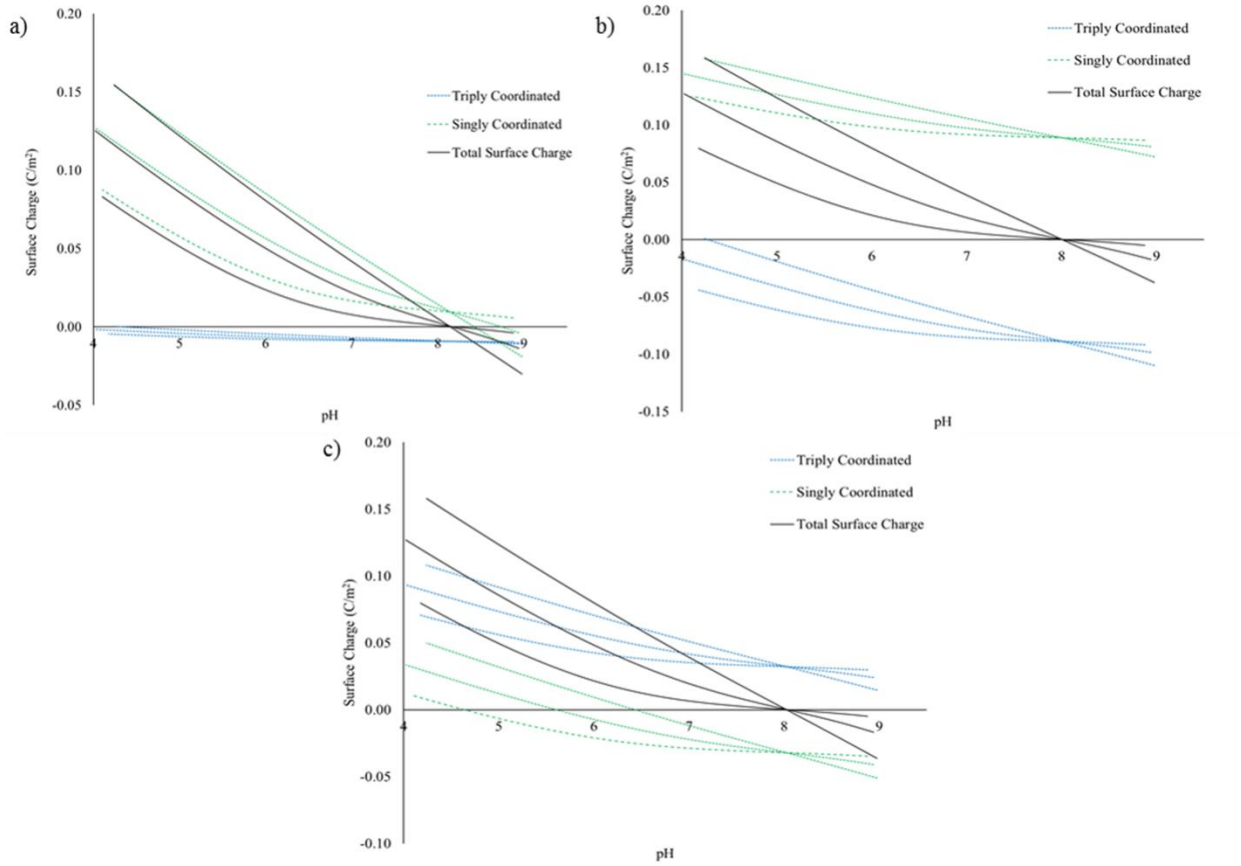

Figure 2-6. Calculated contribution of the singly- coordinated and triply- coordinated surface groups to the overall surface charge of Girvin et al. (1991) FH for a) the 11-site and b) 3-site model 3a and c) 3-site model 3c.

Conversely, the relative contribution of SC and TC sites in the two 3-site models is substantially different. The total site densities of the two groups are identical, however the SC sites are predicted to contribute more positive charge in model 3a and be mostly negatively charged in model 3c. This is because a log K higher than the PZNPC is assigned to the SC groups in model 3a and to TC groups in model 3c, and higher log K groups are protonated first. In model 3a, SC groups have

positive charge even above the PZNPC and TC groups are negatively charged throughout the pH range.

The above analysis leads to the following conundrum:

Models relying on 2 or 3 sites with log Ks that are all set at the PZNPC, which has been the prevailing approach, are not able to describe the charging behavior of FHs with different PZNPC values. Experimental studies indicate that the PZNPC of FH increases with aging, which indicates the presence of at least one type of surface functional group with log K above the PZNPC. This functional group should become more abundant as the crystal morphology changes with aging and crystallite size increases. Although there is limited evidence to this end, TEM observations suggest that the basal planes (001) and $(00\bar{1})$ become more evident in larger crystallite sizes, which would imply that the TC oxygens present on these surfaces have to be the functional groups with log K values exceeding the PZNPC of fresh FH. However, if the log Ks of the SC and TC groups on the more reactive $(1\bar{1}0)$ and $(1\bar{1}1)$ planes are set equal to the PZNPC of fresh FH (8.0), which is a typical approach adopted in the literature, then the relative contribution of SC and TC groups to surface charge appears to be inconsistent with FH behavior for inner sphere complexation. This model also does not support a higher reactivity of large FH particles with increasing size, which was the conclusion of Villacís-García et al. (2015). This would require a higher contribution of SC groups, which are only present on the $(1\bar{1}0)$ and $(1\bar{1}1)$ surfaces. The original 11-site model with decreased contribution of basal planes can, in fact, capture both behaviors. At this point, there is insufficient experimental evidence to support conclusions on FH morphology with aging and its reactivity; for example, the recent Wang et al. (2013) and Villacís-García et al. (2015) offer contradicting evidence in both accounts.

Conclusions

A compilation of surface charge data for FH indicates that there are differences in reported values in two aspects: a) different values both on mass and surface area basis, and b) differences in the PZNPC, which ranges between 8.0 and 8.7. Both aspects appear to be driven by the size of FH crystals, which are in turn related to the precipitation method and specifically aging during and after preparation. Fresh FH suspensions have smaller crystals with higher SSAs and lower PZNPC values, while aged suspensions have smaller SSAs and higher PZNPCs. The supporting experimental information to determine what the term "aging" means and how it translates to particular particle sizes and crystal morphologies is currently lacking. In addition, there is contradictory data, with one recent study (Wang et al. 2013) concluding that there is no difference in reactivity for FH particles of different sizes and crystallinities, and yielding identical PZNPC values of 8.7 for all types of FH. However, the surface charge data they obtained could not be modeled using any of our models and thus the experimental dataset appears to be an outlier.

For the remaining datasets (8 in total), modeling surface charge using the proposed surface structure by Hiemstra (2013) that includes 11 different sites with calculated site densities and protonation constants was successful for fresh FH datasets, however datasets with PZNPC values exceeding 8.4 could not be described. To accommodate large differences in PZNPC, it is necessary to change the contribution of different crystal faces, as has been done in the past for goethite (Villalobos et al. 2009). The Hiemstra (2013) model can only capture high PZNPC values if the contribution of the (001) and $(00\bar{1})$ basal planes are minimized, given that the triply coordinated surface oxygens on these planes are more acidic in this model. Overall, the site densities for singly and triply coordinated groups appear to be reasonable, as their use can describe surface charge values with SSA values in the range 300-600 m^2/g, i.e. much lower and in the expected range

compared to the values fitted in the unified model of Villalobos and Antelo (2012), who based their model on the goethite structure with lower site densities. Still, the approach of normalizing surface charge data to the same range of C/m^2 using fitted SSAs yields results equivalent to fitting individual capacitance values for every dataset. Given that the uncertainty in measured SSAs is high and that capacitance is also a parameter that cannot be measured or easily fixed, surface area normalization reduces uncertainty in the datasets.

Still, the problem of modeling all datasets using a single set of log Ks is not easily solved. Even though the Hiemstra (2013) model works, the number of sites and associated log K values used is too high (seven different log K values are used) to be independently verified through a modeling approach alone, and will also prove cumbersome to adopt when specific ion adsorption and ion exchange reactions are considered. Towards a simplified model, several versions of models using three sites were tested, all of which maintained the total site densities but varied in the type of sites used and the approach to determine log Ks for the sites. Two of the models utilized the same log K values for the SC groups as proposed by Hiemstra (2013). For this scenario, a single TC site was used, but it was not possible to determine a single log K value for this site to describe all eight datasets. Thus, the last approach involved one singly and two triply coordinated oxygens, one of which was placed on the basal planes and one on the more reactive faces of the FH crystal. The singly and triply coordinated groups on these faces were considered to have a log K equal to the PZNPC of fresh FH (8.0), while the basal plane log K was set equal to 9.5, so that an increased contribution of these planes could capture higher PZNPCs. This approach described all eight datasets quite well, but has two drawbacks: there is no experimental evidence to support the variable contributions of crystal faces, and perhaps more importantly, the relative contribution of singly and triply coordinated groups to the overall charge is substantially different compared to

the 11-site model. This may have important implications when one attempts to describe specific adsorption and ion exchange reactions, and is an issue that has not been adequately addressed to date.

References

Antelo, J., Fiol, S., Pérez, C., Mariño, S., Arce, F., Gondar, D., López, R., 2010. Analysis of phosphate adsorption onto ferrihydrite using the CD-MUSIC model. J. Colloid Interface Sci. 347, 112–119. doi:10.1016/j.jcis.2010.03.020

Brunauer, S., Emmett, P.H., Teller, E., 1938. Adsorption of Gases in Multimolecular Layers. J. Am. Chem. Soc. 60, 309–319. doi:10.1021/ja01269a023

Ching-kuo Daniel Hsi, Langmuir, D., 1985. Adsorption of uranyl onto ferric oxyhydroxides: Application of the surface complexation site-binding model. Geochim. Cosmochim. Acta 49, 1931–1941. doi:10.1016/0016-7037(85)90088-2

Cismasu, A.C., Michel, F.M., Stebbins, J.F., Levard, C., Brown Jr., G.E., 2012. Properties of impurity-bearing ferrihydrite I. Effects of Al content and precipitation rate on the structure of 2-line ferrihydrite. Geochim. Cosmochim. Acta 92, 275–291. doi:10.1016/j.gca.2012.06.010

Cornell, R.M., Schwertmann, U., 2003. The Iron Oxides: Structure, Properties, Reactions, Occurrences and Uses. John Wiley & Sons.

Davis, J.A., 1977. Adsorption of trace metals and complexing ligands at the oxide/water interface /.

Davis, J.A., James, R.O., Leckie, J.O., 1978. Surface ionization and complexation at the oxide/water interface. J. Colloid Interface Sci. 63, 480–499. doi:10.1016/S0021-9797(78)80009-5

Drits, V.A., Sakharov, B.A., Salyn, A.L., Manceau, A., 1993. Structural model for ferrihydrite. Clay Miner. 28, 185–207.

Dzombak, D.A., Morel, F.M.M., 1990. Surface Complexation Modeling: Hydrous Ferric Oxide. John Wiley & Sons.

Fukushi, K., Aoyama, K., Yang, C., Kitadai, N., Nakashima, S., 2013. Surface complexation modeling for sulfate adsorption on ferrihydrite consistent with in situ infrared spectroscopic observations. Appl. Geochem. 36, 92–103. doi:10.1016/j.apgeochem.2013.06.013

Fuller, C.C., Davis, J.A., Waychunas, G.A., 1993. Surface chemistry of ferrihydrite: Part 2. Kinetics of arsenate adsorption and coprecipitation. Geochim. Cosmochim. Acta 57, 2271–2282. doi:10.1016/0016-7037(93)90568-H

Gaboriaud, F., Ehrhardt, J.-J., 2003. Effects of different crystal faces on the surface charge of colloidal goethite (α-FeOOH) particles: an experimental and modeling study. Geochim. Cosmochim. Acta, Advances in Oxide and Sulfide Mineral Surface Chemistry 67, 967–983. doi:10.1016/S0016-7037(02)00988-2

Girvin, D.C., Ames, L.L., Schwab, A.P., Mcgarrah, J.E., 1991. Neptunium adsorption on synthetic amorphous iron oxyhydroxide. J. Colloid Interface Sci. 141, 67–78.

Girvin, D.C., Ames, L.L., Schwab, A.P., McGarrah, J.E., 1991. Neptunium adsorption on synthetic amorphous iron oxyhydroxide. J. Colloid Interface Sci. 141, 67–78. doi:10.1016/0021-9797(91)90303-P

Greffié, C., Amouric, M., Parron, C., 2001. HRTEM study of freeze-dried and untreated synthetic ferrihydrites: consequences of sample processing. Clay Miner. 36, 381–387. doi:10.1180/000985501750539472

Gregg, S.J., Sing, K.S.W., Salzberg, H.W., 1967. Adsorption Surface Area and Porosity. J. Electrochem. Soc. 114, 279C–279C. doi:10.1149/1.2426447

Gustafsson, J.P., 2001. Modelling competitive anion adsorption on oxide minerals and an allophane-containing soil. Eur. J. Soil Sci. 52, 639–653. doi:10.1046/j.1365-2389.2001.00414.x

Gustafsson, J.P., Dässman, E., Bäckström, M., 2009. Towards a consistent geochemical model for prediction of uranium(VI) removal from groundwater by ferrihydrite. Appl. Geochem. 24, 454–462. doi:10.1016/j.apgeochem.2008.12.032

Gustafsson, J.P., Tiberg, C., Edkymish, A., Kleja, D.B., 2011. Modelling lead(II) sorption to ferrihydrite and soil organic matter. Environ. Chem. 8, 485. doi:10.1071/EN11025

Hiemstra, T., 2013. Surface and mineral structure of ferrihydrite. Geochim. Cosmochim. Acta 105, 316–325. doi:10.1016/j.gca.2012.12.002

Hiemstra, T., Barnett, M.O., van Riemsdijk, W.H., 2007. Interaction of silicic acid with goethite. J. Colloid Interface Sci. 310, 8–17. doi:10.1016/j.jcis.2007.01.065

Hiemstra, T., Rahnemaie, R., van Riemsdijk, W.H., 2004. Surface complexation of carbonate on goethite: IR spectroscopy, structure and charge distribution. J. Colloid Interface Sci. 278, 282–290. doi:10.1016/j.jcis.2004.06.014

Hiemstra, T., Riemsdijk, W.H.V., Rossberg, A., Ulrich, K.-U., 2009. A surface structural model for ferrihydrite II: Adsorption of uranyl and carbonate. Geochim. Cosmochim. Acta 73, 4437–4451. doi:10.1016/j.gca.2009.04.035

Hiemstra, T., Van Riemsdijk, W.H., 2009. A surface structural model for ferrihydrite I: Sites related to primary charge, molar mass, and mass density. Geochim. Cosmochim. Acta 73, 4423–4436. doi:10.1016/j.gca.2009.04.032

Hiemstra, T., Van Riemsdijk, W.H., 2006. On the relationship between charge distribution, surface hydration, and the structure of the interface of metal hydroxides. J. Colloid Interface Sci. 301, 1–18. doi:10.1016/j.jcis.2006.05.008

Hiemstra, T., Van Riemsdijk, W.H., 1996. A Surface Structural Approach to Ion Adsorption: The Charge Distribution (CD) Model. J. Colloid Interface Sci. 179, 488–508. doi:10.1006/jcis.1996.0242

Hiemstra, T., Venema, P., Riemsdijk, W.H.V., 1996. Intrinsic Proton Affinity of Reactive Surface Groups of Metal (Hydr)oxides: The Bond Valence Principle. J. Colloid Interface Sci. 184, 680–692. doi:10.1006/jcis.1996.0666

Hofmann, A., van Beinum, W., Meeussen, J.C.L., Kretzschmar, R., 2005. Sorption kinetics of strontium in porous hydrous ferric oxide aggregates II. Comparison of experimental results and model predictions. J. Colloid Interface Sci. 283, 29–40. doi:10.1016/j.jcis.2004.08.105

Hwang, Y.S., Lenhart, J.J., 2008. The dependence of hematite site-occupancy standard state triple-layer model parameters on inner-layer capacitance. J. Colloid Interface Sci. 319, 206–213. doi:10.1016/j.jcis.2007.11.032

Jain, A., Raven, K.P., Loeppert, R.H., 1999. Arsenite and Arsenate Adsorption on Ferrihydrite: Surface Charge Reduction and Net OH- Release Stoichiometry. Environ. Sci. Technol. 33, 1179–1184. doi:10.1021/es980722e

Johnston, C.P., Chrysochoou, M., 2012. Investigation of Chromate Coordination on Ferrihydrite by in Situ ATR-FTIR Spectroscopy and Theoretical Frequency Calculations. Environ. Sci. Technol. 46, 5851–5858. doi:10.1021/es300660r

Machesky, M.L., Wesolowski, D.J., Palmer, D.A., Ichiro-Hayashi, K., 1998. Potentiometric Titrations of Rutile Suspensions to 250°C. J. Colloid Interface Sci. 200, 298–309. doi:10.1006/jcis.1997.5401

Michel, F.M., Ehm, L., Antao, S.M., Lee, P.L., Chupas, P.J., Liu, G., Strongin, D.R., Schoonen, M.A.A., Phillips, B.L., Parise, J.B., 2007. The Structure of Ferrihydrite, a Nanocrystalline Material. Science 316, 1726–1729. doi:10.1126/science.1142525

Nagata, T., Fukushi, K., Takahashi, Y., 2009. Prediction of iodide adsorption on oxides by surface complexation modeling with spectroscopic confirmation. J. Colloid Interface Sci. 332, 309–316. doi:10.1016/j.jcis.2008.12.037

Ponthieu, M., Juillot, F., Hiemstra, T., van Riemsdijk, W.H., Benedetti, M.F., 2006. Metal ion binding to iron oxides. Geochim. Cosmochim. Acta 70, 2679–2698. doi:10.1016/j.gca.2006.02.021

Rahnemaie, R., Hiemstra, T., van Riemsdijk, W.H., 2006. A new surface structural approach to ion adsorption: Tracing the location of electrolyte ions. J. Colloid Interface Sci. 293, 312–321. doi:10.1016/j.jcis.2005.06.089

Sahai, N., Sverjensky, D.A., 1997. Evaluation of internally consistent parameters for the triple-layer model by the systematic analysis of oxide surface titration data. Geochim. Cosmochim. Acta 61, 2801–2826. doi:10.1016/S0016-7037(97)00128-2

Salazar-Camacho, C., Villalobos, M., 2010. Goethite surface reactivity: III. Unifying arsenate adsorption behavior through a variable crystal face – Site density model. Geochim. Cosmochim. Acta 74, 2257–2280. doi:10.1016/j.gca.2010.01.025

Sverjensky, D.A., 2005. Prediction of surface charge on oxides in salt solutions: Revisions for 1:1 (M+L−) electrolytes. Geochim. Cosmochim. Acta 69, 225–257. doi:10.1016/j.gca.2004.05.040

Sverjensky, D.A., Sahai, N., 1996. Theoretical prediction of single-site surface-protonation equilibrium constants for oxides and silicates in water. Geochim. Cosmochim. Acta 60, 3773–3797. doi:10.1016/0016-7037(96)00207-4

Tiberg, C., Sjöstedt, C., Persson, I., Gustafsson, J.P., 2013. Phosphate effects on copper(II) and lead(II) sorption to ferrihydrite. Geochim. Cosmochim. Acta 120, 140–157. doi:10.1016/j.gca.2013.06.012

Villalobos, M., Antelo, J., 2012. A unified surface stuctural model for ferrihydrite: proton charge, electrolyte binding, and arsenate adsorption.

Villalobos, M., Cheney, M.A., Alcaraz-Cienfuegos, J., 2009. Goethite surface reactivity: II. A microscopic site-density model that describes its surface area-normalized variability. J. Colloid Interface Sci. 336, 412–422. doi:10.1016/j.jcis.2009.04.052

Villalobos, M., Leckie, J.O., 2000. Carbonate adsorption on goethite under closed and open CO2 conditions. Geochim. Cosmochim. Acta 64, 3787–3802. doi:10.1016/S0016-7037(00)00465-8

Wang, X., Li, W., Harrington, R., Liu, F., Parise, J.B., Feng, X., Sparks, D.L., 2013. Effect of Ferrihydrite Crystallite Size on Phosphate Adsorption Reactivity. Environ. Sci. Technol. 47, 10322–10331. doi:10.1021/es401301z

Wesolowski, D.J., Machesky, M.L., Palmer, D.A., Anovitz, L.M., 2000. Magnetite surface charge studies to 290°C from in situ pH titrations. Chem. Geol. 167, 193–229. doi:10.1016/S0009-2541(99)00209-0

Zeltner, W.A., Anderson, M.A., 1988. Surface charge development at the goethite/aqueous solution interface: effects of CO2 adsorption. Langmuir 4, 469–474. doi:10.1021/la00080a039

Villacís-García M., Ugalde-Arzate M., Vaca-Escobar K., Villalobos M., Zanella R., Martínez-Villegas N., 2015. Laboratory synthesis of goethite and ferrihydrite of controlled particle sizes. Boletín de la Sociedad Geológica Mexicana Volumen 67, núm. 3, 2015, p. 433-446

Appendix – Chapter 2

Titration data sets as used in this study.

Experimental potentiometric surface titration data obtained digitizing graphs from sources as cited above each figure.

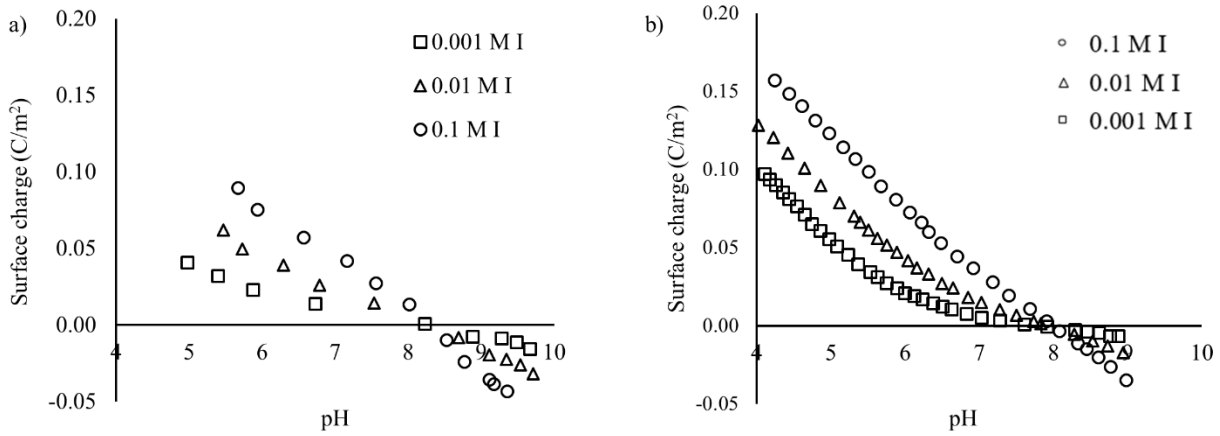

Figure A2-7. Titration of ferrihydrite in $NaNO_3$: a) data from Ching-kuo Daniel Hsi and Langmuir (1985) and b) data from Girvin et al. (1991).

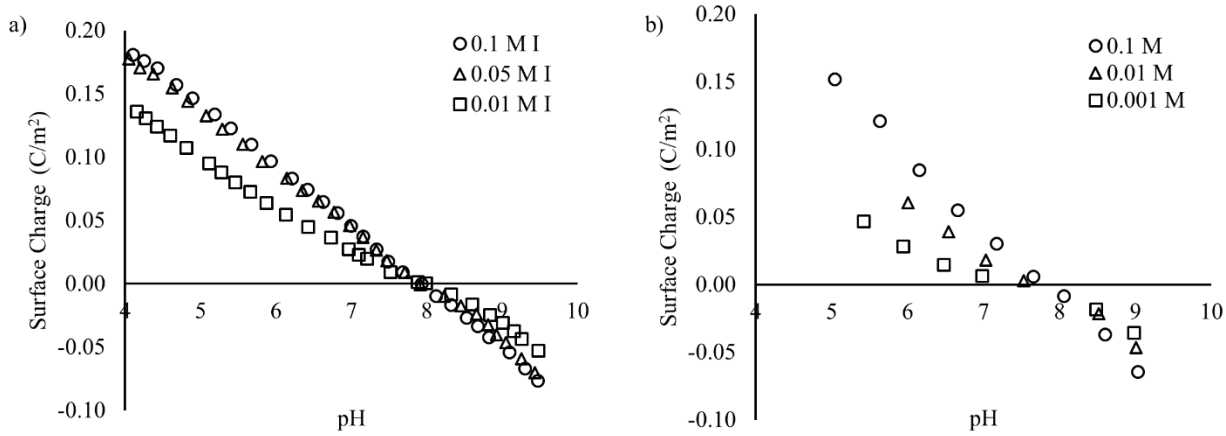

Figure A2-8. Titration of ferrihydrite in $NaNO_3$: a) data from Nagata et al. (2009) and b) data from Davis (1977).

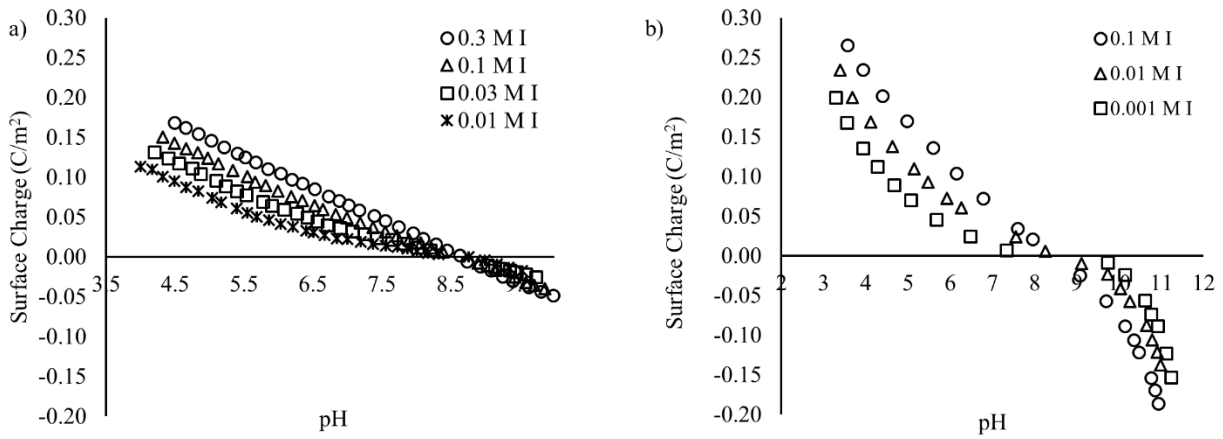

Figure A2-9. Titration of ferrihydrite in a) $NaNO_3$ obtained by (Hofmann et al., 2005) and b) NaCl by Jain et al. (1999)

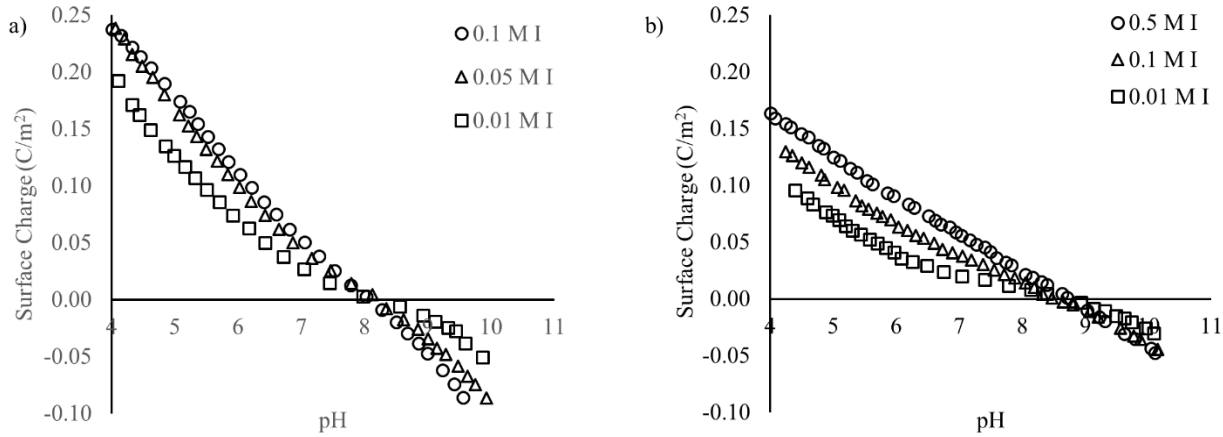

Figure A2-10. Titration of ferrihydrite in: a) NaCl obtained by (Fukushi et al., 2013) and b) KNO_3 obtained by (Antelo et al., 2010)

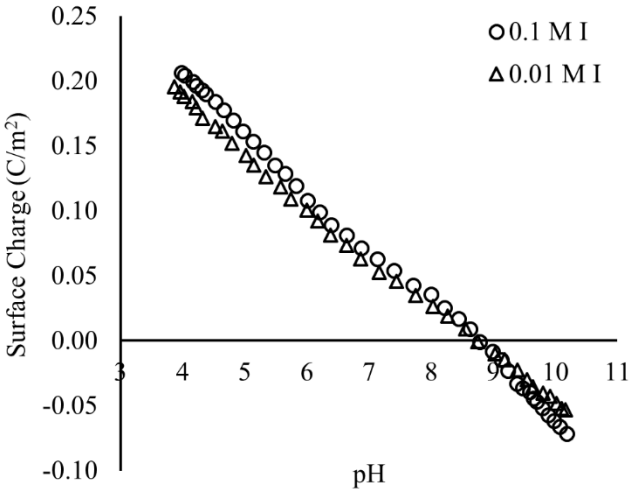

Figure A2-11. Titration of ferrihydrite in KCl obtained by Wang et al. (2013)

Basic surface charge calculations used in the modeling.

The surface protonation constants for singly- and triply- coordinated surface oxygens are given by:

$$K_{Hi} = \frac{\left[\equiv \mathrm{FeOH}_{2i}^{+0.5}\right]}{\left[\equiv \mathrm{FeOH}_{i}^{-0.5}\right]\{H^{+}\}} \exp\left(\frac{zF\psi_0}{RT}\right)$$

$$K_{Hj} = \frac{\left[\equiv \mathrm{Fe_3OH}_{j}^{+0.5}\right]}{\left[\equiv \mathrm{Fe_3O}_{j}^{-0.5}\right]\{H^{+}\}} \exp\left(\frac{zF\psi_0}{RT}\right)$$

Where, F is the Faraday constant (96,485 C/mol), z is the valence of the adsorbing ion, ψ is the surface potential (V), R is the gas constant and T is the absolute temperature (298.15 K).

The basic Stern layer has one fitting parameter, the capacitance, C_1, was used to define the charge – potential relationships:

$$\sigma_0 = C_1(\psi_0 - \psi_{1)}$$

While σ_d, the net charge of electrolytes in the diffuse layer (DL) based on Guoy – Chapman relationship:

$$\sigma_d = (8RT\varepsilon_0\varepsilon_b I\rho_s)^{0.5} \sinh\left(\frac{zF\psi_d}{2RT}\right)$$

Model Parameters

Table A2-8. Electrolyte equilibrium constants for CD-MUSIC model on goethite and ferrihydrite.

Study	LogK Na+	LogK K+	LogK NO3-	LogK Cl-	LogK ClO4-
Hiemstra et al. (2004)	-1		-1	-0.5	-1.7
(Hiemstra and Van Riemsdijk, 2006))	-0.6 ± 0.03	-1.61 ± 0.13	-0.68 ± 0.03	-0.45 ± 0.03	
(Hiemstra et al., 2007a)	-0.61		-0.7		
(Hiemstra et al., 2007b)	-0.61	-1.74	-0.7	-0.44	
(Hiemstra and Van Riemsdijk, 2009)	-0.6		-0.68	-0.45	-1.7
(Antelo et al., 2010)		-1.16	-0.96		
(Tiberg et al., 2013)	-0.6		-0.68		
Adopted in this study	**-0.6**	**-1.61**	**-0.68**	**-0.45**	**-1.7**

Modeling Results

Model 11-sites

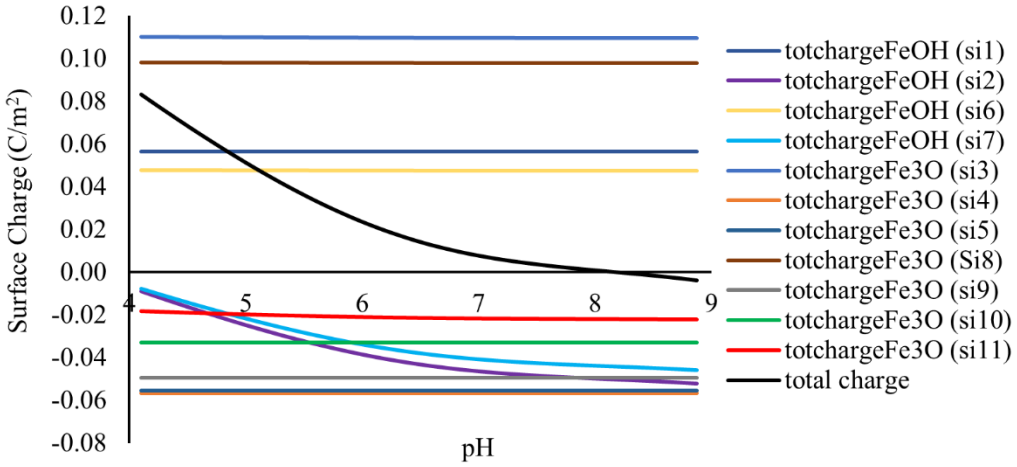

Figure A2-12. Charging behavior of individual sites – 11-site model

Model 3-sites

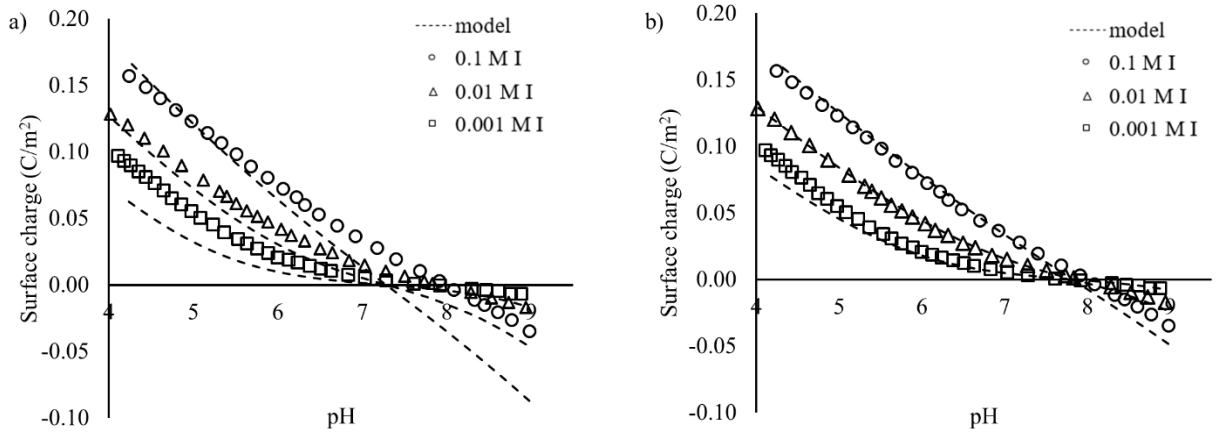

Figure A2-13. Surface charge modeling for 3 site model with two singly- and one triply-coordinated group. Experimental data for fresh FH (symbols) and model simulations (lines) for a triply- coordinated group with a) LogK 6.56 (average) and, b) LogK 7.55 (weighted average).

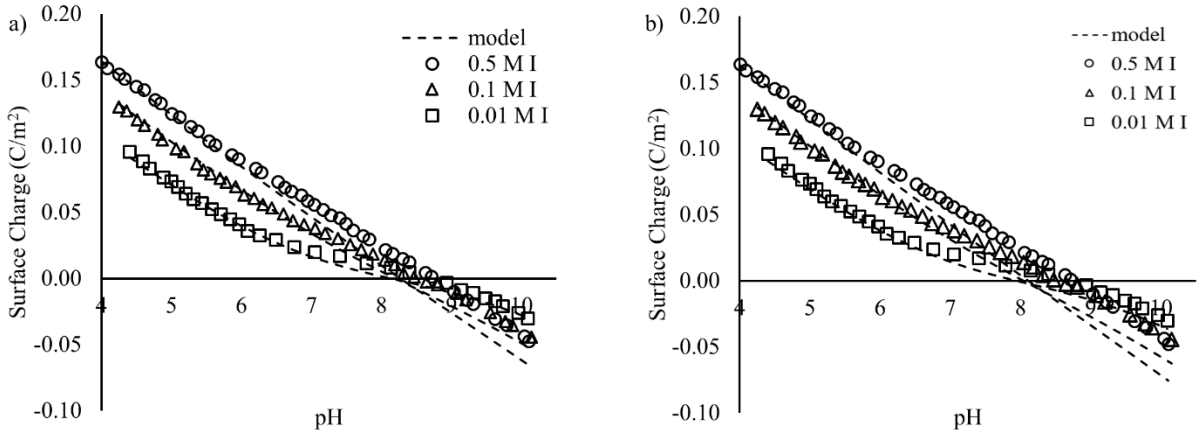

Figure A2-14. Surface charge modeling for 3 site model with two singly- and one triply-coordinated group. Experimental data for aged FH (symbols) and model simulations (lines) for a triply- coordinated group with a) LogK 6.56 (average) and, b) LogK 7.55 (weighted average).

Model 3b

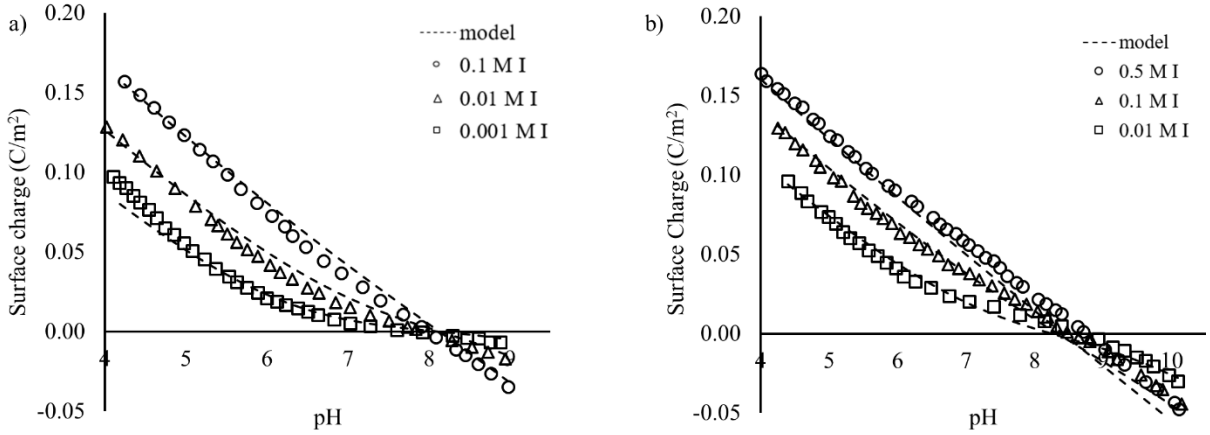

Figure A2-15. Surface charge modeling for 3b site model (one TC with fixed Logk at 8.1). Experimental data (symbols) and model simulations (lines) for a) Girvin et al. (1991) and, b) Antelo et al. (2010) studies.

CHAPTER 3 The MUSE I: A multi – start optimization algorithm for surface complexation parameter estimation

Nefeli Maria Bompoti, Maria Chrysochoou, and Michael Machesky

Submitted, under revision to Environmental Science and Technology

Abstract

The MUSE algorithm has been developed to optimize the thermodynamic parameters for surface complexation modeling (SCM). Although there is a plethora of software for estimation of intrinsic equilibrium constants, the extracted parameters are typically variable and highly correlated. This limits their usefulness and transferability in, for example, reactive transport models. With this in mind, a hybridized optimization approach, based on a multi – start algorithm combined with a local optimizer, has been developed to allow the simultaneous optimization of SCM parameters. In this study, the CD – MUSIC formalism with a Basic Stern electrostatic model was adopted, yet the algorithm can be implemented in any model formulation. This study offers two innovative components to the inverse SCM modeling approach: a) determination of the true global optimum based on the minimization of the mean squared error between the simulated and observed data, and b) quantitative simulation of spectroscopic pH – dependent profiles for two chromate surface complexes. We demonstrate that when MUSE is implemented to determine chromate log Ks, their dependence on other adjustable parameters such as specific surface area (SSA) and capacitance is relatively small (i.e., one unit change for chromate log Ks on ferrihydrite) and can be accounted by mathematical functions determined through the MUSE algorithm. The robustness of the algorithm is demonstrated in the absence of the spectroscopy data as well, with traditional batch tests yielding similar thermodynamic constants as the spectroscopic profiles.

Introduction

Surface complexation models (SCMs) provide a thermodynamic framework to describe adsorption processes, and can, in principle, replace empirical distribution factors for fate and transport modeling of contaminants (Davis et al., 1978; Dzombak and Morel, 1990; Goldberg et al., 2007;

Stumm et al., 1980; Yates et al., 1974). Several SCM formulations exist, arising from combinations of different pK models (1-pK or 2-pK), single or multisite expressions (charge distribution multisite complexation (CD – MUSIC) (Hiemstra and Van Riemsdijk, 1996)), and various electrostatic models (constant capacitance (CCM) (Stumm et al., 1980), basic Stern, diffuse layer model (DLM) (Huang and Stumm, 1973; Stumm et al., 1970), and triple layer model (TLM) (Davis et al., 1978; Yates et al., 1974)). The drawback of using SCMs is the high degree of parameterization, even when pure sorbate-sorbent systems are considered. Certain parameters can be measured, or otherwise constrained, while others are either calculated, assumed or fitted, rendering the transferability of SCMs between systems quite limited.

Experimental parameters include solid-liquid ratio, ionic strength and composition, and the specific surface area (SSA). While the popular N_2-BET (Brunauer et al., 1938; Gregg et al., 1967) method provides accurate SSA results for many materials (Everett et al., 1974), the difficulty of measuring the SSA of poorly crystallized oxy-hydro-oxides, such as ferrihydrite, is well established (Dzombak and Morel, 1990; Villacís-García et al., 2015; Villalobos and Antelo, 2012). The uncertainty in SSA values is such that Villalobos and Antelo (2012) treated it as a normalization parameter for their ferrihydrite studies. Site densities (Ns) are also required and constant values such as 3 sites/nm^2 or 2.3 (Davis and Kent, 1990) sites/nm^2 are often used in modeling studies. Crystallographic considerations tied to microscopy tools, such as transmission electron microscopy (TEM) and atomic force microscopy (AFM) (Gaboriaud and Ehrhardt, 2003; Livi et al., 2017; Villalobos et al., 2009), are being increasingly employed to reveal the crystal faces, and consequently estimate Ns values for well-resolved mineral faces.

Depending on the choice of the electrostatic model, the description of the surface potential may require no electrostatic parameters (as in the case for the diffuse double layer model (DLM)), or

one to two parameters to describe capacitance (CCM, Basic Stern (BS) and TLM), plus additional parameters to describe charge distribution, i.e. the CD factors in the CD – MUSIC model if that is utilized. Capacitance values are treated in various ways; adjusted/ fitted (Venema et al., 1998) to potentiometric titration data, predicted by the radius of the electrolyte cations in a TLM model (Sverjensky, 2001), predicted as a linear combination of the capacitances of different electric double layer structures (Boily, 2014), or even obtained from classical molecular dynamics simulations (Parez et al., 2014). It is also possible to adopt a non-electrostatic SCM, as is typically the case with Generalized Composite models. However, this causes equilibrium constants to become more heavily dependent on experimental conditions and site densities (Stoliker et al., 2011).

Any ligand-specific SCM requires at a minimum four equilibrium constants: protonation (log K_{H+}), electrolyte (log K_{C+}, log K_{A-}), and specific ion/contaminant. If more than one oxygen type (singly- vs. triply- coordinated oxygens on different locations on the surface) and more than one surface species are considered, the number of necessary thermodynamic constants increases. The surface complexes formed are nowadays usually determined from spectroscopy insights (X-ray absorption near edge structure (XANES), attenuated total reflectance Fourier transform infrared spectroscopy (ATR-FTIR), extended X-Ray Absorption fine Structure (EXAFS) (Fukushi et al., 2013; Ponthieu et al., 2006; Rossberg et al., 2009; Tiberg et al., 2013; Villalobos and Leckie, 2001), mostly in a qualitative manner, although notable exceptions include studies that incorporated quantitative analysis of EXAFS (Gu et al., 2016), nuclear magnetic resonance data (NMR) (Ingri et al., 1996), and time resolved laser fluorescence spectroscopy (TRLFS) (Stumpf et al., 2008) spectra. Protonation equilibrium constants attributed to particular surface oxygen groups may be calculated, as in the case of the MUSIC model (Hiemstra et al., 1996), or fitted to

experimental titration data. Electrolyte and specific ion equilibrium constants are usually fitted to describe potentiometric titrations and macroscopic adsorption data, respectively.

A number of fitting algorithms are used to determine model parameters, including FITEQL (Oregon State University. and Westall, 1982), GEOSURF (Sahai and Sverjensky, 1998), ECOSAT-FIT (Keizer and an Riemsdijk, 1999; Kinniburgh, 1993), PEST (Doherty, 1994), and most recently MINFIT (Xie et al., 2016). Some of these programs operate as extensions of geochemical modeling software, e.g., MINEQL and ORCHESTRA, which amplifies their utility. However, that dependence often constraints them to certain types of SCMs and/or a limited choice of optimizable parameters.

Several studies have demonstrated the dependence of equilibrium constants and capacitance on site density (Christl and Kretzschmar, 1999; Goldberg, 1991; Hayes et al., 1991; Hwang and Lenhart, 2008; Katz and Hayes, 1995), capacitance on specific surface area (Hwang and Lenhart, 2008) and equilibrium constants on capacitance (Katz and Hayes, 1995). Hayes et al. (1991) showed a decreasing trend of electrolyte equilibrium constants with increasing site densities in various types of SCMs (CCM, DLM, and TLM), and Hwang and Lenhart (2008) further illustrated a decreasing trend of capacitance with increasing SSA. Sverjensky (2005, 2003) proposed to determine equilibrium constants independent of the solid sorbent properties by normalizing the molar-based equilibrium constants for site density, surface area and solid concentration. However, this approach does not address other interdependencies, such as the correlation of equilibrium constants with capacitance values. Capacitance values are commonly treated as floating parameters and fitted arbitrarily, leading to non – unique fitting solutions (Hayes et al., 1991). It follows from this analysis that the simultaneous optimization of multiple parameters is necessary to enhance the robustness of SCMs.

The goodness of fit to experimental data is often judged subjectively, and not upon specific error criteria. There is little discussion in the literature about global vs local optimization, and non – uniqueness of solutions, with the exception of Jiménez and Mucci (2010) who employed an evolutionary genetic algorithm to detect global optima. The objective of this study is to address the issue of global optimization for multiple parameters, with a MUlti-start optimization algorithm for Surface complexation Equilibrium parameters (MUSE). The MUSE algorithm has been developed to optimize adsorption parameters, such as (but not limited to) equilibrium constants, capacitance values, and SSA. To add to the robustness of MUSE, spectroscopic input is also incorporated in terms of fitting equilibrium constants to multivariate curve resolution with alternating least squares profiles (MCR – ALS) derived from ATR – FTIR spectra.

Materials and Methods

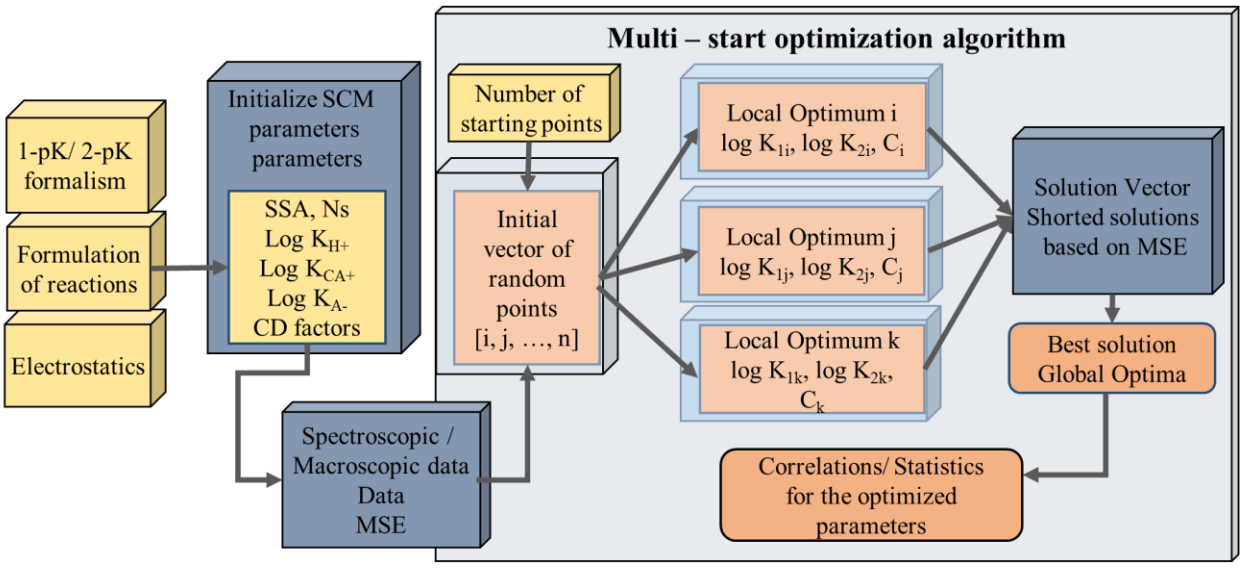

Figure 3-1. Flow chart of MUSE algorithm.

Experimental data

Two types of data were employed for purposes of model fitting: traditional batch adsorption data and concentration profiles for the monodentate and bidentate species of chromate on ferrihydrite

using infrared spectroscopy previously presented in Johnston and Chrysochoou (2016). Detailed experimental methods for both types of adsorption data are provided in Appendix. The utilization of the ATR spectra for modeling purposes required the conversion of the absorbance units to surface coverage units, i.e. mol of adsorbed Cr(VI) per g or m^2 of mineral surface. Other studies performed this conversion using Beer's law (Mitchell et al., 2011; Sabur et al., 2015), which requires an estimate for the molar extinction coefficient (scattering coefficient) of the sorbed species. In this study, we utilized MCR – ALS relative distributions of surface complexes based on direct experimental data obtained in the flow cell, as described in Kabengi et al. (2017). More details about the conversion of spectroscopic data to surface coverage are given in Appendix.

Model Description

The overall flowchart of the MUSE algorithm in shown in Figure 3-1. As with any other modeling approach, it is necessary to choose the formulation of surface reactions and the electrostatics, and for here a 1-pK CD-MUSIC model with a Basic Stern layer was adopted. This was preferred because the 1-pK formalism reduces the number of protonation log Ks needed and the Basic Stern layer requires only one capacitance value for fitting. We also incorporated the adjusted capacitance value for spherical particles as suggested by Hiemstra and Van Riemsdijk (2009). The algorithm can be modified to accommodate any surface reaction formulation and electrostatic model, with limitations imposed mainly by the number of fitting parameters.

The fitting problem treated in this study was to determine the log K values for a ligand with two surface species, i.e. chromate on iron oxides. Three parameters are fitted simultaneously, the two log Ks for the surface species and the capacitance. The algorithm allows for the optimization of more than three parameters at the expense of computing time; depending on the dataset, this could

also lead to overfitting and increase the possibility of non-unique solutions. Reducing the number of fitted parameters ultimately requires fixing others, i.e. the conundrum of optimization and transferability to other systems is not completely resolved. However, it is proposed that it can be mitigated and in this study, the choice of fixed versus fitted parameters was made with end users of SCMs in mind, i.e. users of geochemical software (MINTEQ, PHREEQC and others) that will adopt a model from the literature for a particular mineral and adjust the parameters to describe their data. Typically, adoption of existing SCMs relies on two steps:

- Choosing a database of reactions for a particular surface, which includes protonation, electrolyte and ligand reactions with the associated log Ks.
- Entering system-specific parameters, including the solid concentration, ionic strength and composition, specific surface area and capacitance. Depending on the software, it is possible to choose site densities as well, or these are automatically adopted based on the suggested models within the software.

Addressing the experimental error still remains a challenging issue since datasets with full error characterization are lacking. Although the uncertainty of experimental error is not directly addressed in this study, the uncertainty of the input parameters such as capacitance, is addressed indirectly by performing sensitivity analysis of the extracted parameters.

Choosing log K_{H+} values can be itself an optimization problem, if relying on fitting surface charge data. While calculated values based on theory have been proposed for iron oxides (Hiemstra, 2013; Venema et al., 1998), calculation requires the consideration of multiple types of surface oxygens, e.g., 11 different sites with log K_{H}^{+} ranging from 3 to 12.4 have been proposed for ferrihydrite (Hiemstra, 2013). It is generally impractical to use a large number of variable sites to describe surface charge; Hiemstra et al. (1996) showed that two sites were adequate to describe surface

charge of goethite, while Bompoti et al. (2017) used three sites to describe the surface charge of several FH datasets with variable points of zero net proton charge (PZNPCs). The model developed by Bompoti et al. (2017) for fresh FH with three surface sites is adopted in this study (Table 3-1), including the log Ks for electrolytes. The surface charge of ferrihydrite was simulated by a 3 – site model fully discussed in previous work (Bompoti et al., 2017). Briefly, the model consists of one singly coordinated (SC) hydroxyl group and one triply coordinated (TC) group located on the $(1\bar{1}0)$ and $(1\bar{1}1)$ planes, and one TC group on the (001) and $(00\bar{1})$ faces. The doubly–coordinated surface groups are not considered in the model since their pK is out of the normal environmental pH range and therefore are considered non-reactive (Hiemstra and Van Riemsdijk, 2009). The site densities are taken as the summation of site densities proposed by Hiemstra (2013) and protonation log Ks are taken to 8 for the $(1\bar{1}0)$ and $(1\bar{1}1)$ faces, and 9.5 for the (001) and $(00\bar{1})$ faces. The purpose of this approach was to capture differences, both in terms of charging values on a mass and surface area basis, as well as differences in the PZNPC, which range between 8.0 and 8.7. These variations appear to be driven by the size of FH crystals, which are related to the precipitation methods as well as aging during and after preparation (Villacís-García et al., 2015). The proposed surface model was able to capture the charging behavior of both fresh and aged FH by increasing the contribution of the basal planes. In this study, we used the site densities for the fresh FH model since the chromate pH edge experiments in this study were performed with fresh FH.

Table A3-3 shows the surface complexation reactions, CD factors and equilibrium constants. CD factors may also be treated as variable parameters and will impact the results for log K values (Figure A3-6). However, in this study they were based on the structure of the adsorbed ligand, as

in many other studies (Rietra et al., 1999), and were fixed at -0.5 and -1.0 for the monodentate and bidentate chromate surface species, respectively.

Table 3-1. FH surface structure based on surface three sites as proposed by Bompoti et al. (2017).

Site	Face	Face distribution (%)	Site density (sites/ nm^{-2})	Site density (sites/ nm^{-2}) accounting for face distribution	$LogK_{H+}$
FeOH	$1\bar{1}0$	37.5	17.40	6.53	8.00
Fe_3O	$1\bar{1}1$		15.90	5.96	8.00
Fe_3O	001 $00\bar{1}$	12.5	6.60	0.83	9.50

Optimization Algorithm

The model was built with custom-made Mathematica™ notebooks, versions of which have been previously used to simulate the rutile (Hawkins et al., 2017; Machesky et al., 2015, 1998; Ridley et al., 2005), magnetite (Wesolowski et al., 2000), ferrihydrite (Bompoti et al., 2017) and goethite (Machesky et al., 1991) interfaces. They have also been extended to fit adsorption data to 290° C (Machesky et al., 2001, 1998). The multi – start optimization routine was integrated in the original SCM model to optimize multiple parameters using as criteria the mean squared error (MSE) and Model Selection Criterion (MSC), with larger MSC values indicating a better fit (Machesky et al., 1998; Wesolowski et al., 2000). Both MSE and MSC depend on the experimental data, specifically the number and variability of available data, and number of fitting parameters for the latter; thus, they are used to compare different fits for a single data set. The MUSE algorithm also supports the calculation of statistics, such as standard deviation and correlations among the parameters.

A minimization function was applied, tied to a Nelder – Mead downhill simplex method for optimization. Compared to the other direct search methods available in Mathematica (differential evolution, simulated annealing and random search), Nelder – Mead was free of convergence

problems and required less computing time. Nelder – Mead is a nonlinear, derivative – free adaptive method applicable for non – linear problems and continuous variables (Nelder and Mead, 1965; Olsson and Nelson, 1975). For each iteration, a 3 - dimensional space is formed to minimize the objective function by performing tetrahedral reflections. However, similar to other minimization techniques, Nelder - Mead is dependent on the choice of starting points and boundary conditions, and is often trapped to a local minimum around the initial guesses. To address this problem, the Nelder – Mead method was hybridized with a multi – start algorithm, an approach that has shown promise in other fields for global optimization problems (Huang et al., 1998; Kocsis and György, 2009; Martí et al., 2013).

Briefly, a random number generator was implemented to produce a 3 – dimensional matrix of starting points for the local optimization function. The dimensions of the matrix depend on the number of fitted parameters and their constraints, which was three or four in this case. For each initial point, Nelder – Mead provided an optimal solution; comparison of the solutions using the MSE as selection criterion was done in order to identify the "best local minimum", which is assumed to correspond to the global minimum. From this definition, it follows that finding the true global minimum depends on the number of initial points and parameter boundaries, as defined by the user.

Figure 3-2a illustrates this issue for the spectroscopy dataset, using two different SSA values as constants within the algorithm. The MSE decreases with an increasing number of starting points and plateaus at a minimum value, indicating that the MUSE algorithm successfully detected the global optimum within the selected boundaries for the three parameters. Compared to local optimizers that start with one initial point, the multi – start algorithm provided a solution with an order of magnitude lower MSE (for SSA 600 m^2/g, MSE: $2.36*10^{-13}$ for one starting point,

compared to $2.51*10^{-14}$ for starting points > 200, as shown in Figure 3-2a). Figure 3-2b plots the evolution in the optimized parameters, showing that the identified global minimum had a much lower capacitance and higher log K values compared to the initial solution with one starting point. The number of points for which the algorithm identified a better minimum varied for different datasets and was even different for the same dataset with different SSA values (Figure 3-2a). Generally, however, it was observed that starting with more than 200 points was usually sufficient for all datasets when three parameters were fitted simultaneously. The results presented henceforth were all obtained using 500 initial points.

Figure A3-7 and A3-8 show the distribution of the 500 points used by the algorithm and the local optimization process for three iterations for the spectroscopy dataset, for which the parameter boundaries were chosen to be relatively narrow (5-15 for log K monodentate, 14-23 for log K bidentate and 0.3-3 for the capacitance). In this case, the availability of the spectroscopy profiles enabled narrowing of the boundaries for the two log K values, as these were constrained by the respective species distribution. For the batch tests, the boundaries had to be expanded, given that there was no physical constraint for the two log K values, and were 0 to 22 for monodentate and 10 to 30 for bidentate. The boundaries for the capacitance were maintained at 0.3 to 3, given that values outside this range are physically unrealistic. The expansion of the boundaries of the log K values has two implications: a) the 500 points cover a wider domain and are thus less likely to identify the global minimum; and, b) more equivalent solutions emerge. These issues will be further illustrated in the discussion of the model results for the spectroscopy and batch datasets. The full SCM including the MUSE algorithm is given in the Appendix.

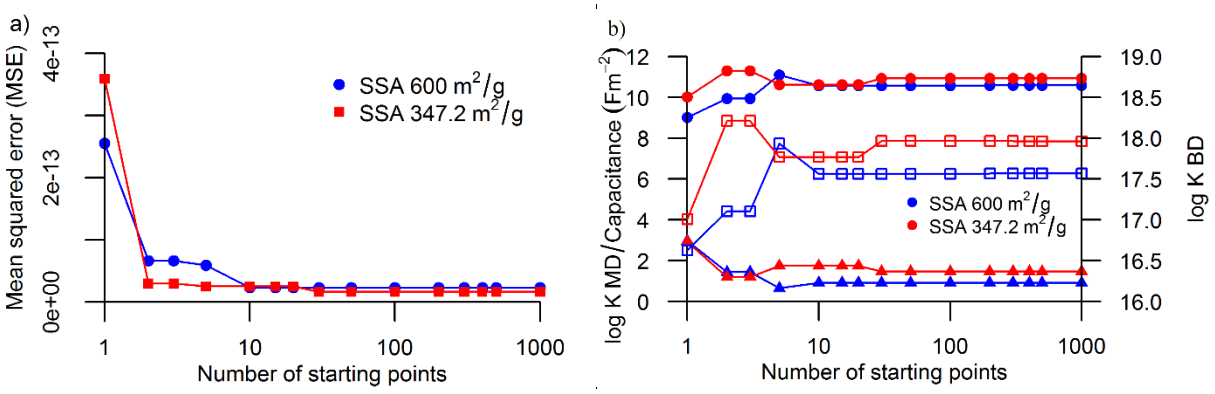

Figure 3-2. MUSE results for the FH spectroscopy dataset using two different SSAs: a) MSE as a function of the number of starting points in the multi – start optimization algorithm, and b) extracted parameters (Capacitance (triangles), monodentate (circles) and bidentate (squares) log K values as a function of the number of starting points.

Results and Discussion

Spectroscopy profiles

Figure 3-3a shows the model fits for the concentration profiles obtained by MCR ALS for two SSA values. Along with Table A3-4, Figure 3-3 also includes the results of a sensitivity analysis performed for the three fitted parameters as a function of SSA. The extraction of these relationships between the four parameters was enabled by the MUSE algorithm. Other algorithms are often trapped in local minima, away from the optimum solution, providing non-unique thermodynamic parameters. For instance, if the capacitance value is not minimized simultaneously with the equilibrium constants, the dependence of those parameters on SSA is not easily observed.

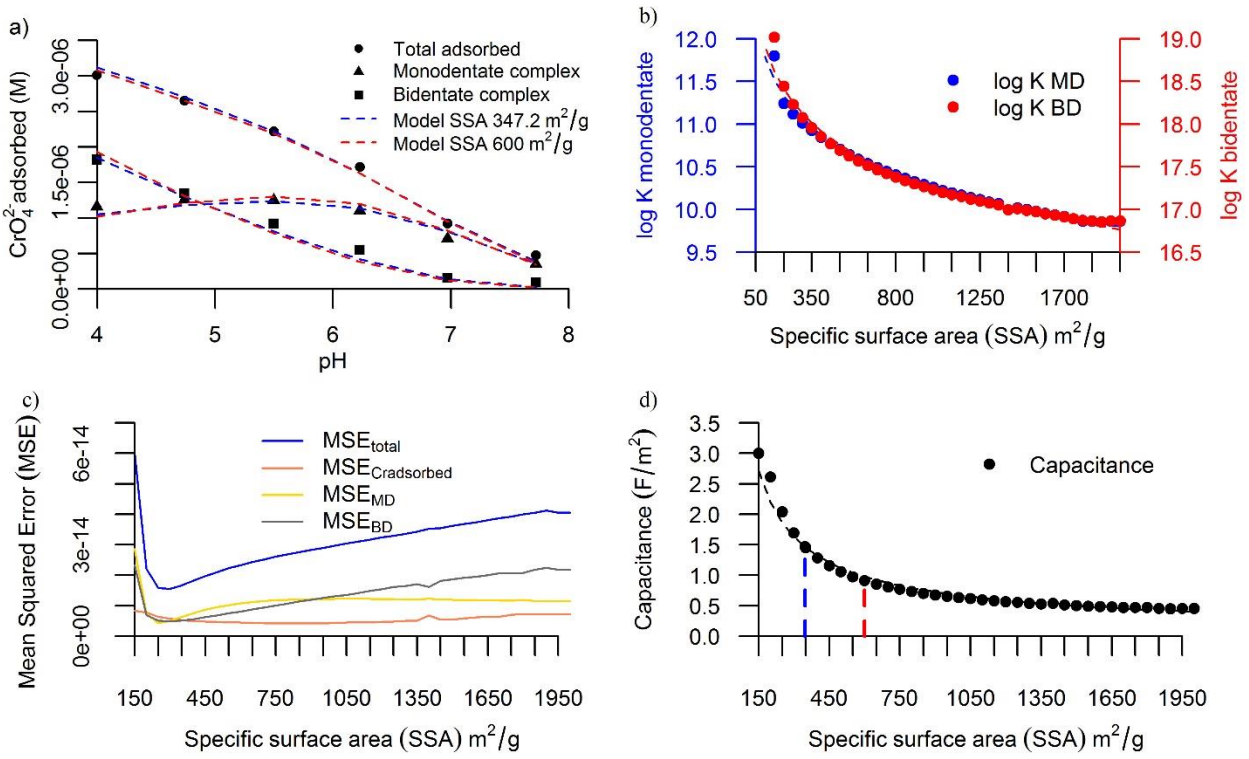

Figure 3-3. Adsorption profiles produced from ATR spectroscopy and MCR ALS (a). Adsorption data (points) and model fits for two SSA values (dashed lines) are shown for total chromate adsorbed and individual surface complexes; corresponding fitted log Ks (b), MSE (c), and capacitance values (d) as a function of SSA. Trend lines represent the relationships for log Ks (c) and Capacitance (d) with SSA: log K MD: -0.664 ln (SSA) + 14.85, log K MD: -0.717 ln (SSA) + 22.215, Capacitance: 108.54 $(SSA)^{-0.736}$.

The results of the sensitivity analysis clearly demonstrate a dependence of all three fitted parameters on SSA, and specifically a decrease with increasing SSA. The SSA range investigated was between 150-2000 m^2/g, which extends beyond the upper and lower limits of plausible SSAs for fresh FH. Assuming individual spherical particles, the theoretical SSA of a 1 nm particle would be 1,680 m^2/g (Villalobos and Antelo, 2012). The TEM analysis of the FH used in this study showed particles of 3.4 nm median diameter, which corresponds to a theoretical SSA of 480 m^2/g.

Both log Ks varied in a consistent manner with SSA, i.e. the difference between the bidentate and monodentate log K was approximately constant (Δlog Ks: 6.97 - 7.22), which is necessary in order for the distribution of the two complexes to remain the same. Both equilibrium constants exhibited a range of approximately two log units across the adopted SSA range, decreasing proportionally to the logarithm of SSA (Figure 3-3b). The bidentate complex exhibits a slight higher range (2.15 versus 1.94) in order to account for the double site occupancy. The dependency of log Ks on SSA has implications on the amount of sites that are occupied by chromate. By increasing the available SSA, the total site concentration is also increasing, meaning that the ratio of Cr – binding sites to singly coordinated sites decreases. For this spectroscopic dataset, the Cr – binding sites account for 31.24 % of the total sites when SSA is 350 m^2/g, while the ratio decreases to 17.31 % for SSA 650 m^2/g. A surface area of 69.4 m^2/g is the theoretical limiting SSA for the spectroscopic dataset that is where all the available sites would be occupied by chromate. The inversely proportional change of the capacitance with SSA (Figure 3-3d) indicates that, mathematically, the capacitance value can account for the majority of the SSA uncertainty when treated as floating parameter. Modeling studies of hematite (Hwang and Lenhart, 2008) and goethite (Boily et al., 2001) surface charge have shown strong correlations between SSA and capacitance, suggesting higher proton capacity of the lower SSA minerals due presumably to their greater surface roughness (Boily et al., 2001).

The sorbent dependency of molar-based equilibrium constants has been previously discussed in a thermodynamic framework by Kulik (2002), as well as the implications of the molar-based mass action expressions regarding the surface properties (Wang and Giammar, 2013). The MUSE algorithm accounts for surface activity by incorporating a surface mole fraction scale for surface species, while, in a similar approach, Sverjensky (2003) proposed the “site occupancy” standard

state to account for different sorbent properties. In this model, the equilibrium constants are expressed as a surface mole fraction, in terms of moles/ m^2. However, we observe that there is still some dependency on the surface area, although the range of the obtained log Ks is relatively narrow for common SSAs. Wang and Giammar (2013) have also mentioned findings similar to Kulik, suggesting that even when accounting for surface activities, "denticity" effects on the thermodynamic constants are not consistently addressed. While the discussion of sorbent dependency on intrinsic equilibrium constants has focused on multidentate species (Benjamin, 2002; Lützenkirchen et al., 2015; Wang and Giammar, 2013), we show that the monodentate thermodynamic constant is also affected by differences in SSA.

A benefit of utilizing the spectroscopy profiles is that additional MSEs can be calculated and used as constraints, i.e. the MSEs for the total adsorption envelope and for the individual profiles of the monodentate and bidentate species, which are also shown in Figure 3-3c. The MSE of the adsorption envelope alone decreased asymptotically with increasing SSA and no true minimum was identified over the range of SSAs tested. Conversely, the individual species profiles both exhibited a clear minimum around 250-350 m^2/g and adding all three MSEs the optimum solution emerged at SSA 300 m^2/g, with a capacitance of 1.69 F/m^2, log K_{MD} 11.01 and log K_{BD} 18.08 (Table A3-4).

The MUSE algorithm was tested for optimization of all four parameters, including SSA, simultaneously. The optimal solution coincided with the results of the sensitivity analysis when running 4,000 starting points (SSA 290 m^2/g, capacitance of 1.74 F/m^2, log K_{MD} 11.03 and log K_{BD} 18.10); having 1,000 initial points yielded an optimal solution at (SSA 327 m^2/g, capacitance of 1.55 F/m^2, log K_{MD} 10.95 and log K_{BD} 18), i.e. 1000 starting points were not sufficient to find the true minimum. Thus, optimizing more parameters requires a greater number of starting points.

The optimum point in terms of the total MSE clearly does not correspond to either the BET measured surface area of 347 m^2/g, or the theoretical surface area of 600 m^2/g that is often used in FH modeling studies. While 290 m^2/g is within the range of SSA previously reported in the literature (Bompoti et al., 2017), it is at the low end, while the optimal capacitance is higher compared to most values used in the literature. In other words, the optimum fit in terms of MSE does not yield a solution that lies within expected values for SSA and capacitance. The two plausible starting points for SSA (BET and theoretical) also yield solutions with very good fits; in fact, every solution within a typical SSA range for FH (300-650 m^2/g) yields a satisfactory fit for both the spectroscopic and the overall adsorption profiles. This begs the question, which log Ks can be considered as the "true" log Ks to be adopted by future modelers of chromate on FH?

Clearly, the strict answer is that there are no "true" log Ks. All log K values are a function of the SSA and capacitance values adopted, as well of other parameters that were treated as constants here (e.g., see Figure A3-6 for effect of CD values). An approach that would best address this issue is to implement functions within geochemical models that will correct log K values for differences in SSA, e.g. in this case the logarithmic functions fitted in Figure 3-3, as well as calculate optimal capacitances, which will relieve the end user of the necessity to pick an arbitrary value for capacitance. When surface charge data are available, the capacitance values can be estimated by fitting those data first. However, charging curve data do not always accompany adsorption data. Moreover, the functional relationships have to be determined for each ligand and surface, which also implies that the functions determined using one specific dataset (the spectroscopic profiles in this study) are transferrable to any other dataset, which is questionable.

Another possibility to deal with this uncertainty for modeling studies is to modify the way that models are fitted, reported and transferred into modeling codes. Instead of reporting ligand log Ks

as constants, we propose to report average log Ks for a range of SSAs, along with the uncertainty for that range. For FH, SSA typically ranges between 300 and 650 m^2/g, considering both BET measurements and theoretical values. The calculated average log Ks for this range are 10.8 ± 0.5 and 17.8 ± 0.5 for monodentate and bidentate chromate surface complexes, respectively. The fluctuations in the log K values are small, and it is plausible that other uncertainties are larger. An end user may then describe their own dataset using the average log Ks (or choose to modify them within the given range if needed), using a BET-based SSA and treating capacitance as a floating parameter to absorb other parameter uncertainties. In this scenario, the end user has to adjust capacitance and evaluate the model fit either visually or by evaluating the MSE, or an alternative goodness of fit criterion.

Application to Macroscopic data

A conventional batch pH-envelope for FH was also fitted using the MUSE algorithm. The SSA was kept constant in this case, at the measured BET value of 347.2 m^2/g. The number and type of surface complexes were varied in order to evaluate the variability of extracted parameters and the model fitting capability with and without the spectroscopic insights. Since quantifiable spectroscopy data are not available for many ligands, it useful to evaluate the performance of the MUSE algorithm under less constrained conditions. The following four optimizations were performed:

Model optimized both MD and BD: Employment of monodentate and bidentate surface complexes with optimization of both log Ks and capacitance. This scenario was evaluated with and without the consideration of competitive CO_2 adsorption, with the CO_2 model and results described in Appendix.

Model only MD: Adoption of only monodentate surface complexes and optimization of the respective log K and capacitance.

Model only BD: Adoption of only bidentate surface complexes and optimization of the respective log K and capacitance.

Model Spectroscopy: Adoption of both surface complexes and log Ks as extracted from spectroscopic profiles, optimizing only capacitance. Specifically, the average calculated log Ks were employed as described previously (10.78 and 17.78 for monodentate and bidentate, respectively).

The simulated adsorption data and extracted parameters for the above scenarios are given in Figure 3-4 and Table 3-2, respectively. Utilizing only a visual assessment of the model fits, all four scenarios provide acceptable fits to the experimental data, except in the pH region 7.0-8.0, in which they fail to predict the sharp decrease in adsorption observed in the data.

For the model with both species' equilibrium constants being optimized, the algorithm clearly suppressed the monodentate species in favor of the bidentate. Several equivalent solutions emerged in this case, in terms of both the MSE and the MSC. All three solutions in this case yield a very low log K_{MD} value because the monodentate species exhibits a flatter slope above pH 7 and worsens the fit in this pH region. In this particular case, there is no added value of choosing one of the equivalent solutions, since in all cases the monodentate complexes are out competed by bidentate complexes. Eliminating the monodentate species completely slightly improves the fit while keeping all values approximately constant, for the same reason.

However, the distribution of species is not similar to those which are constrained by spectroscopic data (Figure A3-10). As such, the alternate approach of using the average log K values to fit the

dataset provides an equally successful fit to the data, since the spectroscopy data is also matched satisfactorily (Figure A3-10c and A3-10d).

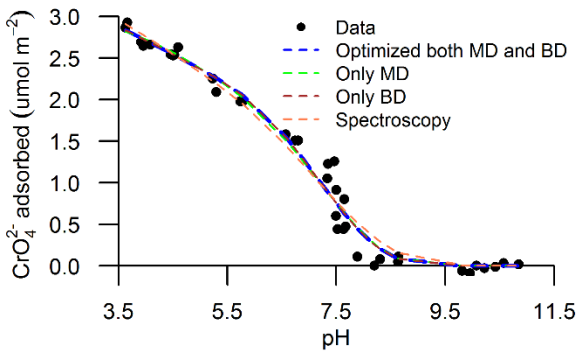

Figure 3-4. Simulated macroscopic adsorption data for FH at ionic strength 0.01 M and SSA 347.2 m^2/g. Data (points) and model simulation (dashed lines) are shown for adsorbed chromate.

Suppression of monodentate species and the variability exhibited by its equilibrium constant puts into question the actual presence of monodentate species or perhaps points to the existence of an outer – sphere complex. DFT calculations on FH have shown more energetically favored outer-sphere complexes compared to monodentate complexes, while inner-sphere bidentate complexes are predicted to be the most energetically favored (Kabengi et al., 2017). For that reason, a model scenario including an outer – sphere complex instead of a monodentate was examined, yielding an equivalent fit to the model with optimized both monodentate and bidentate log Ks (MSC 3.73). The optimized equilibrium constant for the outer – sphere complex was log $K_{outer\text{ - }sphere}$ -3.77, while the bidentate equilibrium constant remained unchanged at log K_{BD} 18.76. Model simulation for the outer sphere case is shown in Figure A3-9. Clearly, the monodentate inner-sphere and the outer-sphere complexes are equivalent from a pure modeling perspective. However, our spectroscopic results suggest that the monodentate complex is inner-sphere for our experimental conditions.

Table 3-2. Optimized parameters and their standard deviation for batch chromate pH – envelope dataset under different modeling scenarios described in text.

Model	log $K_{monodentate}$	log $K_{bidentate}$	Capacitance	MSC	MSE
		FH			
Model_optimized both MD and BD	1.918	18.759	1.010	3.732	7.181E-10
	3.149	18.760	1.010	3.732	7.181E-10
	1.173	18.759	1.011	3.732	7.181E-10
	2.294	18.759	1.011	3.732	7.181E-10
	3.665	18.760	1.010	3.732	7.181E-10
Model_only MD	10.577	-	2.524	3.738	7.507E-10
Model_only BD	-	18.759	1.011	3.784	7.181E-10
Model_Spectroscopy	10.780	17.780	1.709	3.500	9.056E-10

Inclusion of CO_2 in the model. The presence of carbonate species in the experimental data was evaluated. Mineral synthesis and batch experiments were all performed inside a globe bag under N_2 atmosphere, but it is possible that CO_2 was not completely eliminated. Specifically, the remaining CO_2, as measured by an infrared detector, was approximately 20 ppm. Villalobos and Antelo (2012) have previously discussed the potential influence that disregarding CO_2 has on SCM parametrization, pointing out that experimental studies typically underestimate the effort associated with eliminating CO_2 from mineral surfaces and suspensions. Therefore, two model scenarios were performed, one representing the experimental conditions (20 ppm CO_2), and another one at atmospheric conditions (400 ppm). The fits for both scenarios are shown in Figure 3-6.

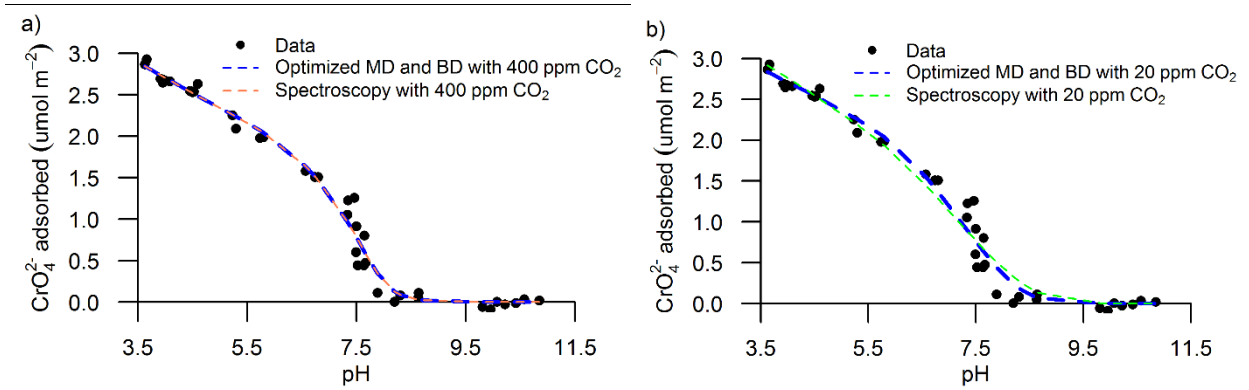

Figure 3-5. Simulated batch chromate data considering CO_2 presence. Data (points) and model simulation (dashed lines) are shown for adsorbed chromate. a) at 400 ppm CO_2 and b) at 20 ppm CO_2.

Addition of 20 ppm CO_2 in the model improved the fit of chromate adsorption slightly, while the fit parameters did not show any substantial differences. On the other hand, incorporation of 400 ppm CO_2 in the model improves the fitting of chromate adsorption data since carbonate competes with chromate adsorption above 6.5 (Figure 3-6). In this case, the optimal fit actually yields values for the two species that are reasonably close to the average log K values obtained from spectroscopy (11.61 compared to 10.78 for log K_{MD} and 17.88 compared to 17.78 for log K_{BD}) (Table 3-3). Adding CO_2 into the model with the spectroscopic log Ks was able to capture the adsorption at higher pH, capturing the steeper slope of the pH envelope between about pH 7.5 and 8. The inclusion of CO_2 in the model gives acceptable results for both optimized and spectroscopic log Ks.

Table 3-3. Optimized parameters for batch chromate pH – envelope dataset with presence of CO_2.

Model	log $K_{monodentate}$	log $K_{bidentate}$	Capacitance	MSC	MSE
Model_optimized both MD and BD with 400 ppm CO_2	11.612	17.883	1.511	4.029	5.333E-10
Model_Spectroscopy with 400 ppm CO_2	10.780	17.780	1.722	3.630	7.949E-10
Model_optimized both MD and BD with 20 ppm CO_2	2.61	18.77	1.008	3.76	6.99E-10
Model_Spectroscopy with 20 ppm CO_2	10.780	17.780	1.7	3.52	8.83E-10

Carbonate species act as competitor reducing the available SSA for chromate to bind to some extent. Thus, we would observe both chromate log Ks to increase in order to account for less adsorption sites. However, adsorption of CO_2 at pH lower than 5.5 is negligible compared to the adsorbing chromate. We observe that when CO_2 is included in the model, the bidentate complexes are decreased (decreased log K) due to CO_2 competition at higher pH, while more monodentate complexes are "forced" to form (increased log K). Overall, the phenomenon of the CO_2 competition is more complex than just decreasing available adsorption sites.

Environmental Significance. The transferability of mineral-specific SCMs to reactive transport modeling is constrained by several lingering problems, including the fact that SCMs have a large number of interdependent parameters. While increased parametrization enhances SCM flexibility, it also increases the uncertainty in thermodynamic constants and end users of geochemical models lack the tools to choose and implement a self-consistent model. Parameters such as those related

to electrostatics are not easily constrained, while others (site densities and specific surface area) can be constrained by physical models or measurements. Ultimately, thermodynamic constants are dependent on all these values, a fact that end users of geochemical modeling software cannot easily account for. The MUSE algorithm addresses this problem by allowing the simultaneous optimization of several parameters and enabling the determination of a global minimum that is not constrained by the initial guesses for the parameter values. Accommodating any type of SCM and choice of parameters, including equilibrium constants, capacitance values and sorbent properties, the MUSE algorithm can be used for optimizing parameters necessary for reactive transport modeling. The incorporated spectroscopy offers insights on surface speciation from the molecular perspective, and expansion of the proposed approach for other ligands could lead towards a consistent database for equilibrium constants that is also constrained by spectroscopic and/or molecular modeling information.

The current approach is built on the premise that the end user will adopt a set of model parameters that were employed to conduct the original fits, specifically the surface structure model (types and concentrations of surface sites), protonation, electrolyte and ligand log Ks, use their own experimental parameters including ionic strength and composition, ligand and solid concentration and SSA, and fit or manually adjust the capacitance. We postulate that when MUSE is implemented to determine ligand log Ks, their dependence on other adjustable parameters such as SSA and capacitance will be relatively small, and certainly smaller compared to traditional single-point optimization (e.g., one unit change for chromate log Ks on ferrihydrite). Ongoing work is geared towards demonstrating the applicability of the MUSE algorithm to a large, diverse dataset of chromate adsorption on multiple iron oxides.

References

Benjamin, M.M., 2002. Modeling the Mass-Action Expression for Bidentate Adsorption. Environ. Sci. Technol. 36, 307–313. https://doi.org/10.1021/es010936n

Boily, J.-F., 2014. The Variable Capacitance Model: A Strategy for Treating Contrasting Charge-Neutralizing Capabilities of Counterions at the Mineral/Water Interface. Langmuir 30, 2009–2018. https://doi.org/10.1021/la403938w

Boily, J.-F., Lützenkirchen, J., Balmès, O., Beattie, J., Sjöberg, S., 2001. Modeling proton binding at the goethite (α-FeOOH)–water interface. Colloids Surf. Physicochem. Eng. Asp. 179, 11–27. https://doi.org/10.1016/S0927-7757(00)00712-3

Bompoti, N., Chrysochoou, M., Machesky, M., 2017. Surface structure of ferrihydrite: Insights from modeling surface charge. Chem. Geol., Adsorption of metals by geomedia III: Fundamentals and implications of metal adsorption 464, 34–45. https://doi.org/10.1016/j.chemgeo.2016.12.018

Bompoti, N., Chrysochoou, M., Machesky, M., 2016. Surface structure of ferrihydrite: Insights from modeling surface charge. Chem. Geol. https://doi.org/10.1016/j.chemgeo.2016.12.018

Brunauer, S., Emmett, P.H., Teller, E., 1938. Adsorption of Gases in Multimolecular Layers. J. Am. Chem. Soc. 60, 309–319. https://doi.org/10.1021/ja01269a023

Christl, I., Kretzschmar, R., 1999. Competitive sorption of copper and lead at the oxide-water interface: Implications for surface site density. Geochim. Cosmochim. Acta 63, 2929–2938. https://doi.org/10.1016/S0016-7037(99)00266-5

Davis, J.A., James, R.O., Leckie, J.O., 1978. Surface ionization and complexation at the oxide/water interface. J. Colloid Interface Sci. 63, 480–499. https://doi.org/10.1016/S0021-9797(78)80009-5

Davis, J.A., Kent, D.B., 1990. Surface complexation modeling in aqueous geochemistry. Rev. Mineral. Geochem. 23, 177–260.

Doherty, J., 1994. PEST: A Unique Computer Program for Model-independent Parameter Optimisation. Water 94 GroundwaterSurface Hydrol. Common Interest Pap. Prepr. Pap. 551.

Dzombak, D.A., Morel, F.M.M., 1990. Surface Complexation Modeling: Hydrous Ferric Oxide. John Wiley & Sons.

Everett, D.H., Parfitt, G.D., Sing, K.S.W., Wilson, R., 1974. The SCI/IUPAC/NPL project on surface area standards. J. Appl. Chem. Biotechnol. 24, 199–219. https://doi.org/10.1002/jctb.2720240404

Fukushi, K., Aoyama, K., Yang, C., Kitadai, N., Nakashima, S., 2013. Surface complexation modeling for sulfate adsorption on ferrihydrite consistent with in situ infrared spectroscopic observations. Appl. Geochem. 36, 92–103. https://doi.org/10.1016/j.apgeochem.2013.06.013

Gaboriaud, F., Ehrhardt, J.-J., 2003. Effects of different crystal faces on the surface charge of colloidal goethite (α-FeOOH) particles: an experimental and modeling study. Geochim. Cosmochim. Acta, Advances in Oxide and Sulfide Mineral Surface Chemistry 67, 967–983. https://doi.org/10.1016/S0016-7037(02)00988-2

Goldberg, S., 1991. Sensitivity of surface complexation modeling to the surface site density parameter. J. Colloid Interface Sci. 145, 1–9. https://doi.org/10.1016/0021-9797(91)90095-P

Goldberg, S., Criscenti, L.J., Turner, D.R., Davis, J.A., Cantrell, K.J., 2007. Adsorption–Desorption Processes in Subsurface Reactive Transport Modeling. Vadose Zone J. 6, 407. https://doi.org/10.2136/vzj2006.0085

Gregg, S.J., Sing, K.S.W., Salzberg, H.W., 1967. Adsorption Surface Area and Porosity. J. Electrochem. Soc. 114, 279C–279C. https://doi.org/10.1149/1.2426447

Gu, C., Wang, Z., Kubicki, J.D., Wang, X., Zhu, M., 2016. X-ray Absorption Spectroscopic Quantification and Speciation Modeling of Sulfate Adsorption on Ferrihydrite Surfaces. Environ. Sci. Technol. 50, 8067–8076. https://doi.org/10.1021/acs.est.6b00753

Hawkins, T., Allen, N., Machesky, M.L., Wesolowski, D.J., Kabengi, N., 2017. Ion Exchange Thermodynamics at the Rutile–Water Interface: Flow Microcalorimetric Measurements and Surface Complexation Modeling of Na–K–Rb–Cl–NO3 Adsorption. Langmuir 33, 4934–4941. https://doi.org/10.1021/acs.langmuir.7b00867

Hayes, K.F., Redden, G., Ela, W., Leckie, J.O., 1991. Surface complexation models: An evaluation of model parameter estimation using FITEQL and oxide mineral titration data. J. Colloid Interface Sci. 142, 448–469. https://doi.org/10.1016/0021-9797(91)90075-J

Hiemstra, T., 2013. Surface and mineral structure of ferrihydrite. Geochim. Cosmochim. Acta 105, 316–325. https://doi.org/10.1016/j.gca.2012.12.002

Hiemstra, T., Van Riemsdijk, W.H., 2009. A surface structural model for ferrihydrite I: Sites related to primary charge, molar mass, and mass density. Geochim. Cosmochim. Acta 73, 4423–4436. https://doi.org/10.1016/j.gca.2009.04.032

Hiemstra, T., Van Riemsdijk, W.H., 1996. A Surface Structural Approach to Ion Adsorption: The Charge Distribution (CD) Model. J. Colloid Interface Sci. 179, 488–508. https://doi.org/10.1006/jcis.1996.0242

Hiemstra, T., Venema, P., Riemsdijk, W.H.V., 1996. Intrinsic Proton Affinity of Reactive Surface Groups of Metal (Hydr)oxides: The Bond Valence Principle. J. Colloid Interface Sci. 184, 680–692. https://doi.org/10.1006/jcis.1996.0666

Huang, C.-P., Stumm, W., 1973. Specific adsorption of cations on hydrous γ-Al2O3. J. Colloid Interface Sci., Kendall Award Symposium 163rd American Chemical Society Meeting 43, 409–420. https://doi.org/10.1016/0021-9797(73)90387-1

Huang, M., Aine, C.J., Supek, S., Best, E., Ranken, D., Flynn, E.R., 1998. Multi-start downhill simplex method for spatio-temporal source localization in magnetoencephalography. Electroencephalogr. Clin. Neurophysiol. Potentials Sect. 108, 32–44. https://doi.org/10.1016/S0168-5597(97)00091-9

Hwang, Y.S., Lenhart, J.J., 2008. The dependence of hematite site-occupancy standard state triple-layer model parameters on inner-layer capacitance. J. Colloid Interface Sci. 319, 206–213. https://doi.org/10.1016/j.jcis.2007.11.032

Ingri, N., Andersson, I., Pettersson, L., Yagasaki, A., Andersson, L., Holmström, K., Undheim, K., Rosendahl, C.N., Haugg, M., Trabesinger-Rüf, N., Weinhold, E.G., 1996. LAKE -- A Program System for Equilibrium Analytical Treatment of Multimethod Data, Especially Combined Potentiometric and Nuclear Magnetic Resonance Data. Acta Chem. Scand. 50, 717–734. https://doi.org/10.3891/acta.chem.scand.50-0717

Johnston, C.P., Chrysochoou, M., 2016. Mechanisms of Chromate, Selenate, and Sulfate Adsorption on Al-Substituted Ferrihydrite: Implications for Ferrihydrite Surface Structure

and Reactivity. Environ. Sci. Technol. 50, 3589–3596. https://doi.org/10.1021/acs.est.5b05529

Kabengi, N.J., Chrysochoou, M., Bompoti, N., Kubicki, J.D., 2017. An integrated flow microcalorimetry, infrared spectroscopy and density functional theory approach to the study of chromate complexation on hematite and ferrihdyrite. Chem. Geol., Adsorption of metals by geomedia III: Fundamentals and implications of metal adsorption 464, 23–33. https://doi.org/10.1016/j.chemgeo.2017.01.017

Katz, L.E., Hayes, K.F., 1995. Surface Complexation Modeling. J. Colloid Interface Sci. 170, 477–490. https://doi.org/10.1006/jcis.1995.1127

Keizer, M., an Riemsdijk, W.H., 1999. ECOSAT (ver. 4.7) Equilibrium Calculation of Speciation and Transport. Wagening. Agric. Univ. Wagening.

Kinniburgh, D.G., 1993. FIT Non-linear Optimization Algorithm and User Manual. Br. Geol. Surv. Nottm. UK.

Kocsis, L., György, A., 2009. Efficient Multi-start Strategies for Local Search Algorithms, in: Machine Learning and Knowledge Discovery in Databases. Presented at the Joint European Conference on Machine Learning and Knowledge Discovery in Databases, Springer, Berlin, Heidelberg, pp. 705–720. https://doi.org/10.1007/978-3-642-04180-8_63

Kulik, D.A., 2002. Gibbs energy minimization approach to modeling sorption equilibria at the mineral-water interface: Thermodynamic relations for multi-site-surface complexation. Am. J. Sci. 302, 227–279. https://doi.org/10.2475/ajs.302.3.227

Livi, K.J.T., Villalobos, M., Leary, R., Varela, M., Barnard, J., Villacís-García, M., Zanella, R., Goodridge, A., Midgley, P., 2017. Crystal Face Distributions and Surface Site Densities of

Two Synthetic Goethites: Implications for Adsorption Capacities as a Function of Particle Size. Langmuir. https://doi.org/10.1021/acs.langmuir.7b01814

Lützenkirchen, J., Marsac, R., Kulik, D.A., Payne, T.E., Xue, Z., Orsetti, S., Haderlein, S.B., 2015. Treatment of multi-dentate surface complexes and diffuse layer implementation in various speciation codes. Appl. Geochem., Geochemical Speciation Codes and Databases 55, 128–137. https://doi.org/10.1016/j.apgeochem.2014.07.006

Machesky, M.L., Andrade, W.O., Rose, A.W., 1991. Adsorption of gold(III)-chloride and gold(I)-thiosulfate anions by goethite. Geochim. Cosmochim. Acta 55, 769–776. https://doi.org/10.1016/0016-7037(91)90340-B

Machesky, M.L., Předota, M., Ridley, M.K., Wesolowski, D.J., 2015. Constrained Surface Complexation Modeling: Rutile in RbCl, NaCl, and NaCF3SO3 Media to 250 °C. J. Phys. Chem. C 119, 15204–15215. https://doi.org/10.1021/acs.jpcc.5b02841

Machesky, M.L., Wesolowski, D.J., Palmer, D.A., Ichiro-Hayashi, K., 1998. Potentiometric Titrations of Rutile Suspensions to 250°C. J. Colloid Interface Sci. 200, 298–309. https://doi.org/10.1006/jcis.1997.5401

Machesky, M.L., Wesolowski, D.J., Palmer, D.A., Ridley, M.K., 2001. On the Temperature Dependence of Intrinsic Surface Protonation Equilibrium Constants: An Extension of the Revised MUSIC Model. J. Colloid Interface Sci. 239, 314–327. https://doi.org/10.1006/jcis.2001.7584

Martí, R., Resende, M.G.C., Ribeiro, C.C., 2013. Multi-start methods for combinatorial optimization. Eur. J. Oper. Res. 226, 1–8. https://doi.org/10.1016/j.ejor.2012.10.012

Mitchell, W., Goldberg, S., Al-Abadleh, H.A., 2011. In situ ATR–FTIR and surface complexation modeling studies on the adsorption of dimethylarsinic acid and p-arsanilic acid on iron-

(oxyhydr)oxides. J. Colloid Interface Sci. 358, 534–540. https://doi.org/10.1016/j.jcis.2011.02.040

Nelder, J.A., Mead, R., 1965. A Simplex Method for Function Minimization. Comput. J. 7, 308–313. https://doi.org/10.1093/comjnl/7.4.308

Olsson, D.M., Nelson, L.S., 1975. The Nelder-Mead Simplex Procedure for Function Minimization. Technometrics 17, 45–51. https://doi.org/10.2307/1267998

Oregon State University., J.C., Westall, 1982. FITEQL : a computer program for determination of chemical equilibrium constants from experimental data. Dept. of Chemistry, Oregon State University, Corvallis, Or. :

Parez, S., Předota, M., Machesky, M., 2014. Dielectric Properties of Water at Rutile and Graphite Surfaces: Effect of Molecular Structure. J. Phys. Chem. C 118, 4818–4834. https://doi.org/10.1021/jp4128012

Ponthieu, M., Juillot, F., Hiemstra, T., van Riemsdijk, W.H., Benedetti, M.F., 2006. Metal ion binding to iron oxides. Geochim. Cosmochim. Acta 70, 2679–2698. https://doi.org/10.1016/j.gca.2006.02.021

Ridley, M.K., Machesky, M.L., Wesolowski, D.J., Palmer, D.A., 2005. Surface complexation of neodymium at the rutile-water interface: A potentiometric and modeling study in NaCl media to 250°C. Geochim. Cosmochim. Acta 69, 63–81. https://doi.org/10.1016/j.gca.2004.06.028

Rietra, R.P.J.J., Hiemstra, T., van Riemsdijk, W.H., 1999. The relationship between molecular structure and ion adsorption on variable charge minerals. Geochim. Cosmochim. Acta 63, 3009–3015. https://doi.org/10.1016/S0016-7037(99)00228-8

Rossberg, A., Ulrich, K.-U., Weiss, S., Tsushima, S., Hiemstra, T., Scheinost, A.C., 2009. Identification of Uranyl Surface Complexes on Ferrihydrite: Advanced EXAFS Data Analysis and CD-MUSIC Modeling. Environ. Sci. Technol. 43, 1400–1406. https://doi.org/10.1021/es801727w

Sabur, M.A., Goldberg, S., Gale, A., Kabengi, N., Al-Abadleh, H.A., 2015. Temperature-Dependent Infrared and Calorimetric Studies on Arsenicals Adsorption from Solution to Hematite Nanoparticles. Langmuir 31, 2749–2760. https://doi.org/10.1021/la504581p

Sahai, N., Sverjensky, D.A., 1998. GEOSURF: a computer program for modeling adsorption on mineral surfaces from aqueous solution. Comput. Geosci. 24, 853–873. https://doi.org/10.1016/S0098-3004(97)00142-8

Stoliker, D.L., Kent, D.B., Zachara, J.M., 2011. Quantifying Differences in the Impact of Variable Chemistry on Equilibrium Uranium(VI) Adsorption Properties of Aquifer Sediments. Environ. Sci. Technol. 45, 8733–8740. https://doi.org/10.1021/es202677v

Stumm, W., Huang, C.P., Jenkins, S.R., 1970. Specific chemical interaction affecting stability of dispersed systems. Croat. Chem. Acta 42, 223.

Stumm, W., Kummert, R., Sigg, L., 1980. A ligand-exchange model for the adsorption of inorganic and organic-ligands at hydrous oxide interfaces. Croat. Chem. Acta 53, 291–312.

Stumpf, S., Stumpf, T., Lützenkirchen, J., Walther, C., Fanghänel, T., 2008. Immobilization of trivalent actinides by sorption onto quartz and incorporation into siliceous bulk: Investigations by TRLFS. J. Colloid Interface Sci. 318, 5–14. https://doi.org/10.1016/j.jcis.2007.09.080

Sverjensky, D.A., 2005. Prediction of surface charge on oxides in salt solutions: Revisions for 1:1 (M+L−) electrolytes. Geochim. Cosmochim. Acta 69, 225–257. https://doi.org/10.1016/j.gca.2004.05.040

Sverjensky, D.A., 2003. Standard states for the activities of mineral surface sites and species. Geochim. Cosmochim. Acta 67, 17–28. https://doi.org/10.1016/S0016-7037(02)01074-8

Sverjensky, D.A., 2001. Interpretation and prediction of triple-layer model capacitances and the structure of the oxide-electrolyte-water interface. Geochim. Cosmochim. Acta 65, 3643–3655. https://doi.org/10.1016/S0016-7037(01)00709-8

Tiberg, C., Sjöstedt, C., Persson, I., Gustafsson, J.P., 2013. Phosphate effects on copper(II) and lead(II) sorption to ferrihydrite. Geochim. Cosmochim. Acta 120, 140–157. https://doi.org/10.1016/j.gca.2013.06.012

Venema, P., Hiemstra, T., Weidler, P.G., van Riemsdijk, W.H., 1998. Intrinsic Proton Affinity of Reactive Surface Groups of Metal (Hydr)oxides: Application to Iron (Hydr)oxides. J. Colloid Interface Sci. 198, 282–295. https://doi.org/10.1006/jcis.1997.5245

Villacís-García, M., Ugalde-Arzate, M., Vaca-Escobar, K., Villalobos, M., Zanella, R., Martínez-Villegas, N., 2015. Laboratory synthesis of goethite and ferrihydrite of controlled particle sizes. Bol. Soc. Geológica Mex. 67, 433.

Villalobos, M., Antelo, J., 2012. A unified surface stuctural model for ferrihydrite: proton charge, electrolyte binding, and arsenate adsorption.

Villalobos, M., Cheney, M.A., Alcaraz-Cienfuegos, J., 2009. Goethite surface reactivity: II. A microscopic site-density model that describes its surface area-normalized variability. J. Colloid Interface Sci. 336, 412–422. https://doi.org/10.1016/j.jcis.2009.04.052

Villalobos, M., Leckie, J.O., 2001. Surface Complexation Modeling and FTIR Study of Carbonate Adsorption to Goethite. J. Colloid Interface Sci. 235, 15–32. https://doi.org/10.1006/jcis.2000.7341

Villegas-Jiménez, A., Mucci, A., 2010. Estimating Intrinsic Formation Constants of Mineral Surface Species Using a Genetic Algorithm. Math. Geosci. 42, 101. https://doi.org/10.1007/s11004-009-9259-8

Wang, Z., Giammar, D.E., 2013. Mass Action Expressions for Bidentate Adsorption in Surface Complexation Modeling: Theory and Practice. Environ. Sci. Technol. 47, 3982–3996. https://doi.org/10.1021/es305180e

Wesolowski, D.J., Machesky, M.L., Palmer, D.A., Anovitz, L.M., 2000. Magnetite surface charge studies to 290°C from in situ pH titrations. Chem. Geol. 167, 193–229. https://doi.org/10.1016/S0009-2541(99)00209-0

Xie, X., Giammar, D.E., Wang, Z., 2016. MINFIT: A Spreadsheet-Based Tool for Parameter Estimation in an Equilibrium Speciation Software Program. Environ. Sci. Technol. 50, 11112–11120. https://doi.org/10.1021/acs.est.6b03399

Yates, D.E., Levine, S., Healy, T.W., 1974. Site-binding model of the electrical double layer at the oxide/water interface. J. Chem. Soc. Faraday Trans. 1 Phys. Chem. Condens. Phases 70, 1807. https://doi.org/10.1039/f19747001807

Appendix – Chapter 3

Experimental Methods

Mineral synthesis and characterization

2 - line FH was synthesized according to Schwertmann and Cornell (2008) inside a CO_2-free glove bag. Briefly, a 0.2 M $Fe(NO_3)_3 \cdot 9H_2O$ solution was titrated with 1 M carbonate – free KOH (Dilut – it) up to pH 7.5, under vigorous stirring in a Nalgene flask. At first, the base was added quickly (within 5 min), while dropwise addition followed (20 min). The freshly prepared suspension was immediately centrifuged and dialyzed to remove excess electrolytes until the conductivity was less than ~ 20 μS/cm. During the centrifuging and dialyzing the mineral came into contact with the atmosphere, and therefore some CO_2 might have contaminated the mineral suspension. The suspension was then titrated with 0.1 M HNO_3 down to pH 4.5, under continuous stirring, to remove excess CO_2 from the surface. The concentration of the suspension was estimated gravimetrically to 31.9 g/L. Specific Surface Area (SSA) was measured to be 347.2 m^2/g by N_2 adsorption isotherms using the BET method (Brunauer et al., 1938). The FH sample was air – dried, and ground and outgassed for 3 h at 150 °C. A Quantochrome NovaWin surface area analyzer with an 11 – point data calculation was used. Transmission electron microscopy (TEM) images (Figure A3-5) were obtained using a FEI TEM Talos F200X instrument. The TEM samples were prepared by sonicating 0.3 g/L suspensions for 3 h, diluting 1 drop of suspension with 10 drops of ethanol and then deposited to a lacey carbon coated copper grid. The particle size for FH has range of 1.5 - 5.7 nm with a median value of 3.4 nm (Figure A3-5). Villacis-Garcia et al. (2015) reported a similar particle size (3.4 nm) with a BET value of 311 m^2/g.

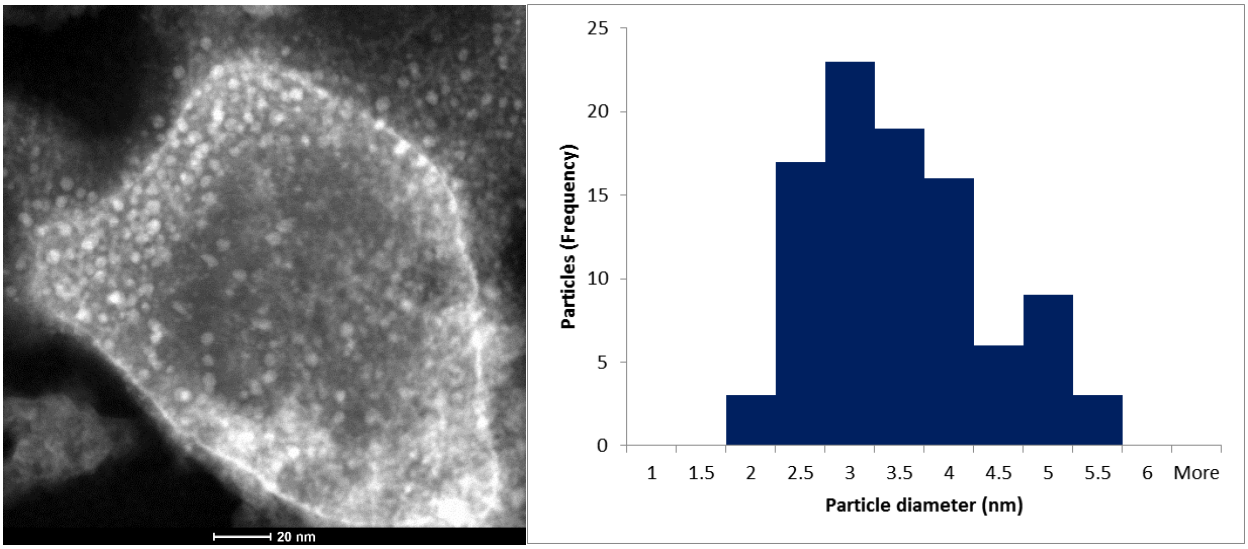

Figure A3-5. TEM images of ferrihydrite particles (white dots) and histogram of particle sizes.

Batch tests

Chromate adsorption (CrO_4^{2-}) on FH was measured in batch experiments at different pH values in 0.01 M NaCl background electrolyte. The experiments were performed under a CO_2 – free atmosphere inside a glove bag that was equilibrated with argon gas for 5 h before the beginning of experiments. However, we are aware of the fact that the CO_2 inside the glove bag was not zero, there was still some residual CO_2 remaining. We have confirmed this recently by measuring the CO_2 gas concentration with a CO_2 infrared detector. The remaining partial pressure of CO_2 was measured at 20 ppm. ACS certified reagents were used and the batches were prepared in 50 mL polypropylene centrifuge tubes. A 10 mM CrO_4^{2-} stock solution was prepared from Na_2CrO_4 the same day of the experiments. A solution of the 1mM CrO_4^{2-}, ionic strength (0.01 M NaCl) and different amounts of acid (0.1 M HCl) or base (0.1 M NaOH) were added to each tube. The FH suspension was then added to each tube to yield a concentration of 0.5 g/L. After shaking for 24 h, the suspensions were centrifuged for 10 min at 3500 rpm and filtered (0.2 μm membranes). The

supernatants were analyzed for chromate using the EPA7196A colorimetric method with a GENESYS^{TM} 20 Visible Spectrophotometer. The pH of the supernatant was measured with a Metrohm pH Unitrode PT1000 glass electrode that was previously calibrated with three Metrohm calibration buffers (4, 7, 9).

ATR-FTIR

Spectroscopic information for chromate surface complexes was incorporated into the model in two ways: 1) by formulating the monodentate and bidentate complexation reactions, as mentioned in the main text, and 2) by optimizing the chromate log Ks with profiles obtained by multivariate curve resolution (MCR) with alternating least squares (ALS) derived from flow through ATR – FTIR experiments. Recent studies (Veselská et al., 2016; Xie et al., 2015) incorporate both inner – sphere complexes, however the pH - dependent distribution of monodentate and bidentate complexes has not yet been included in SCMs. Although the MCR - ALS profiles represent only a relative distribution of the complexes, they may be translated to surface coverage of adsorbed chromate on the mineral surface. Previous studies have related ATR – FTIR spectra to surface coverage on hematite and ferrihydrite films (Kabengi et al., 2017; Sabur et al., 2015). Data for FH were adopted from Johnston and Chrysochoou (2016). Briefly, experiments were performed by depositing a FH film on the ATR diamond and flowing through a solution of 100 μM CrO_4^{2-} in a background electrolyte solution of 0.01 M NaCl. The pH was adjusted with 0.1 M HCl / NaOH and the spectra were recorded at equilibrium (Johnston and Chrysochoou, 2016). The ATR-FTIR experiment had a better control of the CO_2 contamination since the mineral was placed a closed flow cell and flushed with the electrolyte solution at high pH (10-11) until the peak of CO_2 in the ATR-FTIR became negligible. Therefore, no CO_2 was present in the spectroscopic data. The MCR-ALS analysis of the resulting pH envelope provided a relative distribution of monodentate

and bidentate species as a function of pH. To convert the relative distribution of surface complexes into surface coverage, the experimental liquid: solid (L:S) ratio was adjusted in order to obtain surface coverage values comparable to the batch experiments (2.3 umol/m^2 for FH at the lowest pH). This is only an approximation, given that the actual L:S ratio was not recorded in equilibrium experiments; chromate solution was passed through the flow cell until the ATR signal was constant. However, the estimated L:S ratio was comparable to flow through experiments with actual measurements reported in Kabengi et al. (2017) (0.004 g/L compared to 0.0025 g/L in Kabengi et al. (2017)).

Surface Complexation Model

The Surface Complexation model was built with reactions contained in Table A3-3.

Table A3-3. CD – MUSIC surface complexation reactions for protonation, electrolyte, chromate, and carbonate binding.

Protonation reactions	**log K**	**ΔZ_0**	**ΔZ_1**
$\equiv FeOH_i^{-0.5} + H^+ \leftrightarrow \equiv FeOH_{2i}^{+0.5}$	log K_i	1	
$\equiv Fe_3O_j^{-0.5} + H^+ \leftrightarrow \equiv Fe_3OH_j^{+0.5}$	log Kj	1	
Electrolytes – surface reactions	**log K**	**ΔZ_0**	**ΔZ_1**
$\equiv FeOH_i^{-0.5} + Na^+ \leftrightarrow [\equiv FeOH^{-0.5}\text{-}Na^+]^{+0.5}$	-0.60		1
$\equiv Fe_3O_j^{-0.5} + Na^+ \leftrightarrow [\equiv Fe_3O_j^{-0.5}\text{-}Na^+]^{+0.5}$	-0.60		1
$\equiv FeOH_i^{-0.5} + Cl^- + H^+ \leftrightarrow [\equiv FeOH_{2i}^{+0.5}\text{-}Cl^-]^{-0.5}$	-0.45	1	-1
$\equiv Fe_3O_j^{-0.5} + Cl^- + H^+ \leftrightarrow [\equiv Fe_3OH_j^{+0.5}\text{-}Cl^-]^{-0.5}$	-0.45	1	-1
Outer sphere complexation reactions	**log K**	**ΔZ_0**	**ΔZ_1**
$\equiv FeOH_i^{-0.5} + H^+ + CrO_4^{2-} \leftrightarrow [\equiv FeOH_{2i}^{+0.5}\text{-}CrO_4^{2-}]^{-1.5}$	Fitted	1	-2
Inner sphere complexation reactions	**log K**	**ΔZ_0**	**ΔZ_1**
$\equiv FeOH_i^{-0.5} + H^+ + CrO_4^{2-} \leftrightarrow \equiv FeOCrO_3^{-1.5} + H_2O$	Fitted	0.5	-1.5
$2\equiv FeOH_i^{-0.5} + 2H^+ + CrO_4^{2-} \leftrightarrow (\equiv FeO)_2CrO_2^{-1} + 2H_2O$	Fitted	1	-1

$2{\equiv}FeOH_i^{-0.5} + 2H^+ + CO_3^{2-} \leftrightarrow (\equiv FeO)_2CO^{-1} + 2H_2O$	21.3	1	-1
$2{\equiv}FeOH_i^{-0.5} + 2H^+ + CO_3^{2-} \leftrightarrow [(\equiv FeOH_2)_2\text{-}CO_3^{2-}]^{-1}$	-5.3	1.6	-1.6

Briefly, protons were placed on the 0 – plane, electrolyte ions (Na^+, Cl^-) on the 1 – plane, and chromate and carbonate inner sphere complexes were distributed between the 0 – and 1– planes by fixing the CD values to the commonly accepted values for monodentate and bidentate species. The electrolyte equilibrium constants were adopted from studies employing CD – MUSIC modeling on iron oxides, as previously discussed by Bompoti et al. (2017). For inner – sphere complexation, two surface species for chromate were considered, a non-protonated monodentate and a non-protonated bidentate complex, according to previous spectroscopic studies on FH (Johnston and Chrysochoou, 2012, 2016). When considering an outer sphere chromate complex instead of an inner sphere monodentate complex, the outer sphere chromate was placed at the 1-plane.

The CO_2 model

For carbonate adsorption, an inner-sphere non – protonated bidentate complex and a binuclear outer sphere/ hydrogen bonded carbonate complex were considered. Based on spectroscopic observations on hematite (α-Fe_2O_3) (Bargar et al., 2005) and goethite (α-FeOOH) (Hiemstra et al., 2004), carbonate forms bidentate complexes on singly – coordinated sites, while Bargar et al. (2005) also noticed an outer-sphere/ hydrogen bonded complex at the hematite interface. To optimize equilibrium constants for both species, carbonate adsorption data on FH obtained from Zachara et al. (1987) were fitted in previous work (Chrysochoou et al., 2013). The SSA was maintained at 600 m2/g, as was suggested by Zachara et al. (1987), although better fits have been reported in the literature for higher SSAs (Hiemstra et al., 2009). The log K for the non-protonated bidentate species was optimized at 21.3, and at -5.3 for the outer – sphere. The reactions are given

in Table A3-3. However, more research is needed to elucidate the carbonate adsorption mechanisms by FH and optimization of thermodynamic constants, which is ongoing in our laboratory.

CD factors sensitivity analysis

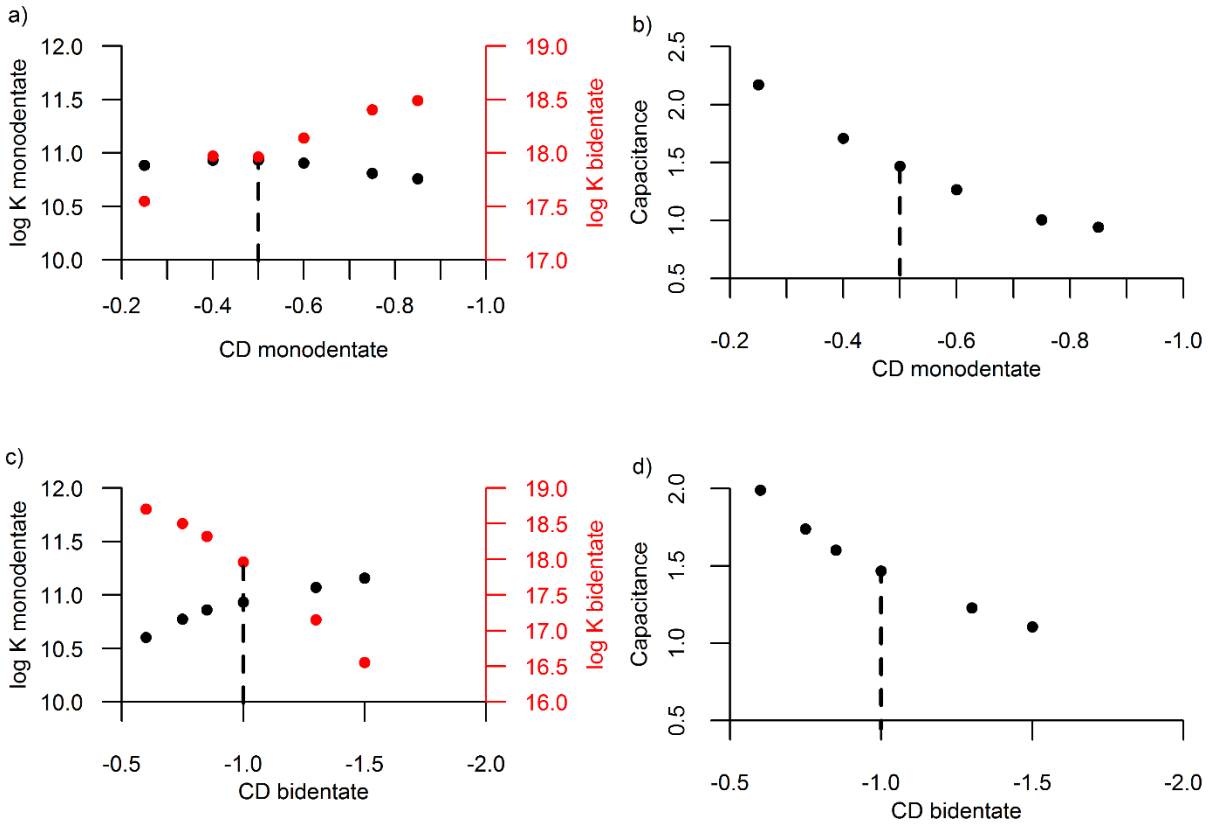

Figure A3-6. Sensitivity analysis of extracted parameters (log Ks and Capacitance) on CD factors for monodentate chromate complexes (a) and (b), and bidentate chromate complexes (c) and (d). The dotted vertical lines represent the values adopted in the study.

Performing a sensitivity analysis on CD factors for both complexes reveals two main trends: a) when the CD factor increases (becomes more negative), more chromate charge is attributed to the

z_0 plane and less to the z_1 plane. This has the effect of increasing log K values (Figure A3-6). b) Increasing the CD factors also has the effect of decreasing capacitance values, thus increasing the distance of the Stern plane from the surface.

Optimization results

The number of optimization starting points, which in this case is 500, are shown in Figure A3-7. Starting from these points, the local optimizer (Nelder – Mead) performs a local minimization around each point. The search pattern of the algorithm around three points is shown in the Figure A3-8.

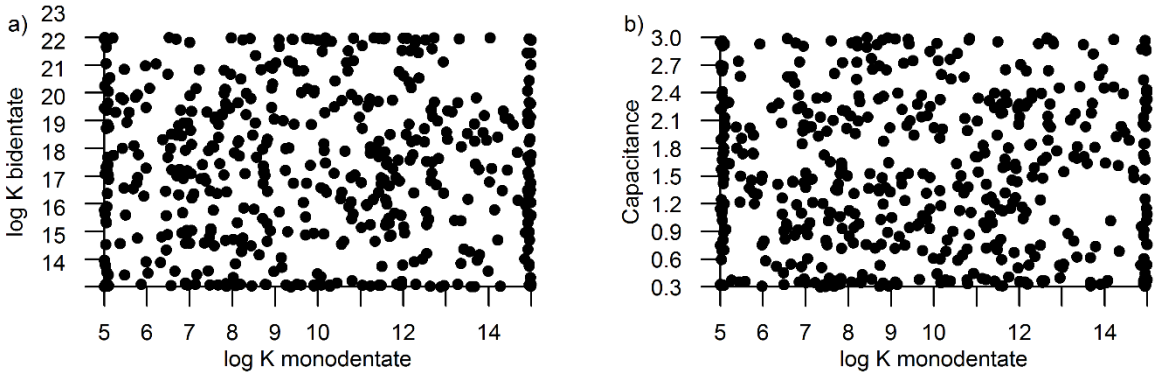

Figure A3-7. Grid of 500 starting points for MUSE for the spectroscopy dataset; monodentate vs bidentate equilibrium constant (a), and monodentate equilibrium constant and capacitance values (b). The boundary conditions were log $K_{monodentate}$ [5, 15], log $K_{bidentate}$ [14, 23] and Capacitance [0.3, 3.0]

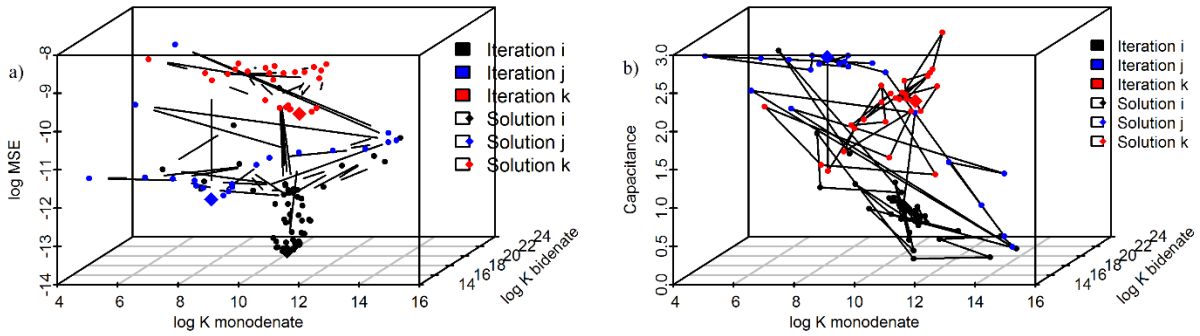

Figure A3-8. MUSE results for 3 selected iterations: a) log MSE as a function of log Ks, and b) the 3 – D solution matrix (log $K_{monodentate}$, log $K_{bidentate}$, Capacitance). The iteration i (black points) is the best solution for SCM parameters, iteration j (blue points) is an intermediate one, and iteration k (red points) is the worst one in terms of MSE.

Sensitivity analysis results

Surface area sensitivity analysis

Table A3-4. Sensitivity analysis results with regard to SSA for MCR – ALS spectroscopy profiles.

SSA (m^2/g)	log K_{MD}	log K_{BD}	C	MSC	MSE_{TOTAL}	MSE1 (total Cr adsorbed)	MSE2 (MD profile)	MSE3 (BD profile)	Δlog Ks	SSA x C
2000	9.8645	16.87	0.5	3.72	4.055E-14	7.24E-15	1.15E-14	2.18449E-14	7.00	914.06
1950	9.86	16.87	0.46	3.72	4.05E-14	7.24E-15	1.15E-14	2.18E-14	7.00	891.20
1900	9.85	16.86	0.45	3.71	4.12E-14	7.31E-15	1.14E-14	2.25E-14	7.00	856.27
1850	9.86	16.87	0.46	3.72	4.05E-14	7.24E-15	1.15E-14	2.18E-14	7.00	845.50
1800	9.86	16.87	0.47	3.70	4.00E-14	7.37E-15	1.19E-14	2.08E-14	7.01	846.14
1750	9.89	16.89	0.47	3.75	3.93E-14	7.05E-15	1.16E-14	2.07E-14	7.00	823.47
1700	9.92	16.92	0.47	3.85	3.87E-14	6.36E-15	1.17E-14	2.07E-14	7.00	805.59
1650	9.94	16.93	0.48	3.83	3.81E-14	6.47E-15	1.17E-14	2.00E-14	7.00	792.39
1600	9.96	16.95	0.49	3.88	3.74E-14	6.15E-15	1.18E-14	1.95E-14	7.00	781.15

1550	9.98	16.97	0.49	3.94	3.68E-14	5.83E-15	1.18E-14	1.92E-14	6.99	764.43
1500	10.00	16.99	0.50	4.00	3.62E-14	5.49E-15	1.20E-14	1.87E-14	6.99	754.17
1450	10.02	17.01	0.51	4.00	3.55E-14	5.48E-15	1.20E-14	1.81E-14	6.99	741.07
1400	10.00	17.00	0.54	3.78	3.53E-14	6.81E-15	1.24E-14	1.61E-14	7.00	756.97
1350	10.07	17.06	0.53	4.06	3.43E-14	5.16E-15	1.20E-14	1.71E-14	6.99	713.62
1300	10.09	17.08	0.54	4.08	3.36E-14	5.04E-15	1.21E-14	1.65E-14	6.99	703.90
1250	10.12	17.10	0.55	4.14	3.30E-14	4.76E-15	1.22E-14	1.61E-14	6.98	691.44
1200	10.14	17.12	0.57	4.15	3.24E-14	4.72E-15	1.22E-14	1.54E-14	6.98	680.35
1150	10.17	17.15	0.58	4.20	3.17E-14	4.50E-15	1.23E-14	1.49E-14	6.98	667.31
1100	10.20	17.18	0.60	4.19	3.11E-14	4.52E-15	1.23E-14	1.42E-14	6.98	656.84
1050	10.22	17.20	0.62	4.19	3.04E-14	4.52E-15	1.23E-14	1.35E-14	6.98	647.31
1000	10.26	17.24	0.63	4.23	2.97E-14	4.34E-15	1.23E-14	1.31E-14	6.98	632.05
950	10.29	17.27	0.65	4.26	2.90E-14	4.20E-15	1.22E-14	1.26E-14	6.98	620.92
900	10.33	17.30	0.68	4.26	2.83E-14	4.22E-15	1.22E-14	1.19E-14	6.97	609.96
850	10.37	17.34	0.70	4.27	2.76E-14	4.18E-15	1.21E-14	1.14E-14	6.97	598.24
800	10.41	17.38	0.73	4.27	2.69E-14	4.20E-15	1.19E-14	1.07E-14	6.97	587.34
750	10.45	17.42	0.77	4.27	2.61E-14	4.19E-15	1.18E-14	1.01E-14	6.97	576.45
700	10.49	17.47	0.81	4.24	2.52E-14	4.30E-15	1.15E-14	9.45E-15	6.97	565.95
650	10.54	17.51	0.86	4.22	2.43E-14	4.39E-15	1.12E-14	8.76E-15	6.98	556.90
600	10.59	17.57	0.91	4.20	2.33E-14	4.49E-15	1.08E-14	8.08E-15	6.98	547.52
550	10.65	17.63	0.98	4.19	2.23E-14	4.53E-15	1.02E-14	7.51E-15	6.98	537.10
500	10.71	17.70	1.06	4.16	2.10E-14	4.67E-15	9.53E-15	6.84E-15	6.99	528.86
450	10.78	17.77	1.16	4.13	1.97E-14	4.81E-15	8.66E-15	6.23E-15	7.00	520.84
400	10.84	17.86	1.29	4.08	1.82E-14	5.07E-15	7.58E-15	5.58E-15	7.01	515.15
350	10.93	17.96	1.45	4.04	1.67E-14	5.24E-15	6.32E-15	5.16E-15	7.03	509.22
347.2	10.93	17.96	1.47	4.03	1.66E-14	5.29E-15	6.25E-15	5.09E-15	7.03	509.59
300	11.01	18.08	1.69	3.96	1.55E-14	5.71E-15	4.98E-15	4.82E-15	7.06	508.24
250	11.12	18.23	2.04	3.85	1.58E-14	6.35E-15	4.31E-15	5.13E-15	7.11	510.67
200	11.24	18.45	2.61	3.65	2.21E-14	7.74E-15	7.43E-15	6.93E-15	7.20	522.77
150	11.80	19.02	3.00	3.57	6.04E-14	8.40E-15	2.86E-14	2.34E-14	7.22	449.99
100	13.14	20.23	3.00	2.09	2.36E-13	3.69E-14	1.13E-13	8.58E-14	7.09	300.00
80	13.91	20.94	3.00	1.69	3.78E-13	5.51E-14	1.91E-13	1.32E-13	7.03	240.00

Outer sphere scenario

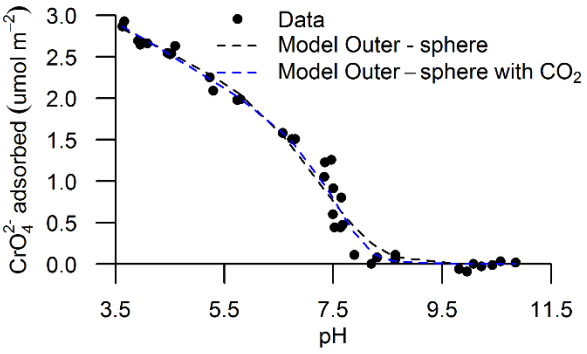

Figure A3-99. Simulated batch chromate data considering an outer – sphere and an inner-sphere bidentate complex for SSA 347.2 m^2/g. Data (points) and model simulation (dashed lines) are shown for chromate adsorbed with and without presence of 400 ppm CO_2.

Table A3-5. Optimized parameters for batch chromate pH – envelope dataset considering an outer – sphere and a bidentate complex with and without presence of CO_2.

Model	log $K_{outer-sphere}$	log $K_{bidentate}$	Capacitance	MSC	MSE
		FH			
Model_optimized both outer-sphere and BD without CO_2	-3.77	18.76	1.01	3.73	7.18E-10
Model_optimized both outer-sphere and BD with CO_2	3.85	16.88	2.98	4.01	5.45E-10

Surface speciation

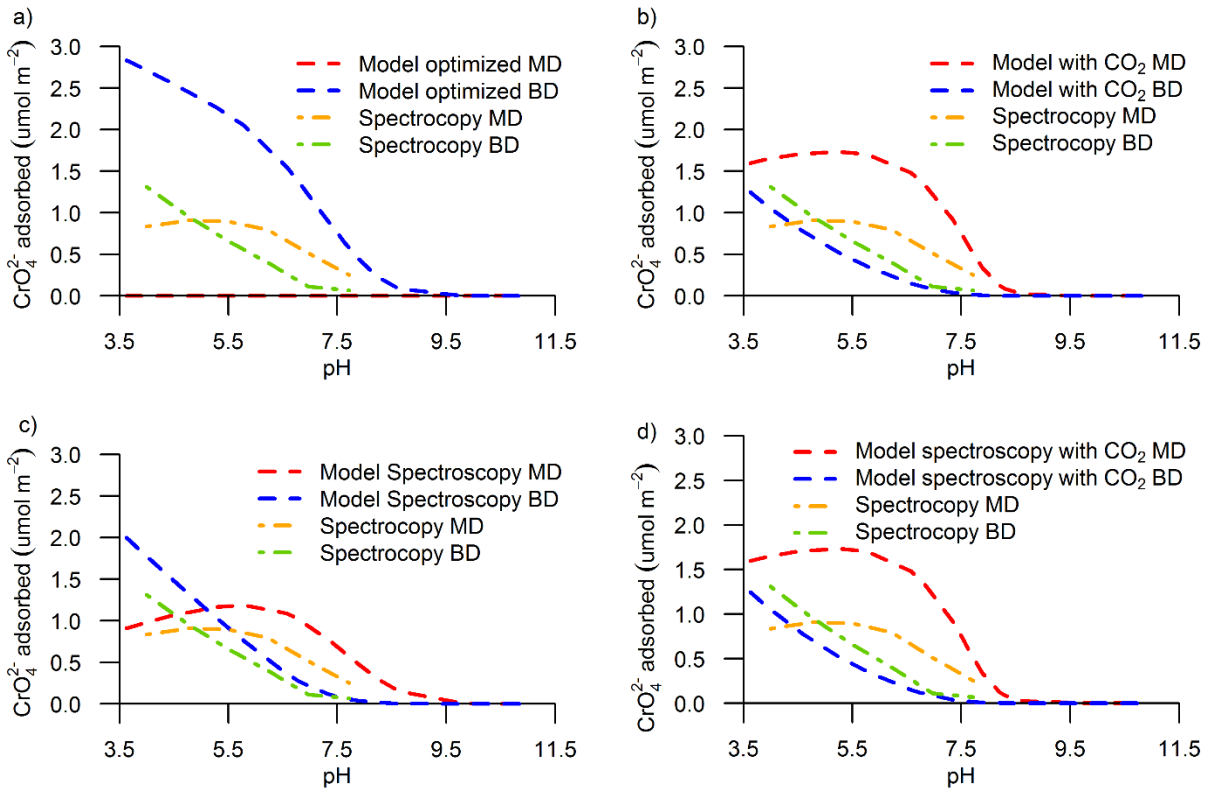

Figure A3-1010. Surface species distribution for macroscopic data compared with spectroscopic speciation based on MCR – ALS profiles. (a) Model with optimized both MD [1.92] and BD [18.759], (b) Model including CO_2 and optimized both MD [11.61] and BD [17.88], (c) Model with average log K values from the spectroscopy analyses MD [10.78] and BD [17.78], (d) Model including CO_2 and average log K values from the spectroscopy analyses MD [10.78] and BD [17.78].

Mathematica SCM and MUSE algorithm

```
Clear[aH, acNa, acCl, totNa, totCl, totCrO4, totFeOHa, totFe3Oa, totFe3Ob];
totalmatrixA :=
```

"species↓" "components→"	FeOHa	Fe3Oa	Fe3Ob	aH	Na	acNa	Cl	acCl	CrO4
aH	0	0	0	1	0	0	0	0	0
Na	0	0	0	0	1	0	0	0	0
Cl	0	0	0	0	0	0	1	0	0
CrO4	0	0	0	0	0	0	0	0	1
FeOHa	1	0	0	0	0	0	0	0	0
Fe3Oa	0	1	0	0	0	0	0	0	0
Fe3Ob	0	0	1	0	0	0	0	0	0
aOH	0	0	0	-1	0	0	0	0	0
HCrO4	0	0	0	1	0	0	0	0	1
H2CrO4 (*10*)	0	0	0	2	0	0	0	0	1
Cr2O7	0	0	0	2	0	0	0	0	2
NaCrO4	0	0	0	0	1	1	0	0	1
FeOH2a	1	0	0	1	0	0	0	0	0
Fe3OHa	0	1	0	1	0	0	0	0	0
Fe3OHb	0	0	1	1	0	0	0	0	0
FeOHaNa	1	0	0	0	1	1	0	0	0
FeOH2aCl	1	0	0	1	0	0	1	1	0
Fe3OaNa	0	1	0	0	1	1	0	0	0
Fe3ObNa	0	0	1	0	1	1	0	0	0
Fe3OHaCl (*20*)	0	1	0	1	0	0	1	1	0
Fe3OHbCl	0	0	1	1	0	0	1	1	0
FeOCrO3a (*monodenate*)	1	0	0	1	0	0	0	0	1
Fe2O2CrO2a (*bidentate*)	2	0	0	2	0	0	0	0	1
totals	totFeOHa	totFe3Oa	totFe3Ob	totaH	totNa	□	totCl	□	totCrO4

```
(*matrixes*)

totalmatrixA // MatrixForm;
Most[totalmatrixA] // MatrixForm;
totalslistA = Drop[Rest[Flatten[Take[totalmatrixA, -1]]], -1] ; (* only totals *)
logkmatrixA = Rest[Take[Most[totalmatrixA], All, {-1}]]; (* only logKs *)
logklistA = Flatten[logkmatrixA];
speciesmatrixA = Rest[Take[Most[totalmatrixA], All, {1}]];
(* only names of species *)
specieslistA = Flatten[speciesmatrixA];
specieslistA2 = Drop[specieslistA, 8] ;
(* names of species without ions and surface components*)
solutiontextspecieslistA = Table[specieslistA[[1]], {1, 8, 12}];
(* only solution species names *)
surfacetextspecieslistA =
  Table[ToString[specieslistA[[1]]], {1, 13, Length[specieslistA]}];
(* only surface species names *)
componentsmatrixA = Drop[Drop[Extract[Most[totalmatrixA], 1], 1], -1] ;
(* names of species, surfaces and electrost  - 1rst raw *)
electrocomponentsA = Take[componentsmatrixA, -3];(* names of elxctrastatics*)
```

	acCrO4	$e^{((-F*\psi 0)/(r*temp))}$	$e^{((-F*\psi 1)/(r*temp))}$	$e^{((-F*\psi 2)/(r*temp))}$	$\log K_T$
	0	0	0	0	0
	0	0	0	0	0
	0	0	0	0	0
	0	0	0	0	0
	0	0	0	0	0
	0	0	0	0	0
	0	0	0	0	0
	0	0	0	0	lkw
	1	0	0	0	lkHCrO4
	1	0	0	0	lkH2CrO4
	2	0	0	0	lkCr2O7
	1	0	0	0	lkNaCrO4
	0	1	0	0	lkFeOH2a
	0	1	0	0	lkFe3OHa
	0	1	0	0	lkFe3OHb
	0	0	1	0	lkFeOHaNa
	0	1	-1	0	lkFeOH2a + lkFeOH2aCl
	0	0	1	0	lkFe3OaNa
	0	0	1	0	lkFe3ObNa
	0	1	-1	0	lkFe3OHa + lkFe3OHaCl
	0	1	-1	0	lkFe3OHb + lkFe3OHbCl
	1	1 + cdCrO4a	-2 - cdCrO4a	0	lkFeOCrO3a - monocorr1
	1	2 + cdCrO4b	-2 - cdCrO4b	0	lkFe2O2CrO2a - bicorr1
		$(\sigma_0$ - refcharge) / F	σ_1 / F	σ_2 / F	

```
speciescomponentsA = Drop[componentsmatrixA, -3] ; (*names of species and surfaces *)
stoichmatrixA = Transpose[Drop[Drop[Transpose[Drop[Most[totalmatrixA], {1}]], 1], -1]];
(* only stoichiometric coefficients - species, surfaces, electrostatics *)
stoichspeciesA = Drop[stoichmatrixA, 8] ;
(* only stoichiometric coefficients - species,
surfaces, electrostatics but not free ions *)
stoichspeciesA2 = Transpose[stoichspeciesA];
Transpose[Transpose[stoichmatrixA] * componentsmatrixA] // MatrixForm;
(* matrix names x stoiciometric coeff *)
Transpose[Transpose[stoichmatrixA] * componentsmatrixA] * Flatten[logkmatrixA] //
  MatrixForm; (* matrix names x stoiciometric coeff x logKs *)


(*Parameters*)
 consts = {F = 96 487, r = 8.314, pv = 8.854 * 10^-12};
vconsts = {temp = 298.15, dw = 78.45, mws = 85, lkw = -13.9914,
    rpart = 1.7 * 10^-9, dr = 0.35 * 10^-9, surfarea1 = 347.2, gsold1 = 0.50};
sitecharges = {zFeOHa = -0.50, zFe3Oa = -0.5, zFe3Ob = -0.5};
(* charges correspond to surface components *)
speciescharges = {zH = 1, zNa = 1, zCl = -1, zCrO4 = -2};
(* charges correspond to solution components *)
sitedensities = {ns1 = 1.0833 * 10^-5, ns2 = 9.899 * 10^-6, ns3 = 1.369 * 10^-6};
(* units: moles/m2 =((sites/nm2)*10^18)/6.023*10^23 *)      (* Hiemstra 2013*)
fixparams =
   {cp = 0.95, c2 = 10000, cs = 1 / ((1 / c1) + (1 / c2)), cdCrO4a = -0.5, cdCrO4b = -1.0,
    lkFeOH2a = 8, lkFe3OHa = 8, lkFe3OHb = 9.5, lkFeOHaNa = -0.6, lkFeOH2aCl = -0.45,
    lkFe3OaNa = lkFeOHaNa, lkFe3ObNa = lkFeOHaNa, lkFe3OHaCl = lkFeOH2aCl,
    lkFe3OHbCl = lkFeOH2aCl, lkFeOCrO3a = 11.5, lkFe2O2CrO2a = 18.6};
(* The fixparams list contains the capacitance, charge distribution,
and log K values for the surface species  *)
sollogks = { lkHCrO4 = 6.50, lkH2CrO4 = 6.30, lkCr2O7 = 14.53, lkNaCrO4 = 0.70};
(* The log K values for the solution
 species are input in the list immediately above. *)
totconcs = {totFeOHa = ns1, totFe3Oa = ns2, totFe3Ob = ns3};

seivefunc1[x_] := Take[x, {1, Length[x], 1}]

(* Input data set *)

(*first adsorption pH edge data set. 0.87x 10^-3 total Fe, under N2*)
pH1 = {3.623, 3.657, 3.914, 3.95, 3.979, 4.082, 4.45, 4.501,
    4.521, 4.593, 5.229, 5.292, 5.731, 5.79, 6.569, 6.739, 6.8, 7.335,
    7.344, 7.459, 7.489, 7.5, 7.519, 7.635, 7.646, 7.67, 7.887, 8.197, 8.302,
    8.634, 8.637, 9.808, 9.955, 10.072, 10.218, 10.419, 10.572, 10.85};
mt1 = {0.01, 0.01, 0.01, 0.01, 0.01, 0.01, 0.01, 0.01, 0.01, 0.01, 0.01, 0.01,
    0.01, 0.01, 0.01, 0.01, 0.01, 0.01, 0.01, 0.01, 0.01, 0.01, 0.01, 0.01, 0.01,
    0.01, 0.01, 0.01, 0.01, 0.01, 0.01, 0.01, 0.01, 0.01, 0.01, 0.01, 0.01};
```

```
acNaa = {0.91267, 0.91267, 0.91267, 0.91267, 0.91267, 0.91267, 0.91267,
    0.91267, 0.91267, 0.91267, 0.91267, 0.91267, 0.91267, 0.91267, 0.91267,
    0.91267, 0.91267, 0.91267, 0.91267, 0.91267, 0.91267, 0.91267, 0.91267,
    0.91267, 0.91267, 0.91267, 0.91267, 0.91267, 0.91267, 0.91267, 0.91267,
    0.91267, 0.91267, 0.91267, 0.91267, 0.91267, 0.91267, 0.91267};
totCrO4a = {0.001, 0.001, 0.001, 0.001, 0.001, 0.001, 0.001, 0.001, 0.001,
  0.001, 0.001, 0.001, 0.001, 0.001, 0.001, 0.001, 0.001, 0.001, 0.001, 0.001,
  0.001, 0.001, 0.001, 0.001, 0.001, 0.001, 0.001, 0.001, 0.001, 0.001, 0.001,
  0.001, 0.001, 0.001, 0.001, 0.001, 0.001, 0.001}(*total chromate conc.*);
solwt1 = {1000., 1000., 1000., 1000., 1000., 1000., 1000., 1000., 1000.,
  1000., 1000., 1000., 1000., 1000., 1000., 1000., 1000., 1000., 1000.,
  1000., 1000., 1000., 1000., 1000., 1000., 1000., 1000., 1000., 1000.,
  1000., 1000., 1000., 1000., 1000., 1000., 1000., 1000., 1000.};
CrO4ads1 = {4.97752496638547*^-04, 5.08643074526445*^-04, 4.67803407446829*^-04,
    4.59635474030906*^-04, 4.65080762974855*^-04, 4.6235811850288*^-04,
    4.41938284963072*^-04, 4.39215640491098*^-04, 4.40576962727085*^-04,
    4.56912829558932*^-04, 3.91569362231546*^-04, 3.62981595275815*^-04,
    3.43923083971995*^-04, 3.45284406207982*^-04, 2.74495649936648*^-04,
    2.62243749812763*^-04, 2.62324151530584*^-04, 1.83367461843327*^-04,
    2.13316551035045*^-04, 2.18761839978994*^-04, 1.0441077215607*^-04,
    1.58863661595558*^-04, 7.7184327436326*^-05, 7.7184327436326*^-05,
    1.39805150291737*^-04, 8.26296163802748*^-05, 2.00087935248638*^-05,
    9.50282221043208*^-07, 1.45635045809152*^-05, 9.11821563696635*^-06,
    2.00087935248638*^-05, -9.94029566685439*^-06, -1.53855846108031*^-05,
    9.50282221043208*^-07, -4.49500672290548*^-06, -1.77236225093114*^-06,
    6.39557116499201*^-06, 3.67292669301755*^-06}(*adsorbed chromate conc.*);
mt1adj = 0.5 * (mt1 * zNa^2 + mt1 * zCl^2 + 2 * totCrO4a + (totCrO4a - CrO4ads1) * zCrO4^2);
(*Ionic Strength including background electrolyte,
sodiun chromate and non adsorbed chromate*)

acNaa = 10^(-0.50 * zNa^2 * (mt1adj^0.5 / (1 + mt1adj^0.5) - 0.3 * mt1adj)) ;
(*activity coefficient for Na based on Davies equation*)
acCrO4 = 10^(-0.50 * zCrO4^2 * (mt1adj^0.5 / (1 + mt1adj^0.5) - 0.3 * mt1adj));
(*activity coefficient for CrO4 based on Davies equation*)
relwts1 = {1., 1., 1., 1., 1., 1., 1., 1., 1., 1., 1., 1., 1., 1., 1., 1.,
    1., 1., 1., 1., 1., 1., 1., 1., 1., 1., 1., 1., 1., 1., 1., 1., 1.};
dilfac1 := Table[solwt1[[1]] / solwt1[[1]], {1, Length[solwt1]}]

(*second adsorption pH edge data set. 17.4 x 10^-3 total Fe, under N2*)



(* Join data sets *)
pHexp = Join[pH1];
aH := 10^-pHexp
mt = Join[mt1adj];
acNa = Join[acNaa];
```

```
acCl = acNa;
(*acCrO4=acCl^(zCrO4*zCrO4);*)
totNa = mt;
totCl = mt;
totCrO4 = Join[totCrO4a];
relwts = Join[relwts1];
CrO4ads = Join[CrO4ads1];
dilfac = Join[dilfac1]; (* for the error *)


(* Calculations *)

c1 = cp * (rpart + dr) / rpart;(**Hiemstra adjustement for spherical particles*)
CrO4ads1sc = CrO4ads1 * ((solwt1 * .001 * F * -zCrO4) / (gsolid1 * surfarea1));
solwts = Join[{(solwt1 * (.001 / (surfarea1 * gsolid1)))}];
dis = 1 / ((1 / dw) + ((-0.206 / dw) * mt) + (.0051 * mt));
mtm = mt(*(mt*sd)/(1+(.001*mt*mws))*);
xt = ((8 * temp * r * pv * dis * mtm * 1000) ^0.5);
kappa = Sqrt[((2 * (F^2) * mtm * 1000) / (dis * pv * r * temp))];

(*bicorr=Log[10,(gsolid1*surfarea1*ns1*solwt1*.001)];*)
monocorr1 = Log[10, (solwts) * dilfac];
bicorr1 = Log[10, ns1] + monocorr1;
(*bicorr2=Log[10,ns2]+monocorr1;*)

myfunc := (refcharge = Sum[F * sitecharges[[i]] * sitedensities[[i]], {i, 1, Length[sitecharges]}];
  masslaweqs = Table[specieslistA[[1]] ==
      10^logklistA[[1]] * Product[componentsmatrixA[[j]]^stoichmatrixA[[1, j]],
        {j, Length[componentsmatrixA]}], {1, Length[specieslistA]}];

massbalanceeqs = Table[Sum[specieslistA[[1]] * stoichmatrixA[[1, j]],
      {1, Length[specieslistA]}], {j, Length[componentsmatrixA]}];

  σ0elec = (ψ0 - ψ1) * c1;
σ1elec = ((ψ1 - ψ2) * c2) - σ0elec;
σdelec = (((-2 * dis * pv * kappa * r * temp) / F) * Sinh[(F * ψ2) / (2 * r * temp)]) *
    Sqrt[1 + (2 / ((rpart * kappa) * Cosh[(F * ψ2) / (4 * r * temp)]^2)) +
      (8 * Log[Cosh[((F * ψ2) / (4 * r * temp))]] /
          (((kappa * rpart)^2) * Sinh[((F * ψ2) / (2 * r * temp))]^2))];
σ2elec = (σdelec + (c2 * (ψ1 - ψ2)));
  diffns1 = (massbalanceeqs[[1]] - ns1) / ns1;
diffns2 = (massbalanceeqs[[2]] - ns2) / ns2;
diffns3 = (massbalanceeqs[[3]] - ns3) / ns3;
  diffNa = (massbalanceeqs[[5]] - (totNa * 1)) / totNa;
diffCl = (massbalanceeqs[[7]] - (totCl * 1)) / totCl;
```

```
diffCrO4 = (massbalanceeqs[[9]] - (totCrO4 * solwts)) / (totCrO4 * solwts);
  diffσ0 = ((massbalanceeqs[[11]] * F) + refcharge) - σ0elec;
diffσ1 = ((massbalanceeqs[[12]] * F) - σ1elec) / 10;
diffσ2 = ((massbalanceeqs[[13]] * F) - σ2elec) / 10;
  preeqs = Total[{diffns1, diffns2,
      diffns3, diffNa, diffCl, diffCrO4, diffσ0, diffσ1, diffσ2}^2];
  solall[f_] := Table[f[[i]] /. rtsols[[i]], {i, Length[pHexp]}];
rtsolsa = Map[FindMinimum[#,
      (*0<ATiOH<1/1000&&0<ATi2O<1/1000&&BTiOH≥0&&BTi2O≥0&&0<M1<1&&0<A1<1&&
        M2≥0&&M3≥0&&A2≥0&&-1<ψ0<1&&-1<ψ1<1&&-1<ψ2<1&&-1<ψ3<1&&-1<ψ4<1},*)
      {{FeOHa, ns1}, {Fe3Oa, ns2}, {Fe3Ob, ns3}, {Na, 10 / 1000}, {Cl, 10 / 1000},
       {CrO4, 1 / 100 000 000 000 000 000}, {ψ0, 5 / 10}, {ψ1, 1 / 11}, {ψ2, 1 / 11}},
      Method → {"LevenbergMarquardt"}, MaxIterations → 80 000] &, Chop[preeqs]];

  rtsols = rtsolsa[[All, 2]];
  (*wtsumsqsadst=relwts*
     ((((totCrO4-Sum[solall[specieslistA[[1]]]/solwts,{1,9,12}]-(((CrO4/.rtsols)/
                 solwts)/1))*solwts*F*-zCrO4)-(CrO4ads*solwts*F*-zCrO4))^2);*)
  Total[Abs[(CrO4 /. rtsols) - CrO4ads1]];
  freeCrO4 = (CrO4 /. rtsols) / solwts ; (*Free A2 conc (molal)*)
  adsCrO4cal = totCrO4 - Sum[solall[specieslistA[[1]]] / solwts, {1, 9, 12}] - freeCrO4;
  MSE = Apply[Plus,
     (Take[CrO4ads, Length[pH1]] - Take[adsCrO4cal, Length[pH1]])^2] / Length[pH1];

  wtsumsqs1 = MSE)

myfunc
lwtsumsqstot := Log[10, wtsumsqs1]
Clear[lkFeOCrO3a, lkFe2O2CrO2a, c1];
PatchFunction[p1_?NumberQ, p2_?NumberQ, p3_?NumberQ] :=
Block[{lkFeOCrO3a = p1, lkFe2O2CrO2a = p2, c1 = p3}, (myfunc)]
methods = {"NelderMead"};
solns = Table[{1, Reap[NMinimize[{PatchFunction[lkFeOCrO3a, lkFe2O2CrO2a, c1],
         0 < lkFeOCrO3a < 25 && 15 < lkFe2O2CrO2a < 30 && 0.3 < c1 < 3.0},
 {lkFeOCrO3a, lkFe2O2CrO2a, c1}, Method → {#, "RandomSeed" → 1},
       WorkingPrecision → 6, MaxIterations -> 500]]}, {1, 0, 500}] & /@ methods
solns = solns //. {x_List} :> x;
sortedsols = SortBy[solns, #[[2]] &]
bestsol = sortedsols[[1]]
Print["Best solution  =  ", bestsol]

bestsol = Flatten[bestsol]

(*Initialize the parameters with the best solution*)
lkFeOCrO3a = lkFeOCrO3a /. bestsol[[3]];
```

```
Print["Best solution lkFeOCrO3a  =   ", lkFeOCrO3a]
lkFe2O2CrO2a = lkFe2O2CrO2a /. bestsol[[4]];
Print["Best solution lkFe2O2CrO2a  =   ", lkFe2O2CrO2a]
c1 = c1 /. bestsol[[5]];
Print["Best solution c1  =   ", c1]


(*Model with the best solution*)
refcharge = Sum[F * sitecharges[[i]] * sitedensities[[i]], {i, 1, Length[sitecharges]}];
masslaweqs = Table[specieslistA[[1]] =
    10^logklistA[[1]] * Product[componentsmatrixA[[j]]^stoichmatrixA[[1, j]],
      {j, Length[componentsmatrixA]}], {1, Length[specieslistA]}];

massbalanceeqs = Table[Sum[specieslistA[[1]] * stoichmatrixA[[1, j]],
    {1, Length[specieslistA]}], {j, Length[componentsmatrixA]}];

σ0elec = (ψ0 - ψ1) * c1;
σ1elec = ((ψ1 - ψ2) * c2) - σ0elec;
σdelec = (((-2 * dis * pv * kappa * r * temp) / F) * Sinh[(F * ψ2) / (2 * r * temp)]) *
   Sqrt[1 + (2 / ((rpart * kappa) * Cosh[(F * ψ2) / (4 * r * temp)]^2)) +
     (8 * Log[Cosh[((F * ψ2) / (4 * r * temp))]] /
        (((kappa * rpart)^2) * Sinh[((F * ψ2) / (2 * r * temp))]^2))];
σ2elec = (σdelec + (c2 * (ψ1 - ψ2)));
diffns1 = (massbalanceeqs[[1]] - ns1) / ns1;
diffns2 = (massbalanceeqs[[2]] - ns2) / ns2;
diffns3 = (massbalanceeqs[[3]] - ns3) / ns3;
diffNa = (massbalanceeqs[[5]] - (totNa * 1)) / totNa;
diffCl = (massbalanceeqs[[7]] - (totCl * 1)) / totCl;
diffCrO4 = (massbalanceeqs[[9]] - (totCrO4 * solwts)) / (totCrO4 * solwts);
diffσ0 = ((massbalanceeqs[[11]] * F) + refcharge) - σ0elec;
diffσ1 = ((massbalanceeqs[[12]] * F) - σ1elec) / 10;
diffσ2 = ((massbalanceeqs[[13]] * F) - σ2elec) / 10;
preeqs = Total[
   {diffns1, diffns2, diffns3, diffNa, diffCl, diffCrO4, diffσ0, diffσ1, diffσ2}^2];
solall[f_] := Table[f[[i]] /. rtsols[[i]], {i, Length[pHexp]}];
rtsolsa = Map[FindMinimum[#,
     (*0<ATiOH<1/1000&&0<ATi2O<1/1000&&BTiOH≥0&&BTi2O≥0&&0<M1<1&&0<A1<1&&
       M2≥0&&M3≥0&&A2≥0&&-1<ψ0<1&&-1<ψ1<1&&-1<ψ2<1&&-1<ψ3<1&&-1<ψ4<1},*)
     {{FeOHa, ns1}, {Fe3Oa, ns2}, {Fe3Ob, ns3}, {Na, 10 / 1000}, {Cl, 10 / 1000},
      {CrO4, 1 / 10 000 000 000 000 000 000 000}, {ψ0, 1 / 3}, {ψ1, 1 / 15}, {ψ2, 1 / 15}},
     Method → {"LevenbergMarquardt"}, MaxIterations → 80 000] &, Chop[preeqs]];

rtsols = rtsolsa[[All, 2]];
wtsumsqsadst = relwts *
   ((((totCrO4 - Sum[solall[specieslistA[[1]]] / solwts, {1, 9, 12}]) - (((CrO4 /. rtsols) /
```

```
                solwts) / 1)) * solwts * F * -zCrO4) - (CrO4ads * solwts * F * -zCrO4)) ^ 2);
freeCrO4 = (CrO4 /. rtsols) / solwts ;(*Free A2 conc (molal)*)

Print["total Cr adsorbed"];
adsCrO4cal = totCrO4 - Sum[solall[[specieslistA[[1]]]] / solwts, {1, 9, 12}] - freeCrO4
(*"Calculated Adsorbed A2 conc (molal)*)

Fe2O2CrO2acal = solall[masslaweqs[[23]]] / solwts;
FeOCrO3acal = solall[masslaweqs[[22]]] / solwts;
MSE = Apply[Plus,
    (Take[CrO4ads, Length[pH1]] - Take[adsCrO4cal, Length[pH1]]) ^ 2] / Length[pH1];


wtsumsqs1
Print["FeOCrO3a"]; FeOCrO3acal = solall[masslaweqs[[22]]] / solwts

Print["Fe2O2CrO2a"]; Fe2O2CrO2acal = solall[masslaweqs[[23]]] / solwts

MSE
ListPlot[{Transpose[{pH1, Take[adsCrO4cal, Length[pH1]]}],
  Transpose[{pH1, Take[CrO4ads, Length[pH1]]}]},
 Joined → {True, False}, AxesOrigin -> {3, 0}, PlotMarkers → {{○, 14}, {●, 14}},
 PlotStyle → {Directive[Black], Directive[Red]}, ImageSize → Medium]
rtsols = rtsolsa[[All, 2]];


ListPlot[{Transpose[{pH1, Take[FeOCrO3acal, Length[pH1]]}],
  Transpose[{pH1, Take[Fe2O2CrO2acal, Length[pH1]]}],
  Transpose[{pH1, Take[adsCrO4cal, Length[pH1]]}]}, Joined → {True, True, False},
 AxesOrigin -> {3, 0}, PlotMarkers → {{○, 14}, {△, 14}, {●, 14}},
 PlotStyle → {Directive[Black], Directive[Red]}, ImageSize → Medium]

monodentate
ListPlot[{Transpose[{pH1, Take[FeOCrO3acal, Length[pH1]]}]},
 Joined → {True, True, False}, AxesOrigin -> {3, 0},
 PlotMarkers → {{○, 14}, {△, 14}, {●, 14}},
 PlotStyle → {Directive[Black], Directive[Red]}, ImageSize → Medium]


bidentate
ListPlot[{Transpose[{pH1, Take[Fe2O2CrO2acal, Length[pH1]]}]},
 Joined → {True, True, False}, AxesOrigin -> {3, 0},
 PlotMarkers → {{○, 14}, {△, 14}, {●, 14}},
 PlotStyle → {Directive[Black], Directive[Red]}, ImageSize → Medium]

(*Statistics routine*)
parvals = {lkFeOCrO3a, lkFe2O2CrO2a, c1};
```

```
mean1 = Apply[Plus, Take[CrO4ads, Length[pH1]]] / Length[pH1];
sumsuct1 = Apply[Plus, (Take[CrO4ads, Length[pH1]] - mean1)^2];
wtsumsqstot1 =
 Apply[Plus, (Take[CrO4ads, Length[pH1]] - Take[adsCrO4cal, Length[pH1]])^2]
mscs1 = Log[((sumsuct1)) / wtsumsqstot1] - (2 * Length[parvals]) / Length[pH1];
Print["Model Selection Criterion  =  ", mscs1]


(*statistics routine*)
mystatfunc := (masslaweqs = Table[specieslistA[[i]] =
      10^logklistA[[i]] * Product[componentsmatrixA[[j]]^stoichmatrixA[[i, j]],
        {j, Length[componentsmatrixA]}], {i, Length[specieslistA]}];

   massbalanceeqs = Table[Sum[specieslistA[[i]] * stoichmatrixA[[i, j]],
      {i, Length[specieslistA]}], {j, Length[componentsmatrixA]}];

σ0elec = (ψ0 - ψ1) * c1;
σ1elec = ((ψ1 - ψ2) * c2) - σ0elec;
σdelec = (((-2 * dis * pv * kappa * r * temp) / F) * Sinh[(F * ψ2) / (2 * r * temp)]) *
     Sqrt[1 + (2 / ((rpart * kappa) * Cosh[(F * ψ2) / (4 * r * temp)]^2)) +
       (8 * Log[Cosh[((F * ψ2) / (4 * r * temp))]] /
          (((kappa * rpart)^2) * Sinh[((F * ψ2) / (2 * r * temp))]^2))];
σ2elec = (σdelec + (c2 * (ψ1 - ψ2)));
   diffns1 = (massbalanceeqs[[1]] - ns1) / ns1;
diffns2 = (massbalanceeqs[[2]] - ns2) / ns2;
diffns3 = (massbalanceeqs[[3]] - ns3) / ns3;
   diffNa = (massbalanceeqs[[5]] - (totNa * 1)) / totNa;
diffCl = (massbalanceeqs[[7]] - (totCl * 1)) / totCl;
diffCrO4 = (massbalanceeqs[[9]] - (totCrO4 * solwts)) / (totCrO4 * solwts);
   diffσ0 = ((massbalanceeqs[[11]] * F) + refcharge) - σ0elec;
diffσ1 = ((massbalanceeqs[[12]] * F) - σ1elec) / 10;
diffσ2 = ((massbalanceeqs[[13]] * F) - σ2elec) / 10;
   preeqs = Total[{diffns1, diffns2,
       diffns3, diffNa, diffCl, diffCrO4, diffσ0, diffσ1, diffσ2}^2];
   solall[f_] := Table[f[[i]] /. rtsols[[i]], {i, Length[pHexp]}];
rtsolsa = Map[FindMinimum[#,
       (*0<ATiOH<1/1000&&0<ATi2O<1/1000&&BTiOH≥0&&BTi2O≥0&&0<M1<1&&0<A1<1&&
         M2≥0&&M3≥0&&A2≥0&&-1<ψ0<1&&-1<ψ1<1&&-1<ψ2<1&&-1<ψ3<1&&-1<ψ4<1},*)
       {{FeOHa, ns1}, {Fe3Oa, ns2}, {Fe3Ob, ns3}, {Na, 10 / 1000}, {Cl, 10 / 1000},
        {CrO4, 1 / 100 000 000 000 000 000}, {ψ0, 1 / 10}, {ψ1, 1 / 11}, {ψ2, 1 / 11}},
       Method → {"LevenbergMarquardt"}, MaxIterations → 80 000] &, Chop[preeqs]];

   rtsols = rtsolsa[[All, 2]];
   freeCrO4 = (CrO4 /. rtsols) / solwts;
   adsCrO4cal = totCrO4 - Sum[solall[specieslistA[[i]]] / solwts, {i, 9, 12}] - freeCrO4);
 (*Free A2 conc (molal)*)
```

```
Off[FindRoot::precw];
Off[FindRoot::lstol];
diffach := 1.000001;
diffacl := 1 / diffach;
parvals = {c1, lkFeOCrO3a, lkFe2O2CrO2a};

parsymbols = {"c1", "lkFeOCrO3a", "lkFe2O2CrO2a"};
suctfitdiff1hs := Block[{c1 = c1 * diffach}, mystatfunc];
suctfitdiff1ls := Block[{c1 = c1 * diffacl}, mystatfunc];
suctderiv1hs = (adsCrO4cal - suctfitdiff1hs) / (parvals[[1]] - (parvals[[1]] * diffach));
suctderiv1ls = (adsCrO4cal - suctfitdiff1ls) / (parvals[[1]] - (parvals[[1]] * diffacl));
suctderiv1s = (suctderiv1hs + suctderiv1ls) / 2;
suctfitdiff2hs := Block[{lkFeOCrO3a = lkFeOCrO3a * diffach}, mystatfunc];
suctfitdiff2ls := Block[{lkFeOCrO3a = lkFeOCrO3a * diffacl}, mystatfunc];
suctderiv2hs = (adsCrO4cal - suctfitdiff2hs) / (parvals[[2]] - (parvals[[2]] * diffach));
suctderiv2ls = (adsCrO4cal - suctfitdiff2ls) / (parvals[[2]] - (parvals[[2]] * diffacl));
suctderiv2s = (suctderiv2hs + suctderiv2ls) / 2;
suctfitdiff3hs := Block[{lkFe2O2CrO2a = lkFe2O2CrO2a * diffach}, mystatfunc];
suctfitdiff3ls := Block[{lkFe2O2CrO2a = lkFe2O2CrO2a * diffacl}, mystatfunc];
suctderiv3hs = (adsCrO4cal - suctfitdiff3hs) / (parvals[[3]] - (parvals[[3]] * diffach));
suctderiv3ls = (adsCrO4cal - suctfitdiff3ls) / (parvals[[3]] - (parvals[[3]] * diffacl));
suctderiv3s = (suctderiv3hs + suctderiv3ls) / 2;

suctderivtots = {suctderiv1s, suctderiv2s, suctderiv3s};
transsuctderivtots = Transpose[suctderivtots];
pr2 = Print["Temp = ", temp];
pr3 = Print["I.S. = ", mt[[1]]];

varcormats = Inverse[Dot[suctderivtots, transsuctderivtots]] // MatrixForm
pr8 = Print["Variance-Covariance Matrix  =   ", varcormats];
(*Data set one*)
chisqtots1 = MSE / (Length[pH1] - Length[parvals]);
pr9 = Print["Chisquared Value for dataset1  =   ", chisqtots1];
stdevpar1s1 = Sqrt[varcormats[[1, 1, 1]] * chisqtots1];
stdevpar2s1 = Sqrt[varcormats[[1, 2, 2]] * chisqtots1];
stdevpar3s1 = Sqrt[varcormats[[1, 3, 3]] * chisqtots1];


corrpar1par1s = varcormats[[1, 1, 1]] / Sqrt[varcormats[[1, 1, 1]] * varcormats[[1, 1, 1]]]
corrpar1par2s = varcormats[[1, 1, 2]] / Sqrt[varcormats[[1, 1, 1]] * varcormats[[1, 2, 2]]];
corrpar1par3s = varcormats[[1, 1, 3]] / Sqrt[varcormats[[1, 1, 1]] * varcormats[[1, 3, 3]]];
corrpar2par2s = varcormats[[1, 2, 2]] / Sqrt[varcormats[[1, 2, 2]] * varcormats[[1, 2, 2]]];
corrpar2par3s = varcormats[[1, 2, 3]] / Sqrt[varcormats[[1, 2, 2]] * varcormats[[1, 3, 3]]];
corrpar3par3s = varcormats[[1, 3, 3]] / Sqrt[varcormats[[1, 3, 3]] * varcormats[[1, 3, 3]]];
```

10 | FH_3 sites Cr.nb

```
corrmats = ColumnForm[
    {{corrpar1par1s, corrpar1par2s, corrpar1par3s(*,corrpar1par4s,corrpar1par5s*)},
     {corrpar2par2s, corrpar2par3s(*,corrpar2par4s,corrpar2par5s*)},
     {corrpar3par3s(*,corrpar3par4s,corrpar3par5s*)}(*,
     {corrpar4par4s,corrpar4par5s},{corrpar5par5s}*)}];
pr15 = Print["Parameter correlations = ", corrmats];
stdevpar1s1 = Sqrt[varcormats[[1, 1, 1]] * chisqtots1];
stdevpar2s1 = Sqrt[varcormats[[1, 2, 2]] * chisqtots1];
stdevpar3s1 = Sqrt[varcormats[[1, 3, 3]] * chisqtots1];

pr13 = Print["Parameters for first dataset"];
pr10 = Print[parsymbols[[1]], " = " , parvals[[1]],  " (+/-) ",  stdevpar1s1];
pr11 = Print[parsymbols[[2]], " = " , parvals[[2]],  " (+/-) ",  stdevpar2s1];
pr12 = Print[parsymbols[[3]], " = " , parvals[[3]],  " (+/-) ",  stdevpar3s1];
```

References

Bargar, J.R., Kubicki, J.D., Reitmeyer, R., Davis, J.A., 2005. ATR-FTIR spectroscopic characterization of coexisting carbonate surface complexes on hematite. Geochim. Cosmochim. Acta 69, 1527–1542. https://doi.org/10.1016/j.gca.2004.08.002

Bompoti, N., Chrysochoou, M., Machesky, M., 2017. Surface structure of ferrihydrite: Insights from modeling surface charge. Chem. Geol., Adsorption of metals by geomedia III: Fundamentals and implications of metal adsorption 464, 34–45. https://doi.org/10.1016/j.chemgeo.2016.12.018

Brunauer, S., Emmett, P.H., Teller, E., 1938. Adsorption of Gases in Multimolecular Layers. J. Am. Chem. Soc. 60, 309–319. https://doi.org/10.1021/ja01269a023

Chrysochoou M.; Machesky M.; Johnston C. A new surface complexation model for chromate adsorption on ferrihydrite. Proceedings of the 13th International Conference on Environmental Science and Technology, paper 687, Athens, Greece, 5-7 September 2013.

Hiemstra, T., Rahnemaie, R., van Riemsdijk, W.H., 2004. Surface complexation of carbonate on goethite: IR spectroscopy, structure and charge distribution. J. Colloid Interface Sci. 278, 282–290. https://doi.org/10.1016/j.jcis.2004.06.014

Hiemstra, T., Riemsdijk, W.H.V., Rossberg, A., Ulrich, K.-U., 2009. A surface structural model for ferrihydrite II: Adsorption of uranyl and carbonate. Geochim. Cosmochim. Acta 73, 4437–4451. https://doi.org/10.1016/j.gca.2009.04.035

Johnston, C.P., Chrysochoou, M., 2016. Mechanisms of Chromate, Selenate, and Sulfate Adsorption on Al-Substituted Ferrihydrite: Implications for Ferrihydrite Surface Structure

and Reactivity. Environ. Sci. Technol. 50, 3589–3596. https://doi.org/10.1021/acs.est.5b05529

Johnston, C.P., Chrysochoou, M., 2012. Investigation of Chromate Coordination on Ferrihydrite by in Situ ATR-FTIR Spectroscopy and Theoretical Frequency Calculations. Environ. Sci. Technol. 46, 5851–5858. https://doi.org/10.1021/es300660r

Kabengi, N.J., Chrysochoou, M., Bompoti, N., Kubicki, J.D., 2017. An integrated flow microcalorimetry, infrared spectroscopy and density functional theory approach to the study of chromate complexation on hematite and ferrihdyrite. Chem. Geol., Adsorption of metals by geomedia III: Fundamentals and implications of metal adsorption 464, 23–33. https://doi.org/10.1016/j.chemgeo.2017.01.017

Sabur, M.A., Goldberg, S., Gale, A., Kabengi, N., Al-Abadleh, H.A., 2015. Temperature-Dependent Infrared and Calorimetric Studies on Arsenicals Adsorption from Solution to Hematite Nanoparticles. Langmuir 31, 2749–2760. https://doi.org/10.1021/la504581p

Schwertmann, U., Cornell, R.M., 2008. Iron Oxides in the Laboratory: Preparation and Characterization. John Wiley & Sons.

Veselská, V., Fajgar, R., Číhalová, S., Bolanz, R.M., Göttlicher, J., Steininger, R., Siddique, J.A., Komárek, M., 2016. Chromate adsorption on selected soil minerals: Surface complexation modeling coupled with spectroscopic investigation. J. Hazard. Mater. 318, 433–442. https://doi.org/10.1016/j.jhazmat.2016.07.002

Villacís-García, M., Ugalde-Arzate, M., Vaca-Escobar, K., Villalobos, M., Zanella, R., Martínez-Villegas, N., 2015. Laboratory synthesis of goethite and ferrihydrite of controlled particle sizes. Bol. Soc. Geológica Mex. 67, 433.

Villalobos, M., Antelo, J., 2012. A unified surface stuctural model for ferrihydrite: proton charge, electrolyte binding, and arsenate adsorption.

Xie, J., Gu, X., Tong, F., Zhao, Y., Tan, Y., 2015. Surface complexation modeling of Cr(VI) adsorption at the goethite–water interface. J. Colloid Interface Sci. 455, 55–62. https://doi.org/10.1016/j.jcis.2015.05.041

Zachara, J., Girvln, D., Schmidt, R., Resch, C., 1987. Chromate Adsorption on Amorphous Iron Oxyhydroxide in the Presence of Major Groundwater Ions. US Dep. Energy Publ.

CHAPTER 4 The MUSE II: Application to chromate binding on iron oxides

Nefeli Maria Bompoti, Maria Chrysochoou, and Michael Machesky

Under preparation, to be submitted at Environmental Science and Technology

Introduction

Fate and transport of pollutants in the subsurface is influenced by chemical reactions between mineral surfaces and aqueous solutions. Substantial effort has been devoted to characterize, simulate, and predict mineral - solution interactions under different environmental conditions. For the last 30 years, surface complexation models (SCMs) have been proven superior tools compared to traditional distribution factors (K_d), to describe adsorption processes and estimate the partitioning of ions at the solid – solution interface (Goldberg et al., 2007). Although SCMs are mechanistic and thus can potentially perform under different environmental conditions, they have been used mostly for the description of laboratory adsorption experiments. Their transferability to real systems is hindered by the high degree of parametrization required and the subsurface transport modeling is usually performed by empirical relationships or by generalized component (GC) models, which treats all soil components as one generic surface (Davis et al., 1998, 2004; Goldberg et al., 2007). Reducing the number of parameters to be determined or estimated in a natural system could be accomplished by considering various classes of surfaces, instead of individual minerals, as in the Particle Assemblage Model of Lofts and Tipping (1998), adopted later by Bonten et al. (2008) and Serrano et al. (2009). These studies utilized either non-electrostatic models or only a diffuse layer, in order to simplify the approach and reduce the number of fitted parameters. Surface types include organic matter, iron oxides, aluminum oxides, manganese oxides, silicates and clay minerals (Lofts and Tipping, 1998). The success of this approach is difficult to judge on the basis of these studies, which utilized real soils with highly variable properties. Specifically, it is difficult to distinguish between errors caused by faulty input (insufficient characterization of the soil) or the model itself.

The objective of this study is to adopt the particle assemblage approach for one surface class (iron oxyhydroxides and specifically goethite (GH), ferrihydrite (FH) and hematite (HT)) and one contaminant (chromate, CrO_4^{2-}), and investigate whether a single unified model can capture a variety of experimental conditions used in studies obtained from the literature and in studies conducted by the authors. The parameters required can be obtained from crystallographic studies (site densities, mineral face distribution), estimated by the properties in each individual system (specific surface area (SSA), solid concertation (Gs), or optimized by fitting experimental data (capacitance, proton, electrolyte, and ligand constants). Over the past decade, the RES^{3}T (Rossendorf Expert System for Surface and Sorption Thermodynamics) provided a digitized version of a thermodynamic sorption database (Brendler et al., 2003). In the following graph (Figure 4-1), the RES^{3}T thermodynamic constants for chromate adsorption on ferrihydrite and goethite (there are no SCM studies for chromate on hematite) are plotted for three types of SCMs. Summarized values are also shown in boxplots (Figure A4-5). The variability exhibited in both log Ks is relatively high; four and two log units for monodentate and bidentate complexes, respectively, for all three SCMs. Nevertheless, there is still considerable parameter variability within a given model (Figure 4-1), which further complicates the choice of thermodynamic constants for reactive transport modeling, even if a particular model is used.

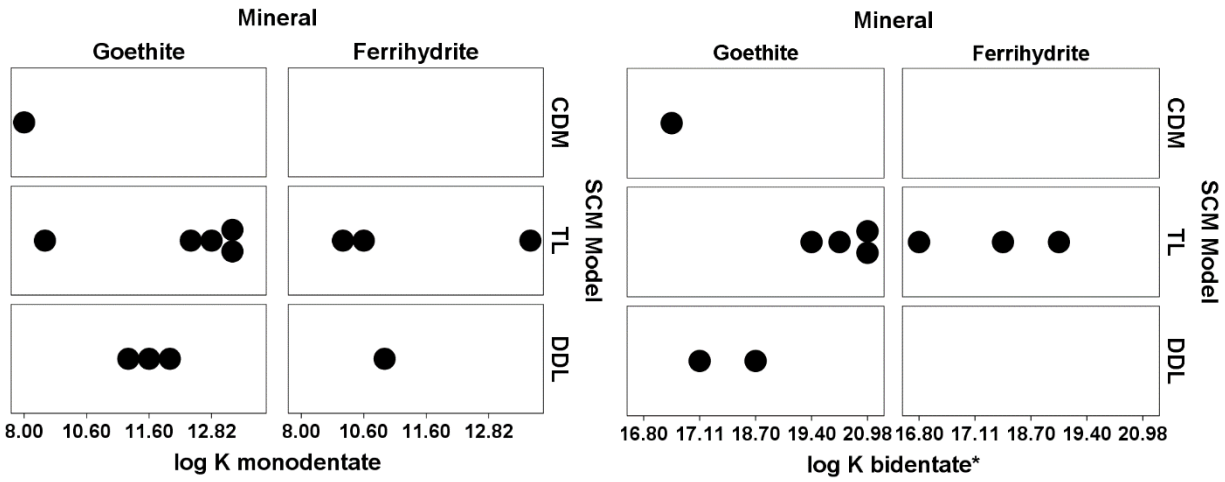

Figure 4-1. Thermodynamic constants for chromate adsorption on ferrihydrite and goethite reported by RES^{3}T database, plotted by surface complex, mineral, and SCM model (CDM: charge distribution multi - site surface complexation model (CD- MUSIC) (Hiemstra and Van Riemsdijk, 1996), TL: Triple –Layer Model (Davis et al., 1978; Yates et al., 1974), and DDL: (Dzombak and Morel, 1990; Stumm et al., 1970)). *The surface complex is suspected to be a bidentate species, although most the studies refer to it as a protonated monodentate species. Recent spectroscopic studies have shown that chromate forms two inner – sphere complexes, one modentate and one bidentate, on both ferrihydrite and goethite (Fendorf et al., 1997; Johnston and Chrysochoou, 2012).

We hypothesize that there are four possible reasons for parameter variability:

1. Optimization inconsistencies: That is the inability to find the global optimum parameters since algorithms are often trapped in local minima. In addition, subjective judgement on goodness of fit, instead of specific error criteria, might also lead to local optima. Better optimization tools are needed to facilitate the extraction of parameters that may lead to a consistent thermodynamic database. To optimize multiple parameters simultaneously, we

have recently proposed a new multi–start optimization algorithm for surface complexation parameter estimation (MUSE) (MUSE I).

2. Interdependency of SCM parameters: Thermodynamic constants for surface equilibrium depend on other parameters (i.e. capacitance, site density, surface area) (Hayes et al., 1991; Hwang and Lenhart, 2008; Sverjensky, 2003, 2005). Optimizing certain parameters implies fixing others, quite often arbitrarily, which often results in inconsistent results. The structural model for a particular mineral surface can differ among studies, thus increasing the variability of other parameters.
3. Other physical constraints that influence the affinity of the adsorbing ion for the surface. Adsorption affinity can vary with surface coverage. Thus studies encompassing different degrees of surface coverage may result in different fitted parameters.
4. Experimental or analytical error. Errors in pH, solid, and ligand concentration measurements increase the uncertainty of extracted parameters. However, quantifying those errors is difficult and is rarely even attempted.

Previous attempts have been made on unifying parameters for the same mineral surface. Dzombak and Morel (1990) described ion adsorption on FH by combing datasets from different studies using a generic 2-pK protonation formulation in combination with the Guoy-Chapman diffuse layer model. Although the FH structure was not yet known, the authors used mean and median values of site densities estimated by experimental data. Later studies employed the goethite surface structure and adjusted the proportion of crystallographic faces to describe the FH surface, such as the CD-MUSIC approach for adsorption of uranyl and carbonate (Hiemstra et al., 2009), and a 2-pK TLM for proton and arsenate adsorption (Villalobos and Antelo, 2012). Similarly, Ponthieu et al. (2006) used the CD – MUSIC

formalism to describe cation binding on both ferrihydrite and goethite using the goethite surface structure as a proxy and adjusted the crystallographic faces and capacitance values to describe FH behavior.

This study will build upon previous approaches by addressing three fundamental questions:

- Is the variability of log Ks driven by structural differences between the three iron oxides?
- What is the driving force for the uncertainty in log Ks?
- Can a unified model capture chromate adsorption on the three iron oxides?

Materials and Methods

Surface Complexation Modeling with the MUSE algorithm

In previous work, we have described the development of a MUlti–start algorithm to optimize Surface complexion Equilibrium parameters, the MUSE algorithm (MUSE I). Briefly, the MUSE algorithm is attached to a custom made SCM, built on Mathematica notebooks. The MUSE incorporates two algorithms for parameter optimization: one external that creates a random matrix of the initial matrix of parameters, and one internal (Nelder–Mead) that performs local optimizations for each initial set of parameters. The MUSE algorithm provides the global optimum of multiple parameters by comparing all the possible solutions based on the mean squared error (MSE). This approach is advantageous to the extent that multiple parameters can be optimized simultaneously (the choice of thermodynamic constants, capacitance, surface area, site densities), using a strict fitting criteria. It can also optimize directly quantitative spectroscopic pH – dependent profiles for individual surface complexes, extracting parameters consistent with spectroscopic observations.

Developing a unified model for the surface properties of iron oxides involves two steps: a) developing a unified model for proton adsorption, and/or b) developing a unified model for specific ion adsorption. Proton affinities are driven by the type of oxygen they attach to, as well as by the general electronic environment. The iron oxide contains singly (SC) and triply coordinated (TC) oxygens that contribute to surface charge, while doubly coordinated oxygens are considered inert and non-reactive under common environmental conditions (Hiemstra and Van Riemsdijk, 1996). The MUSIC approach has been used to calculate proton affinities based on bond valence and estimated proton constants can be highly variable for different sites on a surface; for example, the range of calculated log Ks for the ferrihydrite surface is between 3.3 and 12 (Hiemstra 2013). It is generally impractical to use a large number of variable sites to describe the surface charge; Hiemstra et al. (1996) showed that two sites were adequate to describe surface charge of goethite, while Bompoti et al. (2017) used three sites to describe the surface charge of several FH datasets with variable PZNPCs. In this paper, we adopted proton affinities specific to the surface structure of iron oxide and developed a single model for chromate adsorption. This relies on the hypothesis that proton affinity is different for each mineral, which is reflected by the charging curves, while specific ion affinity is similar, at least for chromate on iron oxides. Once the differences in surface structure are taken into account, the interaction energy from sorption of an ion is approximately the same for all iron oxides (Mathur and Dzombak, 2006). The is also supported by spectroscopic investigations of chromate adsorption in three ways: 1) both monodentate and bidentate complexes are formed when chromate binds on FH (Johnston and Chrysochoou, 2012, 2016), HT (Johnston and Chrysochoou, 2014), and GH (Fendorf et al., 1997), 2) both complexes have similar pH – dependency for FH and HT, as shown by optimized MCR – ALS profiles (Johnston and

Chrysochoou, 2014, 2016), and 3) while FH favors monodentate and HT bidentate complexation, this phenomenon is driven by differences in their surface structure (Kabengi et al., 2017).

Specifically, the SCM is based on the 1 - pK CD-MUSIC framework with a Basic Stern layer. Table A4-3 summarizes the surface complexation reactions, CD factors and respective complexation equilibrium constants. Briefly, protons were placed on the 0– plane, electrolyte ions on the 1– plane and chromate inner sphere complexes were distributed between the 0– and 1– planes by adjusting the CD values. The electrolyte equilibrium constants were adopted from studies of CD – MUSIC modeling on iron oxides, as previously discussed by Bompoti et al. (2017).

Ferrihydrite surface charge was simulated by a 3 – site model discussed in previous work (Bompoti et al., 2017). Briefly, the model consists of one SC and one TC group located on the $(1\bar{1}0)$ and $(1\bar{1}1)$ planes, and one TC site on the (001) and $(00\bar{1})$ faces. The site densities are taken as the summation of site densities proposed by Hiemstra (2013) and protonation log Ks are considered 8 for the $(1\bar{1}0)$ and $(1\bar{1}1)$ faces and 9.5 for the (001) and $(00\bar{1})$ faces. Surface properties for hematite and goethite were based on Venema et al. (1998) and included three surface sites: one SC and one TC located on the $(1\bar{1}0)$ face, and one SC on the (001) and (021) face for hematite and goethite, respectively. To describe the platy hematite crystals, the face distribution was taken to be 70% for (001) face and 30% for $(1\bar{1}0)$ face. For goethite, the dominant faces are the $(1\bar{1}0)$ at 90% and the (021) at 10% of the total surface area. To simplify the surface model, sites of the same type located on the same face were merged into one, by summing up their site densities. The protonation log Ks for hematite and goethite were adopted from Venema et al. (1998). For the merged sites, the log K_{H+} were fitted to titration curves. The fitted surface charge curves are shown in the Figure A4-7 and A4-8 in the SI. Table 4-1 summarizes the surface properties for the three minerals as used in the SCM.

Table 4-1. Surface properties for ferrihydrite, goethite and hematite.

Mineral	Site	Face	Face distribution (%)	Site density (sites/ nm^{-2})	Site density (sites/ nm^{-2}) accounting for face distribution	Log K_{H+}
	FeOH	$1\bar{1}0$	37.5	17.40	6.53	8.00
	Fe_3O	$1\bar{1}1$		15.90	5.96	8.00
	Fe_3O	001 $00\bar{1}$	12.5	6.60	0.83	9.50
Hematite[a]	FeOH	$1\bar{1}0$	30	5.00	1.50	7.70
	Fe_3O			5.00	1.50	8.20
	FeOH	001	70	5.00	3.50	10.50[b]
Goethite[a]	FeOH	$1\bar{1}0$	90	3.03	2.73	7.70
	Fe_3O			9.09	8.18	9.50[b]
	FeOH	021	10	7.50	0.75	12.00[b]

[a] Site densities for hematite and goethite from Venema et al., 1998
[b] Fitted values

For chromate adsorption, two surface species were considered, a non-protonated monodentate and a non-protonated bidentate complex, following previous spectroscopic studies on the three minerals (Fendorf et al., 1997; Johnston and Chrysochoou, 2012, 2014). The CD factors were based on the structure of the adsorbed ligand, and were fixed at -0.5 and -1.0 for the monodentate and bidentate chromate surface species, respectively (Rietra et al., 1999). In companion work, the thermodynamic constants for ferrihydrite chromate complexes were optimized by fitting a

spectroscopic dataset. However, we observed that these thermodynamic constants varied with the SSA logarithmically. In this study the equilibrium constants are fitted to chromate adsorption data, and further analyzed.

Cr adsorption datasets

Fitting and validation of the SCM for chromate was done using data collected in this study, as well as with data for chromate adsorption reported in the literature. Description of the experimental techniques for HT synthesis, characterization and collection of chromate batch data are provided at Supplemental Information (Figure A4-6). The chromate pH edges cover a broad range of surface coverage, background electrolyte types and concentrations, and sorbent surface areas. Table 2 summarizes the experimental details for all datasets. For FH, all studies used for SCM modeling FH prepared and aged less than 24 h, so they were considered fresh. While for FH and GH there are several datasets available, for HT the only data reported are from Ajouyed et al. (2010). This particular dataset exhibited atypical adsorption at high pH, showing a "tail" that were previously observed in data collected under CO_2 atmosphere (Wijnja and Schulthess, 2000). Since it is the only available dataset in the literature, it was included in the analysis. Table 4-2 provides the list of studies that were used in the analysis along with experimental details. For HT and GH, the measured BET surface area was used for modeling, while for FH most studies the theoretical value of 600 m^2/g was used.

Table 4-2. Chromate adsorption studies used in the SCM analysis.

Mineral	Study	CO_2 exclusion	Electrolyte	Ionic Strength (M)	Surface area (m^2/g)	Max surface coverage ($umol/m^2$)
Ferrihydrite	Bompoti et al.,	yes, but some CO_2	NaCl	0.01	347.2[a,b]	2.8
	Zachara et al. (1987)	yes	$NaNO_3$	0.1	600[b]	0.005, 0.1
	Davis and Leckie (1980)	yes	$NaNO_3$	0.1	600[b]	0.009
	Benjamin (1983)	yes	$NaNO_3$	0.1	600[b]	0.18
	Honeyman (1984)	no	$NaNO_3$	0.1	182[a], 600[b]	0.00038 - 0.02
	Hsia et al. (1993)	yes	$NaNO_3$	0.01	600[b]	0.86 – 2.11
Hematite	This study	yes, but some CO_2	NaCl	0.01	71.7[a]	2.00
	Ajouyed et al. (2010)	no	$NaNO_3$	0.01-0.1	1.7	0.27-1.31
Goethite	Mesuere and Fish (1992)	yes	KNO3	0.01 - 0.5	66[a]	0.42 - 2.3
	Villalobos and Pérez-Gallegos (2008)	yes	NaClO4	0.1	50[a], 70[a]	0.008, 0.0098
	Grossl et al. (1997)	yes	$NaNO_3$	0.01, 0.1	50[a]	1.9, 1.97
	Xie et al. (2015)	yes	$NaNO_3$	0.001 - 0.1	63.5[a]	0.83 - 2.00
	Weerasooriya and Tobschall (2000)	yes	$NaNO_3$	0.001 – 0.1	95[a]	0.02 -0.54
	Ajouyed et al. (2010)	no	$NaNO_3$	0.01 - 0.1	11.6[a]	0.04, 0.2

[a] BET measurement, [b] Surface area considered for modeling

Results and Discussion

Extracted parameters

Optimization on three parameters (two chromate log Ks and Stern layer capacitance) was performed for each of the datasets. Optimized parameters and fitted data are given in Table A4-4 and Figures A4-9, A4-10, and A4-11. The MUSE model was able to fit the majority of the datasets, with the exception of the HT data provided by Ajouyed et al. (2010). The model underestimated the adsorption at higher pH (pH > 8) and could not also capture the steep slope of the pH envelope. However, since the model was able to describe the acidic part of the pH envelope, the extracted parameters were included in the analysis. The optimized thermodynamic constants exhibited high variability over a broad range (0.03-13.43 and 12.79-21.62 for the monodentate and bidentate constants respectively). The median values are 10.58 for the equilibrium constant of monodentate constant, and 19.37 for the bidentate constant. Detailed descriptive statistics and boxplots are given in Table A4-5 and Figure A4-12 respectively, of the SI.

Effect of Specific Surface area

In companion work, the effect of SSA was quantified with the use of a spectroscopic dataset when three parameters were simultaneously optimized (log Ks and capacitance). To examine to what extent the SSA accounts for the variability of the equilibrium parameters, a sensitivity analysis on the effect of SSA was performed for several datasets. Two FH adsorption datasets (Dataset 1 from Zachara et al. (1987) and Dataset 2 from Honeyman (1984), and two GH datasets (Dataset 5 from Mesuere and Fish (1992) and Dataset 2 from Villalobos and Pérez-Gallegos (2008) were used for the sensitivity analysis. The results are shown in Figure 4-2 while the fit parameters are shown in Table A4-6 of the SI.

For all datasets, the equilibrium constants followed an inverse logarithmic trend with SSA, while the capacitance values also show an inverse relationship, i.e. the higher the SSA the lower the log Ks and capacitance. The logarithmic relationships, although of similar slope, do not follow the spectroscopic equations. For the monodentate constant two of the datasets (Mesuere and Fish (1992) and Zachara et al. (1987)) follow the spectroscopic trend (Figure 4-2a), while the dataset of Honeyman (1984) did not follow a logarithmic trend for some values of surface area. The dataset Villalobos and Pérez-Gallegos (2008) showed a similar trend, but it was shifted towards lower log Ks. Both datasets are for low surface coverage of chromate, 0.0008 umol/m^2 for Honeyman (1984) and 0.00098 umol/m^2 for Villalobos and Pérez-Gallegos (2008). The bidentate adsorption constant decreases logarithmically for all datasets but the trends are offset form each other (Figure 2b).

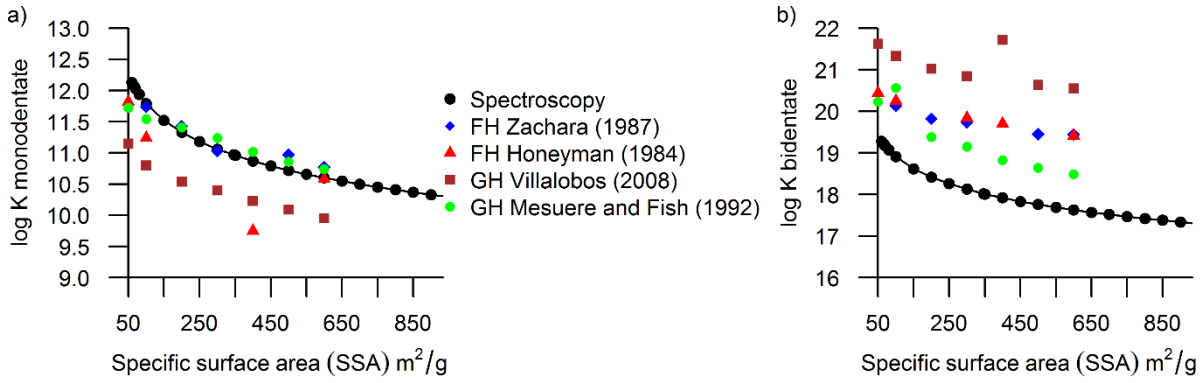

Figure 4-2. Surface area effect on (a) monodentate and (b) bidentate thermodynamic constants. Spectroscopic data set and trend line fitted (shown in MUSE I) (black dots). Logarithmic trend line for the monodentate constant: $\log K_{MD} = -0.664 \times \ln SSA + 14.85$ and bidentate constant: $\log K_{BD} = -0.717 \times \ln SSA + 22.22$.

Even when spectroscopic information is available to constrain the relative distribution between the two complexes, there is still dependency on SSA. An important outcome of this analysis is that the

SSA effect can account for up to two log units of variability for SSAs ranging between 50 and 600 m^2/g. These relationships do not differ between ferrihydrite and goethite, although there is variability among the individual datasets, this variability does not appear to depend on whether the mineral is ferrihydrite or goethite.

Effect of surface coverage

To evaluate the effect of surface coverage, the fit thermodynamic constants are plotted against surface coverage in Figure 4-3. The monodentate constant does show any surface coverage dependence, while the bidentate constant increases with decreasing surface coverage. There were too few data sets to calculate a trend line for hematite. Also, the GH datasets from Ajouyed et al. (2010) and Weerasooriya and Tobschall (2000) are considered outliers and were not included in the analysis. The trend lines for goethite and ferrihydrite have the same slope but the intercepts are offset by the two log units. We hypothesize that this difference can be explained by differences in SSAs, i.e. most FHs were modeled with SSA 600 m^2/g, while for goethite the SSA ranged from 11.6 to 95 m^2/g. If the SSA effect is taken into account by implementing the log K – SSA relationships for chromate, the dependency of the bidentate species on surface coverage is basically the same for all three minerals.

A surface coverage effect has been previously reported by Fendorf et al. (1997) for chromate adsorption on GH where the monodenate complex was favored at low surface coverages, while the bidentate complex was more prevalent at higher surface coverages. Our spectroscopic data exhibit the opposite trend, i.e. the bidentate complex decreases with increasing surface coverage, while the monodentate complex decreases. A surface coverage effect was also observed by Kabengi et al. (2017) who noted that the differential enthalpies of chromate adsorption on both

ferrihydrite and hematite decrease with increasing surface coverage. Similarly, Machesky et al. (1989) showed that adsorption enthalpies for several ions (salicylate, phosphate, iodate, and fluoride) decreased with increasing surface coverage on goethite at pH 4.

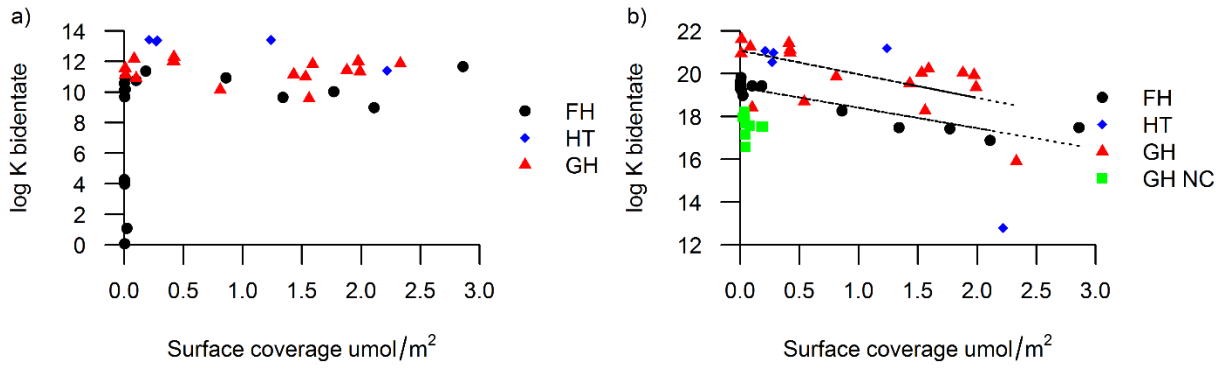

Figure 4-3. Optimized equilibrium constants for (a) monodentate and (b) bidentate complex with respect to surface coverage for the three minerals. The green squares (GH NC) represent the GH data that were not considered in the analysis (Ajouyed et al. (2010) and Weerasooriya and Tobschall (2000)). The linear trend lines shown at (b) are for GH: $\log K_{BD} = -1.11 \times Surface\ Coverage + 21.1, R^2 = 0.4$ and for FH: $\log K_{BD} = -0.96 \times Surface\ Coverage + 19.37, R^2 = 0.86$

Dzombak and Morel (1990) utilized low and high affinity surface groups to describe the adsorption at different densities. For anion adsorption, the affinity of both low and high affinity sites was considered uniform. Based on their approach, the affinity of the surface to the ion becomes too low to compete with the adsorbing protons at high adsorption densities, thus lowering the sorption constants. Specifically, Dzombak and Morel (1990) showed a decrease in the logarithm of the chromate affinity constant (for both high and low affinity sites) from 10.85 to 10.29, for an

estimated surface coverage of 0.001 umol/m^2 and 1.48 umol/m^2, respectively. That decrease was attributed to the decrease of surface charge in presence of chromate. However, the generalized two-layer model does not distinguish between monodentate and bidentate complexes. In comparison with their results, we show a much higher decrease of the bidentate constant, considering one type of surface groups.

Forward modeling

The development of a predictive model that accounts for the dependencies of thermodynamic constants on surface area and surface coverage is certainly not trivial. If we assume that the SSA of iron oxides can be estimated in the field, and that there is also an estimate for the surface coverage (solute and solid concentration). If surface coverage is unknown, then different model scenarios can be created to account for the variable conditions.

Specifically, we found that the monodentate equilibrium constant is not affected by the surface coverage, and therefore the relationship of SSA was considered as is ($\log K_{MD} = -0.664 \times \ln SSA + 14.85$). For the bidentate the effect of surface coverage was incorporated into the model by converting the spectroscopic relationships to different surface coverages. Since the spectroscopic relationships were extracted for a certain surface coverage, i.e. 2.3 umol/m^2, they were converted to three different surface coverages: a) very low ~ 0.0001 umol/m^2: $\log K_{BD} = -0.717 \times \ln SSA + 24.5$, b) intermediate ~ 1.5 umol/m^2: $\log K_{BD} = -0.717 \times \ln SSA + 23$, and c) high ~ 3 umol/m^2: $\log K_{BD} = -0.717 \times \ln SSA + 21.5$. The modeling results for seven random datasets are shown in Figure 4-4. In this modeling exercise, there is no fitting parameter, the capacitance value was considered constant, 0.95 C/m^2 for GH and 1.2 C/m^2 for FH to account for sphericity effects (Hiemstra and Van Riemsdijk, 2009).

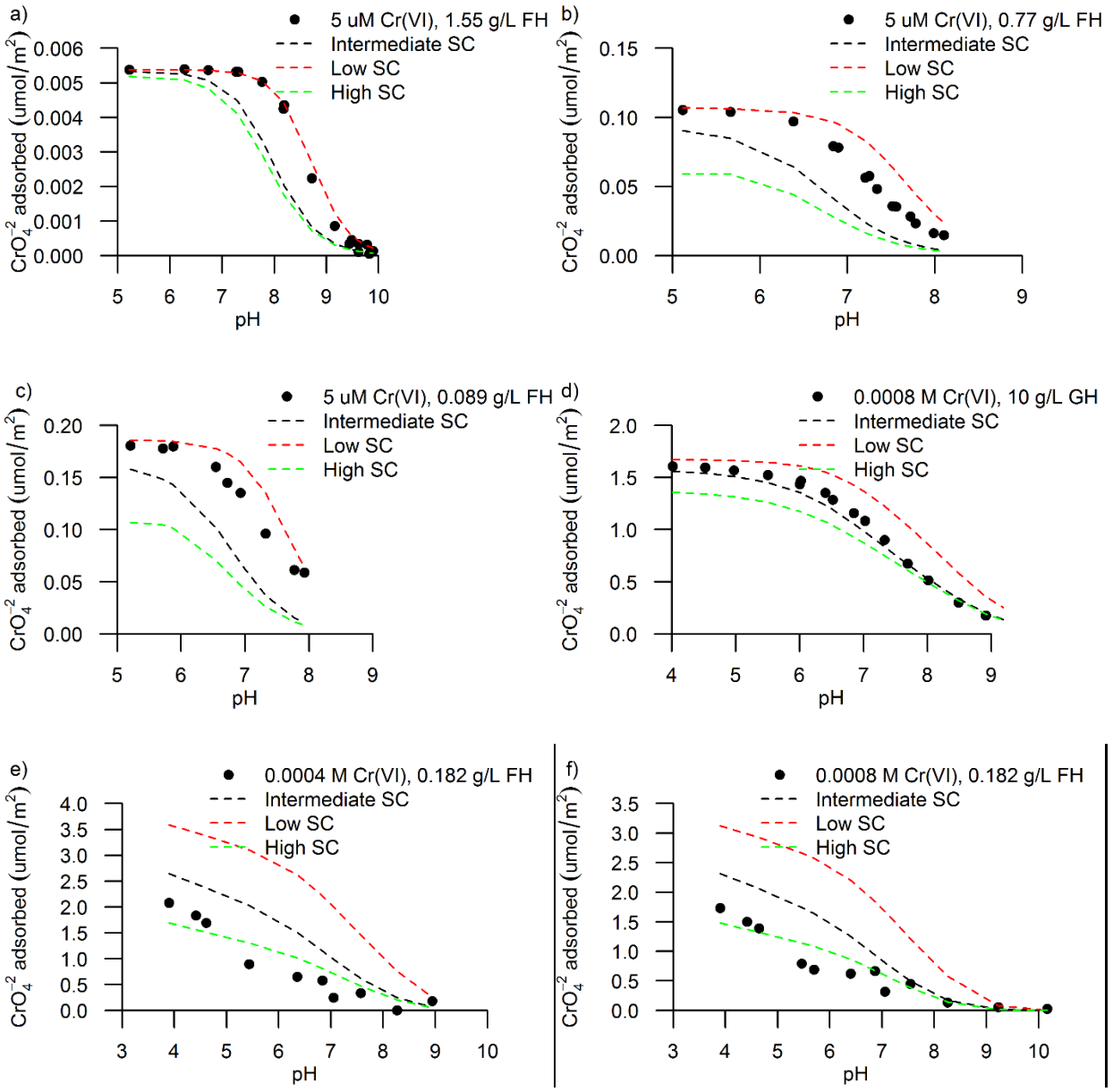
a)
5 uM Cr(VI), 1.55 g/L FH
Intermediate SC
Low SC
High SC
CrO_4^{-2} adsorbed (umol/m^2)
pH
b)
5 uM Cr(VI), 0.77 g/L FH
Intermediate SC
Low SC
High SC
CrO_4^{-2} adsorbed (umol/m^2)
pH
c)
5 uM Cr(VI), 0.089 g/L FH
Intermediate SC
Low SC
High SC
CrO_4^{-2} adsorbed (umol/m^2)
pH
d)
0.0008 M Cr(VI), 10 g/L GH
Intermediate SC
Low SC
High SC
CrO_4^{-2} adsorbed (umol/m^2)
pH
e)
0.0004 M Cr(VI), 0.182 g/L FH
Intermediate SC
Low SC
High SC
CrO_4^{-2} adsorbed (umol/m^2)
pH
f)
0.0008 M Cr(VI), 0.182 g/L FH
Intermediate SC
Low SC
High SC
CrO_4^{-2} adsorbed (umol/m^2)
pH

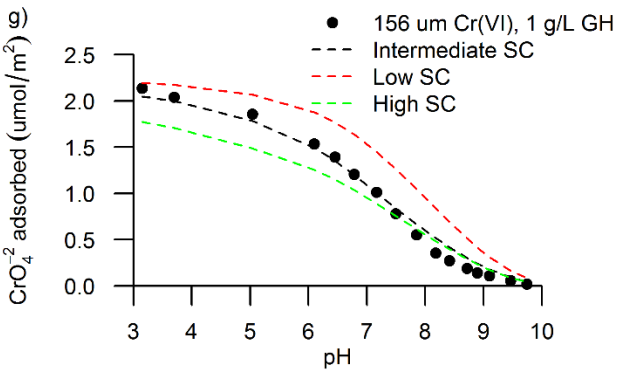

Figure 4-4. Model scenarios at three surface coverages (low, intermediate, high) for: a) Dataset 1 (Zachara et al., 1987), b) Dataset 2 (Zachara et al., 1987), c) Data from Benjamin (1983), d) Dataset 5 from Mesuere and Fish (1992), e) Dataset 1 from Hsia et al. (1993), f) Dataset 2 from Hsia et al. (1993), and g) Dataset 5 from Xie et al. (2015).

References

Ajouyed, O., Hurel, C., Ammari, M., Allal, L.B., Marmier, N., 2010. Sorption of Cr(VI) onto natural iron and aluminum (oxy)hydroxides: Effects of pH, ionic strength and initial concentration. J. Hazard. Mater. 174, 616–622. https://doi.org/10.1016/j.jhazmat.2009.09.096

Benjamin, M.M., 1983. Adsorption and surface precipitation of metals on amorphous iron oxyhydroxide. Environ. Sci. Technol. 17, 686–692. https://doi.org/10.1021/es00117a012

Bompoti, N., Chrysochoou, M., Machesky, M., 2016. Surface structure of ferrihydrite: Insights from modeling surface charge. Chem. Geol. https://doi.org/10.1016/j.chemgeo.2016.12.018

Bonten, L.T.C., Groenenberg, J.E., Weng, L., van Riemsdijk, W.H., 2008. Use of speciation and complexation models to estimate heavy metal sorption in soils. Geoderma 146, 303–310. https://doi.org/10.1016/j.geoderma.2008.06.005

Brendler, V., Vahle, A., Arnold, T., Bernhard, G., Fanghänel, T., 2003. RES3T-Rossendorf expert system for surface and sorption thermodynamics. J. Contam. Hydrol., 8th Internation Conference on Chemistry and Migration Behaviour of Actinides and Fission Products in the Geosphere - Migration 01 61, 281–291. https://doi.org/10.1016/S0169-7722(02)00129-8

Davis, J.A., Coston, J.A., Kent, D.B., Fuller, C.C., 1998. Application of the Surface Complexation Concept to Complex Mineral Assemblages. Environ. Sci. Technol. 32, 2820–2828. https://doi.org/10.1021/es980312q

Davis, J.A., James, R.O., Leckie, J.O., 1978. Surface ionization and complexation at the oxide/water interface. J. Colloid Interface Sci. 63, 480–499. https://doi.org/10.1016/S0021-9797(78)80009-5

Davis, J.A., Leckie, J.O., 1980. Surface ionization and complexation at the oxide/water interface. 3. Adsorption of anions. J. Colloid Interface Sci. 74, 32–43. https://doi.org/10.1016/0021-9797(80)90168-X

Davis, J.A., Meece, D.E., Kohler, M., Curtis, G.P., 2004. Approaches to surface complexation modeling of Uranium(VI) adsorption on aquifer sediments1. Geochim. Cosmochim. Acta 68, 3621–3641. https://doi.org/10.1016/j.gca.2004.03.003

Dzombak, D.A., Morel, F.M.M., 1990. Surface Complexation Modeling: Hydrous Ferric Oxide. John Wiley & Sons.

Fendorf, S., Eick, M.J., Grossl, P., Sparks, D.L., 1997. Arsenate and Chromate Retention Mechanisms on Goethite. 1. Surface Structure. Environ. Sci. Technol. 31, 315–320. https://doi.org/10.1021/es950653t

Goldberg, S., Criscenti, L.J., Turner, D.R., Davis, J.A., Cantrell, K.J., 2007. Adsorption–Desorption Processes in Subsurface Reactive Transport Modeling. Vadose Zone J. 6, 407. https://doi.org/10.2136/vzj2006.0085

Grossl, P.R., Eick, M., Sparks, D.L., Goldberg, S., Ainsworth, C.C., 1997. Arsenate and Chromate Retention Mechanisms on Goethite. 2. Kinetic Evaluation Using a Pressure-Jump Relaxation Technique. Environ. Sci. Technol. 31, 321–326. https://doi.org/10.1021/es950654l

Hayes, K.F., Redden, G., Ela, W., Leckie, J.O., 1991. Surface complexation models: An evaluation of model parameter estimation using FITEQL and oxide mineral titration data. J. Colloid Interface Sci. 142, 448–469. https://doi.org/10.1016/0021-9797(91)90075-J

Hiemstra, T., 2013. Surface and mineral structure of ferrihydrite. Geochim. Cosmochim. Acta 105, 316–325. https://doi.org/10.1016/j.gca.2012.12.002

Hiemstra, T.; Van Riemsdijk, W. H. A surface structural model for ferrihydrite I: Sites related to primary charge, molar mass, and mass density. Geochim. Cosmochim. Acta 2009, 73 (15), 423–4436.

Hiemstra, T., Riemsdijk, W.H.V., Rossberg, A., Ulrich, K.-U., 2009. A surface structural model for ferrihydrite II: Adsorption of uranyl and carbonate. Geochim. Cosmochim. Acta 73, 4437–4451. https://doi.org/10.1016/j.gca.2009.04.035

Hiemstra, T., Van Riemsdijk, W.H., 1996. A Surface Structural Approach to Ion Adsorption: The Charge Distribution (CD) Model. J. Colloid Interface Sci. 179, 488–508. https://doi.org/10.1006/jcis.1996.0242

Hiemstra, T., Venema, P., Riemsdijk, W.H.V., 1996. Intrinsic Proton Affinity of Reactive Surface Groups of Metal (Hydr)oxides: The Bond Valence Principle. J. Colloid Interface Sci. 184, 680–692. https://doi.org/10.1006/jcis.1996.0666

Hsia, T.H., Lo, S.L., Lin, C.F., Lee, D.Y., 1993. Chemical and spectroscopic evidence for specific adsorption of chromate on hydrous iron oxide. Chemosphere 26, 1897–1904. https://doi.org/10.1016/0045-6535(93)90083-H

Hwang, Y.S., Lenhart, J.J., 2008. The dependence of hematite site-occupancy standard state triple-layer model parameters on inner-layer capacitance. J. Colloid Interface Sci. 319, 206–213. https://doi.org/10.1016/j.jcis.2007.11.032

Johnston, C.P., Chrysochoou, M., 2016. Mechanisms of Chromate, Selenate, and Sulfate Adsorption on Al-Substituted Ferrihydrite: Implications for Ferrihydrite Surface Structure and Reactivity. Environ. Sci. Technol. 50, 3589–3596. https://doi.org/10.1021/acs.est.5b05529

Johnston, C.P., Chrysochoou, M., 2014. Mechanisms of chromate adsorption on hematite. Geochim. Cosmochim. Acta 138, 146–157. https://doi.org/10.1016/j.gca.2014.04.030

Johnston, C.P., Chrysochoou, M., 2012. Investigation of Chromate Coordination on Ferrihydrite by in Situ ATR-FTIR Spectroscopy and Theoretical Frequency Calculations. Environ. Sci. Technol. 46, 5851–5858. https://doi.org/10.1021/es300660r

Kabengi, N.J., Chrysochoou, M., Bompoti, N., Kubicki, J.D., 2017. An integrated flow microcalorimetry, infrared spectroscopy and density functional theory approach to the

study of chromate complexation on hematite and ferrihdyrite. Chem. Geol. https://doi.org/10.1016/j.chemgeo.2017.01.017

Lofts, S., Tipping, E., 1998. An assemblage model for cation binding by natural particulate matter. Geochim. Cosmochim. Acta 62, 2609–2625. https://doi.org/10.1016/S0016-7037(98)00183-5

Machesky, M.L., Bischoff, B.L., Anderson, M.A., 1989. Calorimetric investigation of anion adsorption onto goethite. Environ. Sci. Technol. 23, 580–587. https://doi.org/10.1021/es00063a011

Mathur, S.S., Dzombak, D.A., 2006. Chapter 16 - Surface complexation modeling: Goethite, in: Lützenkirchen, J. (Ed.), Interface Science and Technology, Surface Complexation Modelling. Elsevier, pp. 443–468. https://doi.org/10.1016/S1573-4285(06)80060-8

Mesuere, K., Fish, W., 1992. Chromate and oxalate adsorption on goethite. 1. Calibration of surface complexation models. Environ. Sci. Technol. 26, 2357–2364. https://doi.org/10.1021/es00036a004

Ponthieu, M., Juillot, F., Hiemstra, T., van Riemsdijk, W.H., Benedetti, M.F., 2006. Metal ion binding to iron oxides. Geochim. Cosmochim. Acta 70, 2679–2698. https://doi.org/10.1016/j.gca.2006.02.021

Rietra, R.P.J.J., Hiemstra, T., van Riemsdijk, W.H., 1999. The relationship between molecular structure and ion adsorption on variable charge minerals. Geochim. Cosmochim. Acta 63, 3009–3015. https://doi.org/10.1016/S0016-7037(99)00228-8

Serrano, S., O'Day, P.A., Vlassopoulos, D., García-González, M.T., Garrido, F., 2009. A surface complexation and ion exchange model of Pb and Cd competitive sorption on natural soils. Geochim. Cosmochim. Acta 73, 543–558. https://doi.org/10.1016/j.gca.2008.11.018

Stumm, W., Huang, C.P., Jenkins, S.R., 1970. Specific chemical interaction affecting stability of dispersed systems. Croat. Chem. Acta 42, 223.

Sverjensky, D.A., 2005. Prediction of surface charge on oxides in salt solutions: Revisions for 1:1 (M+L−) electrolytes. Geochim. Cosmochim. Acta 69, 225–257. https://doi.org/10.1016/j.gca.2004.05.040

Sverjensky, D.A., 2003. Standard states for the activities of mineral surface sites and species. Geochim. Cosmochim. Acta 67, 17–28. https://doi.org/10.1016/S0016-7037(02)01074-8

Venema, P., Hiemstra, T., Weidler, P.G., van Riemsdijk, W.H., 1998. Intrinsic Proton Affinity of Reactive Surface Groups of Metal (Hydr)oxides: Application to Iron (Hydr)oxides. J. Colloid Interface Sci. 198, 282–295. https://doi.org/10.1006/jcis.1997.5245

Villalobos, M., Antelo, J., 2012. A unified surface stuctural model for ferrihydrite: proton charge, electrolyte binding, and arsenate adsorption.

Villalobos, M., Pérez-Gallegos, A., 2008. Goethite surface reactivity: A macroscopic investigation unifying proton, chromate, carbonate, and lead(II) adsorption. J. Colloid Interface Sci. 326, 307–323. https://doi.org/10.1016/j.jcis.2008.06.026

Weerasooriya, R., Tobschall, H.J., 2000. Mechanistic modeling of chromate adsorption onto goethite. Colloids Surf. Physicochem. Eng. Asp. 162, 167–175. https://doi.org/10.1016/S0927-7757(99)00229-0

Wijnja, H., Schulthess, C.P., 2000. Interaction of Carbonate and Organic Anions with Sulfate and Selenate Adsorption on an Aluminum Oxide. Soil Sci. Soc. Am. J. 64, 898–908. https://doi.org/10.2136/sssaj2000.643898x

Xie, J., Gu, X., Tong, F., Zhao, Y., Tan, Y., 2015. Surface complexation modeling of Cr(VI) adsorption at the goethite–water interface. J. Colloid Interface Sci. 455, 55–62. https://doi.org/10.1016/j.jcis.2015.05.041

Yates, D.E., Levine, S., Healy, T.W., 1974. Site-binding model of the electrical double layer at the oxide/water interface. J. Chem. Soc. Faraday Trans. 1 Phys. Chem. Condens. Phases 70, 1807. https://doi.org/10.1039/f19747001807

Zachara, J., Girvln, D., Schmidt, R., Resch, C., 1987. Chromate Adsorption on Amorphous Iron Oxyhydroxide in the Presence of Major Groundwater Ions. US Dep. Energy Publ.

Appendix – Chapter 4

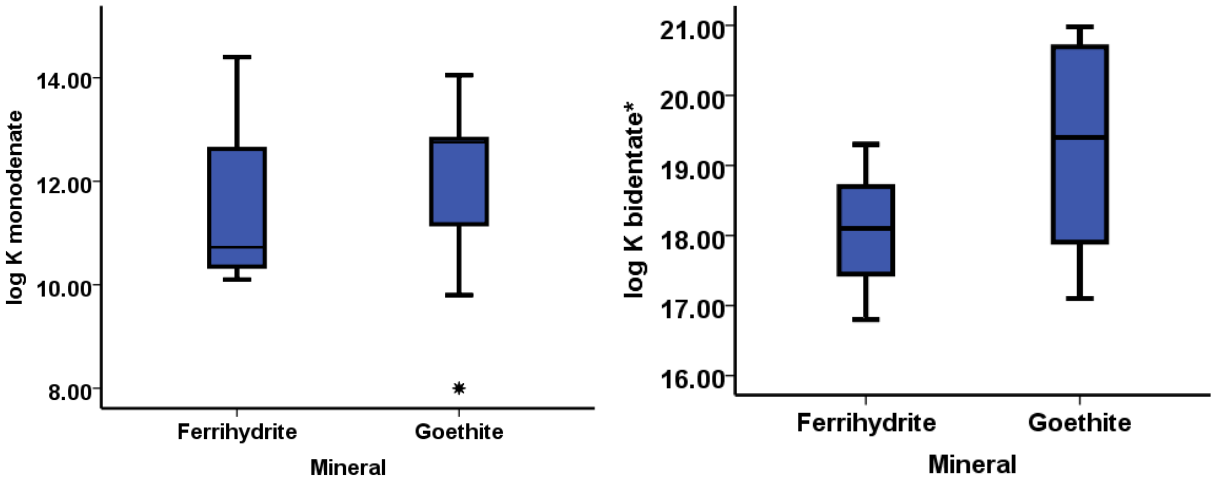

Figure A4-5. Thermodynamic constants for chromate adsorption on ferrihydrite and goethite reported by RES3T database. Boxplots for all SCM models categorized by mineral and type of surface complex.

Experimental Methods

Mineral synthesis and characterization

HT was synthesized by heating 2 L of 0.002 M HNO_3 to 98 °C and adding 16.16 g of $Fe(NO_3)_3 \cdot 9H_2O$ crystals while the solution was continuously stirred (Schwertmann and Cornell, 2000). The freshly prepared suspension was immediately centrifuged and dialyzed to remove excess electrolytes until the conductivity was less than ~ 20 μS/cm. The concentration of the suspension was estimated gravimetrically to be 34.8 g/L. Specific Surface Area (SSA) was measured to be 71.7 m^2/g by N_2 adsorption isotherms using the BET method (Brunauer et al., 1938). The FH sample was air – dried, ground, and then outgassed for 3 h at 150 °C. A Quantochrome NovaWin surface area analyzer with an 11 – point data calculation was used for the BET measurements. Transmission electron microscopy (TEM) images (Figure A4-6) were obtained using a FEI TEM Talos F200X instrument. The TEM samples were prepared by sonicating 0.3 g/L suspensions for 3 h, diluting 1 drop of suspension with 10 drops of ethanol after which an aliquot was deposited to lacey carbon coated copper grid. The hematite particles are mostly diamond shaped with some irregular particles and their diameters ranged from 13 to 51 nm, with a median value of 36 nm. The particle size is in agreement with Method 1 of Schwertmann and Cornell (2000). The high surface area can be attributed to surface irregularities.

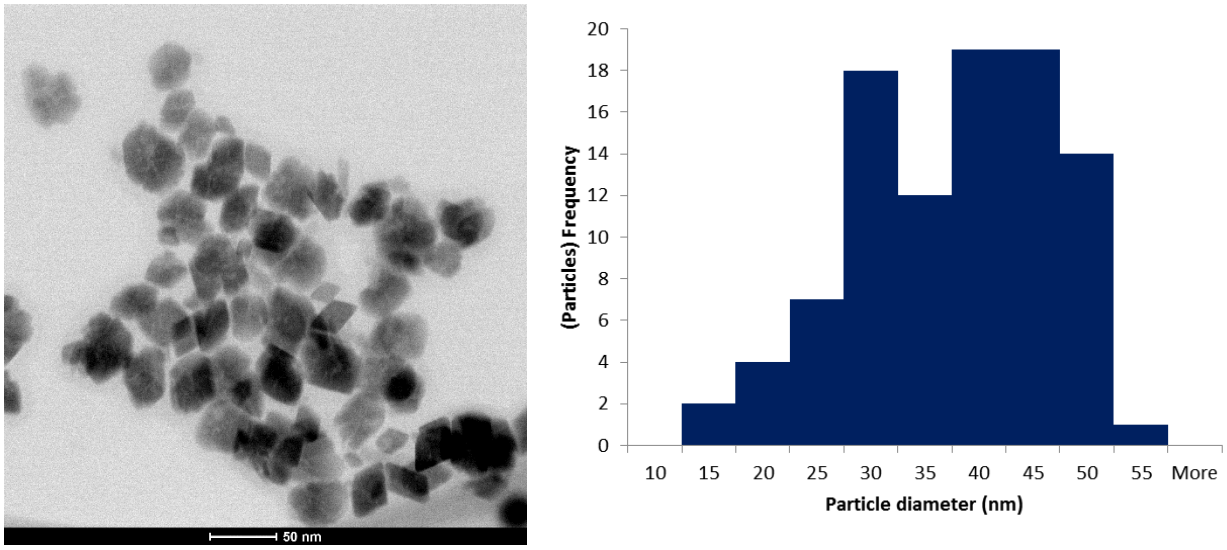

Figure A4-6. TEM images of hematite particles and the histogram of particle sizes.

Batch tests

Chromate adsorption (CrO_4^{2-}) on HT was measured in batch experiments at different pH values at 0.01 M ionic strength (NaCl). ACS certified reagents were used and the batches were prepared in 50 mL polypropylene centrifuge tubes. A 10 mM CrO_4^{2-} stock solution was prepared from Na_2CrO_4 the same day of the experiments. A solution of the 0.5 mM CrO_4^{2-}, ionic strength (0.01 M NaCl) and different amounts of acid (0.1 M HCl) or base (0.1 M NaOH) were added to each batch. The HT suspension was then added to the solutions to yield a concentration of 1 g/L. After shaking for 24 h, the suspensions were centrifuged for 10 min at 3500 rpm and filtered with a 0.2 µm membrane. The supernatant was analyzed for chromate using the EPA7196A colorimetric method with a GENESYS^{TM} 20 Visible Spectrophotometer. The pH of the supernatant was measured with a Metrohm pH Unitrode PT1000 glass electrode that was previously calibrated with three Metrohm calibration buffers.

Surface Complexation Model

The Surface Complexation model incorporated with the surface reactions given in Table A4-3.

Table A4-3. CD – MUSIC surface complexation reactions for protonation, electrolyte ions, chromate, and carbonate binding.

Protonation reactions	**log K**	**ΔZ_0**	**ΔZ_1**
$\equiv FeOH_i^{-0.5} + H^+ \leftrightarrow \equiv FeOH_{2i}^{+0.5}$	log K_i	1	
$\equiv Fe_3O_j^{-0.5} + H^+ \leftrightarrow \equiv Fe_3OH_j^{+0.5}$	log Kj	1	
Electrolytes – surface reactions	**log K**	**ΔZ_0**	**ΔZ_1**
$\equiv FeOH_i^{-0.5} + Na^+ \leftrightarrow [\equiv FeOH^{-0.5}\text{-}Na^+]^{+0.5}$	-0.60		1
$\equiv Fe_3O_j^{-0.5} + Na^+ \leftrightarrow [\equiv Fe_3O_j^{-0.5}\text{-}Na^+]^{+0.5}$	-0.60		1
$\equiv FeOH_i^{-0.5} + K^+ \leftrightarrow [\equiv FeOH^{-0.5}\text{-}K^+]^{+0.5}$	-1.61		1
$\equiv Fe_3O_j^{-0.5} + K^+ \leftrightarrow [\equiv Fe_3O_j^{-0.5}\text{-}K^+]^{+0.5}$	-1.61		1
$\equiv FeOH_i^{-0.5} + Cl^- + H^+ \leftrightarrow [\equiv FeOH_{2i}^{+0.5}\text{-}Cl^-]^{-0.5}$	-0.45	1	-1
$\equiv Fe_3O_j^{-0.5} + Cl^- + H^+ \leftrightarrow [\equiv Fe_3OH_j^{+0.5}\text{-}Cl^-]^{-0.5}$	-0.45	1	-1
$\equiv FeOH_i^{-0.5} + NO_3^- + H^+ \leftrightarrow [\equiv FeOH_{2i}^{+0.5}\text{-}NO_3^-]^{-0.5}$	-0.68	1	-1
$\equiv Fe_3O_j^{-0.5} + NO_3^- + H^+ \leftrightarrow [\equiv Fe_3OH_j^{+0.5}\text{-}NO_3^-]^{-0.5}$	-0.68	1	-1
$\equiv FeOH_i^{-0.5} + ClO_4^- + H^+ \leftrightarrow [\equiv FeOH_{2i}^{+0.5}\text{-}ClO_4^-]^{-0.5}$	-1.70	1	-1
$\equiv Fe_3O_j^{-0.5} + ClO_4^- + H^+ \leftrightarrow [\equiv Fe_3OH_j^{+0.5}\text{-}ClO_4^-]^{-0.5}$	-1.70	1	-1
Outer sphere complexation reactions	**log K**	**ΔZ_0**	**ΔZ_1**
$\equiv FeOH_i^{-0.5} + H^+ + CrO_4^{2-} \leftrightarrow [\equiv FeOH_{2i}^{+0.5}\text{-}CrO_4^{2-}]^{-1.5}$	Fitted	1	-1
Inner sphere complexation reactions	**log K**	**ΔZ_0**	**ΔZ_1**
$\equiv FeOH_i^{-0.5} + H^+ + CrO_4^{2-} \leftrightarrow \equiv FeOCrO_3^{-1.5} + H_2O$	Fitted	0.5	-1.5
$2\equiv FeOH_i^{-0.5} + 2H^+ + CrO_4^{2-} \leftrightarrow (\equiv FeO)_2CrO_2^{-1} + 2H_2O$	Fitted	1	-1
$2\equiv FeOH_i^{-0.5} + 2H^+ + CO_3^{2-} \leftrightarrow (\equiv FeO)_2CO^{-1} + 2H_2O$	21.3	1	-1
$2\equiv FeOH_i^{-0.5} + 2H^+ + CO_3^{2-} \leftrightarrow [(\equiv FeOH_2)_2\text{-}CO_3^{2-}]^{-1}$	-5.3	1.6	-1.6

Briefly, protons were placed on the 0 – plane, electrolyte ions on the 1 – plane, and chromate and carbonate inner sphere complexes were distributed between the 0 – and 1– planes by adjusting the CD values at the commonly accepted values for monodentate and bidentate species. The

electrolyte equilibrium constants were adopted from studies employing CD–MUSIC modeling on iron oxides, as previously discussed by Bompoti et al. (2017). For inner – sphere complexation, two surface species for chromate were considered, a non-protonated monodentate and a non-protonated bidentate complex, according to previous spectroscopic studies on FH (Johnston and Chrysochoou, 2016, 2012).

The ferrihydrite surface charge was simulated by a 3 – site model discussed in previous work (Bompoti et al., 2017). Briefly, the model consists of one SC and one TC group located on the $(1\bar{1}0)$ and $(1\bar{1}1)$ planes, and one TC site on the (001) and $(00\bar{1})$ faces. The site densities are taken as the summation of site densities proposed by Hiemstra (2013) and protonation log Ks are considered 8 for the $(1\bar{1}0)$ and $(1\bar{1}1)$ faces and 9.5 for the (001) and $(00\bar{1})$ faces. The purpose of this approach was to capture differences both in terms of charging values on mass and surface area basis, as well as differences in the PZNPC, which ranges between 8.0 and 8.7. These variations appear to be driven by the size of FH crystals, which are related to the precipitation methods and most likely aging during and after preparation (Villacís-García et al., 2015). The proposed surface model was able to capture the charging behavior of both fresh and aged FH by an increasing the contribution of the basal planes for aged FH. In this study, we used site densities for the fresh FH model since the chromate pH edges in this study were performed with fresh FH.

For carbonate adsorption, a non – protonated bidentate complex and a binuclear outer sphere/ hydrogen bonded carbonate complex were considered. Based on spectroscopic observations of hematite (α-Fe_2O_3) (Bargar et al., 2005) and goethite (α-FeOOH) (Hiemstra et al., 2004), carbonate forms bidentate complexes on singly – coordinated sites, while Bargar et al. (2005) also noticed an outer-sphere/ hydrogen bonded complex at the hematite interface. To optimize equilibrium constants for both species, carbonate adsorption data on FH obtained from Zachara et al. (1987)

were fitted in previous work (Chrysochoou et al., 2013). The SSA was maintained at 600 m2/g, as suggested by Zachara et al. (1987), although better fits have been reported in the literature for higher SSAs (Hiemstra et al., 2009). The optimized log K for the non-protonated bidentate species was 21.3, and the outer – sphere constant was -5.3. However, more research is needed to better elucidate the carbonate adsorption mechanisms by ferrihydrite and to optimize thermodynamic constants, which is ongoing in our laboratory.

Surface Charge Modeling

For HT, the surface structural model was evaluated by fitting potentiometric titrations provided by Venema et al. (1998) and Penners et al. (1986). The modeling was performed by optimizing the capacitance value in order to best fit the surface charge data. The model fits are given in Figure A4-7. The capacitance values optimized were C_{stern} 1.403 F/m^2 for the data of Venema et al. (1998), and 1.34 F/m^2 for Penners et al. (1986). The model was able to capture both the charging values and the PZNPC for the two datasets (9.55 for Venema et al. (1998), and 9.7 for Penners et al. (1986)). For the dataset of Penners et al. (1986), the surface charge at high ionic strength (1 M KCl) was underestimated (Fig. S2b). Deviation of modeling fits at high ionic strengths has been

discussed extensively by Sahai and Sverjensky (1997). This effect could also been attributed to the estimation of activity coefficients. The activity coefficients were estimated with Davies Equation for $I < 0.5$ M while specific ion interaction theory (SIT) was used for $I \geq 0.5$ M. For both datasets, the modeling results were satisfactory for ionic strengths at and below 0.1 M.

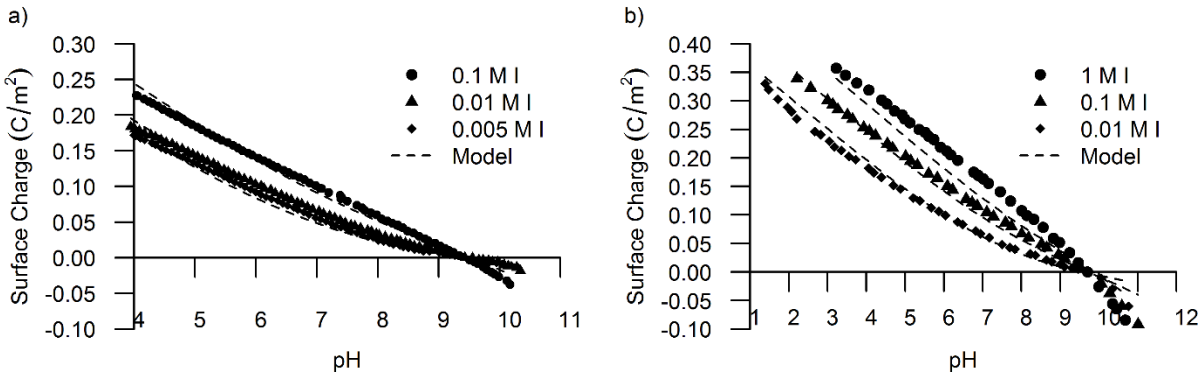

Figure A4-7. Surface charge modeling (dashed lines) and titration data from a) Venema et al. (1998) and b) Penners et al. (1986).

Surface charge data from different GHs were used to test the validity of the GH surface model. The titration datasets included GHs in different background electrolytes (KNO_3, $NaNO_3$, NaCl) and different SSAs (70.8, 95, 70 m^2/g), as given in three different studies (Antelo et al., 2005; Venema et al., 1996; Villalobos and Leckie, 2001). The SCM yielded different capacitance values: C_{stern} of 0.86 F/m^2 (Figure A4-8a), C_{stern} of 0.68 F/m^2 (Figure A4-8b), and 0.98 F/m^2 (Figure A4-8c). In all vases the model was able to capture the PZNPC of 9.3. The capacitance values extracted show an inverse relationship to SSA; datasets with higher SSAs resulted in lower capacitance values. This have been observed in previous studies for HT (Hwang and Lenhart, 2008), but there is also evidence that triple layer model capacitance values depend on the hydrated radii of the electrolyte cation for various minerals. To our understanding capacitance values are interdependent with several parameters, such as SSA and site density, the effect of cation radii is of secondary importance.

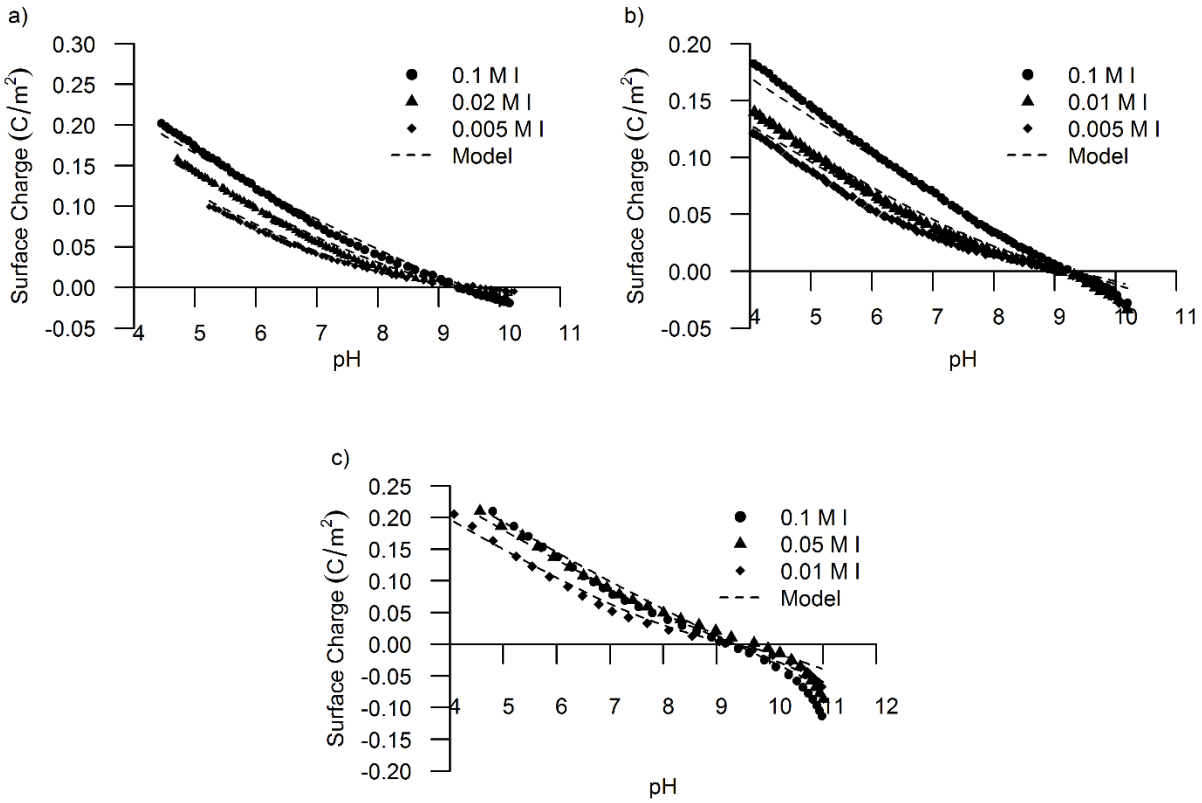

Figure A4-8. Surface charge modeling (dashed lines) and titration data from a) Antelo et al. (2005), b) Venema et al. (1996), and c) Villalobos and Leckie (2001).

Table A4-4. Optimized parameters for all the available chromate adsorption datasets.

Studies	Dataset	SSA (m^2/g)	Max Surface Coverage (umol/m^2)	C_{stern} (C/m^2)	log K MD	log K BD	Mean squared error (MSE)	Model selection criterion (MSC)
			FH					
Bompoti et al., 2018	1	347.2	2.86	1.03	11.67	17.48	5.31E-10	4.0336
Zachara et al. (1987)	1		0.1	0.86	10.77	19.44	5.14E-15	5.570
	2	600	0.0054	2.58	10.92	19.83	4.65E-15	6.554
Davies and Leckie (1980)	1	600	0.0087	1.99	10.18	19.22	2.85E-16	3.717
Benjamin (1983)	1	600	0.18	0.44	11.38	19.44	4.51E-14	4.246

	1	600	0.00038	3.00	4.29	19.33	7.36E-19	2.771
	2	600	0.00083	1.88	10.58	19.41	1.09E-18	2.075
	3	600	0.000365	3.00	4.23	19.62	2.21E-18	2.109
	4	600	0.0024	2.12	10.15	19.42	1.21E-18	2.941
	5	600	0.0029	1.63	0.07	19.36	2.85E-17	3.131
	6	600	0.0029	1.36	9.69	19.40	1.15E-17	3.885
Honeyman	7	600	0.00387	2.99	3.99	19.43	1.73E-17	3.129
(1984)	8	600	0.022	2.57	1.09	18.98	6.60E-18	4.655
	1	600	2.11	1.63	8.99	16.88	3.58E-10	2.227
	2	600	1.77	1.03	10.04	17.42	3.17E-10	1.918
	3	600	1.34	0.98	9.66	17.49	1.92E-10	1.734
Hsia 1993	4	600	0.86	0.50	10.93	18.27	5.13E-11	2.325
				HT				
This study	1	71.7	2.22	2.12	11.40	12.79	6.05E-11	3.716
	1		0.27	0.30	13.30	20.55	3.80E-14	1.642
	2		0.28	0.30	13.41	20.98	3.60E-14	1.683
Ajouyed et	3		0.21	0.30	13.43	21.08	3.62E-14	1.64
al. (2010)	4	1.7	1.24	0.57	13.42	21.19	7.39E-13	2.119
				GH				
	1		0.41	0.37	12.00	21.43		
	2		0.42	0.56	12.01	20.98	7.79E-13	5.750
	3		0.42	0.39	12.30	21.12	1.83E-12	4.609
	4		2.33	1.45	11.87	15.90	1.59E-11	5.851
Mesuere and	5		1.59	1.13	11.82	20.23	3.10E-12	
Fish (1992)	6	66	0.084	0.47	12.19	21.26	4.17E-14	5.234
Villalobos	1	70	0.0071	1.54	11.56	20.95	9.67E-14	3.424
and Pérez-Gallegos (2008)	2	50	0.0098	0.30	11.15	21.62	5.74E-15	5.752
Grossl et al.	1	50	1.88	1.09	11.44	20.05	2.43E-10	5.269
(1997)	2	50	1.975	1.19	12.01	19.94	9.03E-10	3.905
	1		1.43	2.39	11.15	19.54	1.93E-11	3.439
	2		1.53	1.21	11.00	20.04	6.58E-12	4.813
	3		1.56	2.92	9.58	18.27	1.69E-11	
	4		1.99	1.37	11.35	19.37	4.86E-12	5.711
	5		0.81	1.05	10.14	19.86	1.48E-12	5.375
Xie et al. (2015)	6	63.5	0.1	1.28	10.90	18.42	5.96E-14	4.186
	1		0.045	3.00	7.33	16.58	1.83E-13	2.901
	2		0.043	2.96	7.82	17.16	6.58E-12	4.813
	3		0.042	2.95	9.33	17.83	3.42E-13	2.311
	4		0.54	1.12	9.04	18.70	2.76E-11	2.380
Weerasooriya	5		0.178	2.99	7.72	17.53	3.05E-12	2.679
and Tobschall	6		0.079	3.00	8.62	17.56	5.69E-12	0.339
(2000)	7	95	0.022	3.00	0.03	17.96		

	1		0.039	2.10	9.02	17.69	1.85E-14	2.847
	2		0.038	2.46	9.83	17.99	9.34E-15	3.425
Ajouyed et	3		0.038	2.22	10.24	18.24	1.37E-14	3.053
al. (2010)	4	11.6	0.195	2.84	8.71	17.53	2.10E-13	3.661

Simulated datasets

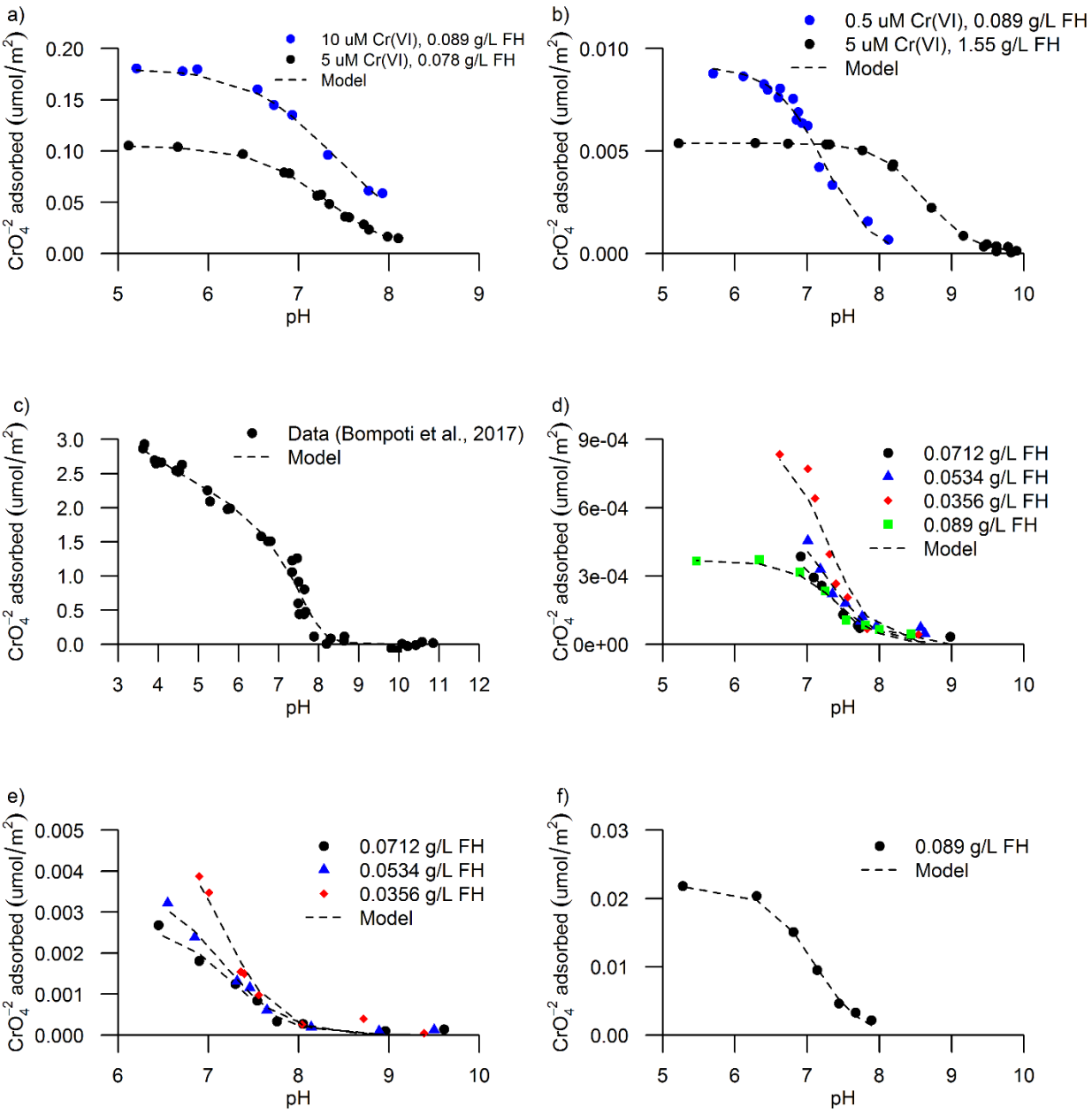

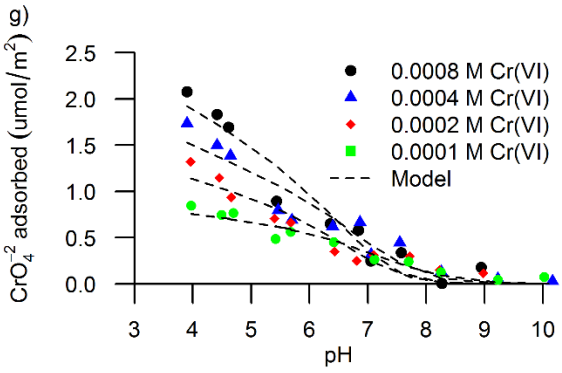

Figure A4-9. Chromate adsorption modeling on FH (dashed lines) at different conditions: a) 5 uM Cr(VI) and 0.078 g/L FH (Zachara et al., 1987), and 10 uM Cr(VI) and 0.089 g/L FH (Benjamin, 1983), b) 5 uM Cr(VI) and 1.54 g/L FH (Zachara et al., 1987) and 0.5 uM Cr(VI) and 0.089 g/L FH (Davis and Leckie, 1980), c) 1 mM and 0.5 g/L FH (Bompoti et al., 2018), d) 0.02 uM Cr(VI) at different solid concentrations (Honeyman, 1984), e) 0.02 uM Cr(VI) at different solid concentrations (Honeyman, 1984) f) 0.02 uM Cr(VI) Honeyman (1984), and g) 0.182 g/L FH at different Cr(VI) concentrations (Hsia et al., 1993).

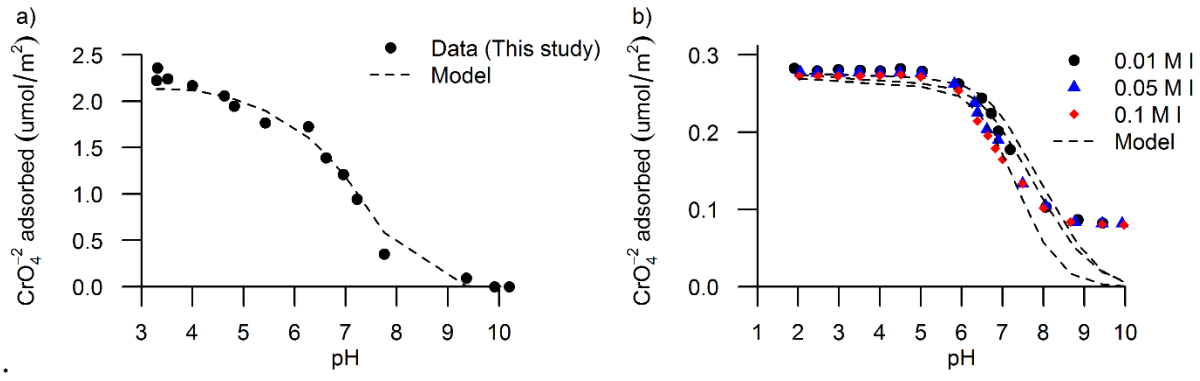

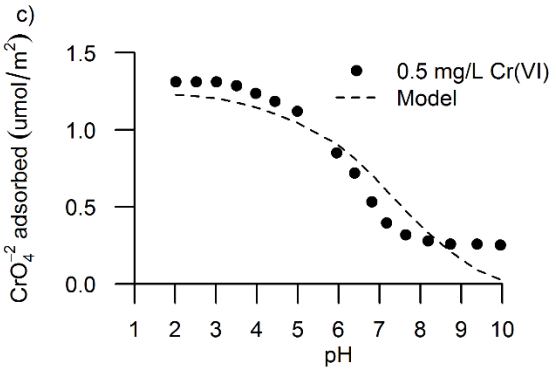

Figure A4-10. Chromate adsorption modeling on HT (dashed lines) at different conditions: a) 1 mM and 1 g/L HT (this study), b) 0.1 mg/ l Cr(VI) at different ionic strength (Ajouyed et al., 2010), and c) 0.01 M I and 0.5 mg/ l Cr(VI) (Ajouyed et al., 2010)

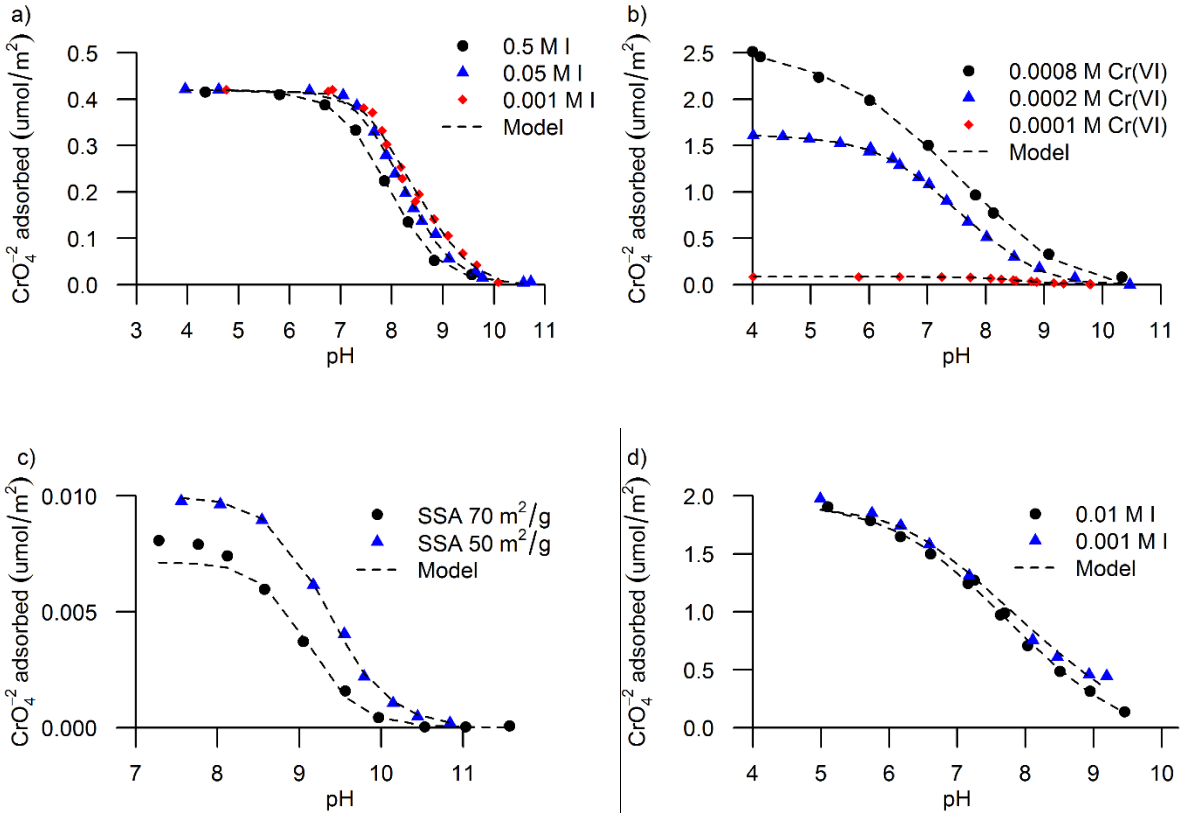

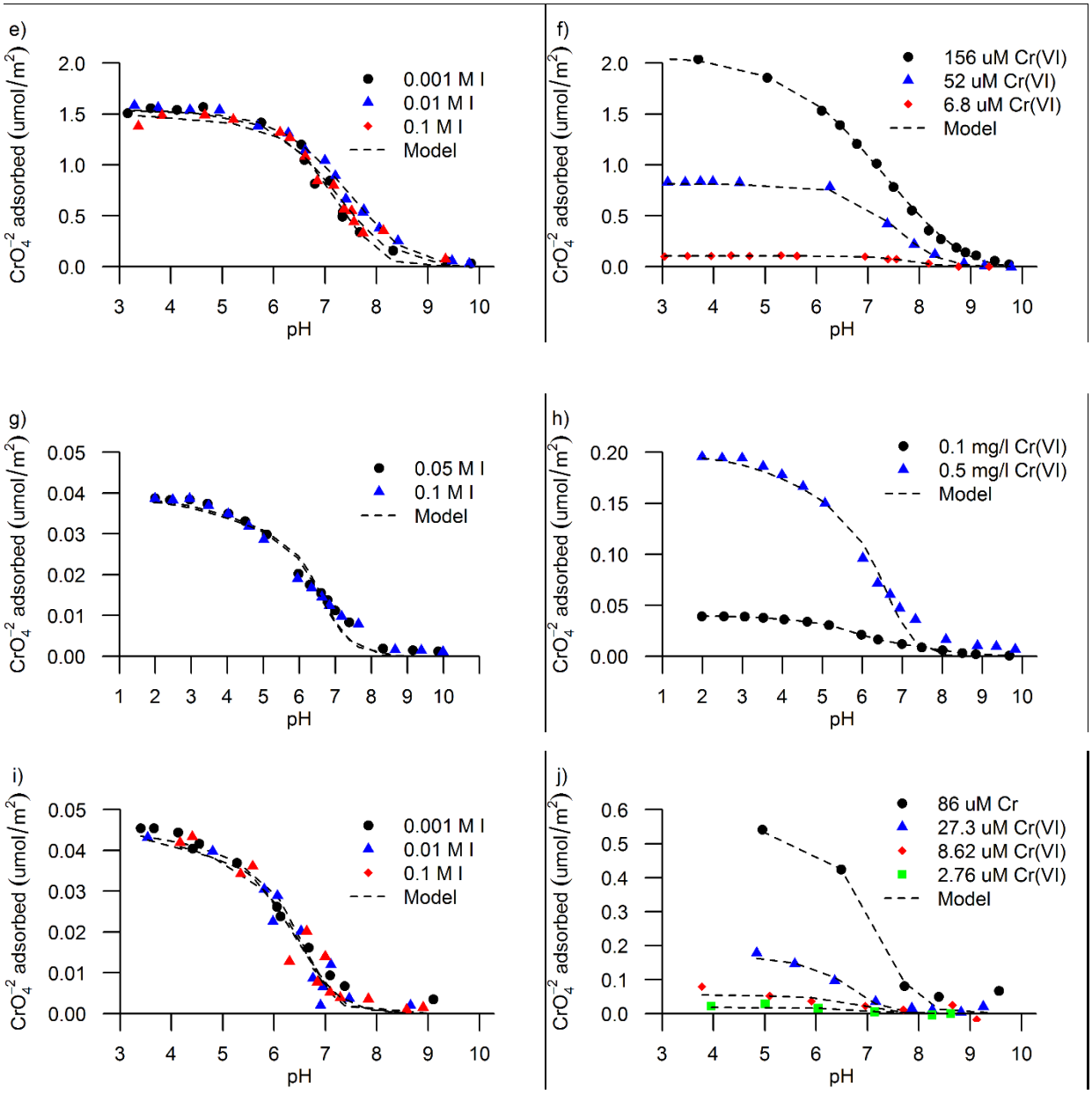

Figure A4-11. Chromate adsorption modeling on GH (dashed lines) at different conditions: a) 50 uM Cr(VI) and different ionic strength (Mesuere and Fish, 1992) b) at 0.01 M I and different Cr (VI) concentrations (Mesuere and Fish, 1992), c) 5 uM and different surface areas (Villalobos and Pérez-Gallegos (2008), d) 1 mM Cr(VI) and different ionic strength (Grossl et al., 1997), e) 1 mM Cr(VI) and different ionic strength (Xie et al., 2015) f) at 0.01 M I and different Cr(VI) concentrations (Xie et al., 2015), g) 0.1 mg/ L Cr(VI) and different ionic strength (Ajouyed et al.,

2010), h) at 0.01 M I and different Cr (VI) concentrations (Ajouyed et al., 2010), i) at 7 uM Cr(VI) and different ionic strength (Weerasooriya and Tobschall, 2000), and j) at 0.001 M I and different Cr (VI) concentrations (Weerasooriya and Tobschall, 2000)

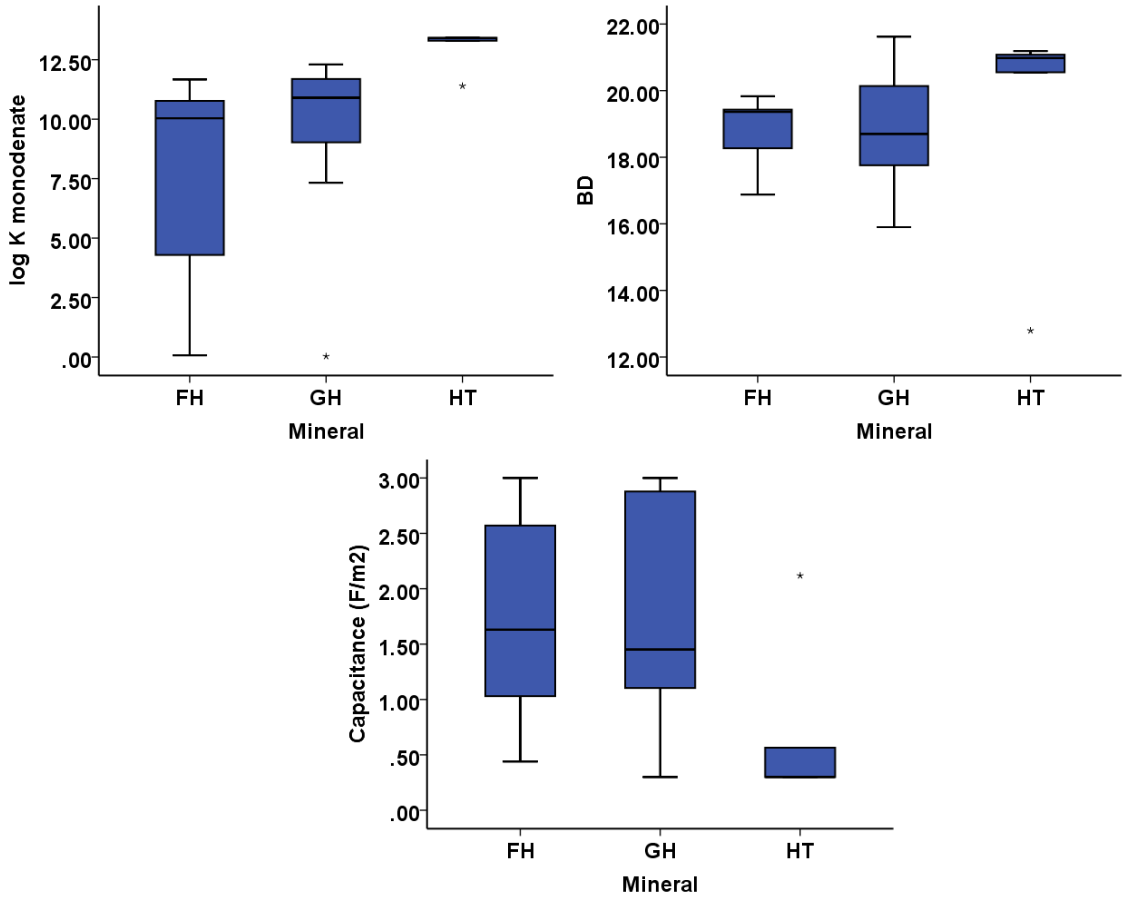

Figure A4-12. Boxplots of optimized parameters for all three minerals

Table A4-5. Descriptive statistics for optimized parameters.

Statistics

		c	MD	BD
N	**Valid**	49	49	49
	Missing	0	0	0
Mean		1.6427	9.6682	18.9952
Median		1.4516	10.5765	19.3700
Std. Deviation		.95754	3.20678	1.68521
Minimum		.30	.03	12.79
Maximum		3.00	13.43	21.62
Percentiles	**25**	.9215	9.0050	17.7600
	50	1.4516	10.5765	19.3700
	75	2.5745	11.6150	20.0450

Surface Area sensitivity analysis

Table A4-6. Optimized parameters based on different surface area

	SSA (m2/g)	log K Monodentate	log K Bidentate	C
Zachara dataset 1	50			
	100	11.74	20.13	2.23
	200	11.43	19.82	1.51
	300	11.03	19.74	1.16
	400			
	500	10.97	19.45	1.05
	600	10.77	19.44	0.86
Honeyman dataset 2	50	11.82	20.44	2.20
	100	11.24	20.25	1.62
	200			
	300	0.77	19.84	1.42
	400	9.75	19.70	1.55
	500			
	600	10.58	19.41	1.88
Mesuere Dataset 5	66	11.72	20.23	1.13
	100	11.54	20.56	0.45
	200	11.41	19.38	0.41
	300	11.24	19.15	0.30
	400	11.02	18.83	0.30
	500	10.86	18.64	0.30
	600	10.74	18.49	0.30
Villalobos Dataset 2	50	11.15	21.62	0.30
	100	10.80	21.33	0.31
	200	10.54	21.02	0.30
	300	10.40	20.84	0.30
	400	10.23	21.72	0.30
	500	10.09	20.63	0.30
	600	9.95	20.55	0.30

References

Ajouyed, O., Hurel, C., Ammari, M., Allal, L.B., Marmier, N., 2010. Sorption of Cr(VI) onto natural iron and aluminum (oxy)hydroxides: Effects of pH, ionic strength and initial concentration. J. Hazard. Mater. 174, 616–622. https://doi.org/10.1016/j.jhazmat.2009.09.096

Antelo, J., Avena, M., Fiol, S., López, R., Arce, F., 2005. Effects of pH and ionic strength on the adsorption of phosphate and arsenate at the goethite–water interface. J. Colloid Interface Sci. 285, 476–486. https://doi.org/10.1016/j.jcis.2004.12.032

Bargar, J.R., Kubicki, J.D., Reitmeyer, R., Davis, J.A., 2005. ATR-FTIR spectroscopic characterization of coexisting carbonate surface complexes on hematite. Geochim. Cosmochim. Acta 69, 1527–1542. https://doi.org/10.1016/j.gca.2004.08.002

Bompoti, N., Chrysochoou, M., Machesky, M., 2016. Surface structure of ferrihydrite: Insights from modeling surface charge. Chem. Geol. https://doi.org/10.1016/j.chemgeo.2016.12.018

Brunauer, S., Emmett, P.H., Teller, E., 1938. Adsorption of Gases in Multimolecular Layers. J. Am. Chem. Soc. 60, 309–319. https://doi.org/10.1021/ja01269a023

Chrysochoou M.; Machesky M.; Johnston C. A new surface complexation model for chromate adsorption on ferrihydrite. Proceedings of the 13th International Conference on Environmental Science and Technology, paper 687, Athens, Greece, 5-7 September 2013

Grossl, P.R., Eick, M., Sparks, D.L., Goldberg, S., Ainsworth, C.C., 1997. Arsenate and Chromate Retention Mechanisms on Goethite. 2. Kinetic Evaluation Using a Pressure-Jump

Relaxation Technique. Environ. Sci. Technol. 31, 321–326. https://doi.org/10.1021/es950654l

Hiemstra, T., 2013. Surface and mineral structure of ferrihydrite. Geochim. Cosmochim. Acta 105, 316–325. https://doi.org/10.1016/j.gca.2012.12.002

Hiemstra, T., Rahnemaie, R., van Riemsdijk, W.H., 2004. Surface complexation of carbonate on goethite: IR spectroscopy, structure and charge distribution. J. Colloid Interface Sci. 278, 282–290. https://doi.org/10.1016/j.jcis.2004.06.014

Hiemstra, T., Riemsdijk, W.H.V., Rossberg, A., Ulrich, K.-U., 2009. A surface structural model for ferrihydrite II: Adsorption of uranyl and carbonate. Geochim. Cosmochim. Acta 73, 4437–4451. https://doi.org/10.1016/j.gca.2009.04.035

Hsia, T.H., Lo, S.L., Lin, C.F., Lee, D.Y., 1993. Chemical and spectroscopic evidence for specific adsorption of chromate on hydrous iron oxide. Chemosphere 26, 1897–1904. https://doi.org/10.1016/0045-6535(93)90083-H

Hwang, Y.S., Lenhart, J.J., 2008. The dependence of hematite site-occupancy standard state triple-layer model parameters on inner-layer capacitance. J. Colloid Interface Sci. 319, 206–213. https://doi.org/10.1016/j.jcis.2007.11.032

Johnston, C.P., Chrysochoou, M., 2016. Mechanisms of Chromate, Selenate, and Sulfate Adsorption on Al-Substituted Ferrihydrite: Implications for Ferrihydrite Surface Structure and Reactivity. Environ. Sci. Technol. 50, 3589–3596. https://doi.org/10.1021/acs.est.5b05529

Johnston, C.P., Chrysochoou, M., 2012. Investigation of Chromate Coordination on Ferrihydrite by in Situ ATR-FTIR Spectroscopy and Theoretical Frequency Calculations. Environ. Sci. Technol. 46, 5851–5858. https://doi.org/10.1021/es300660r

Mesuere, K., Fish, W., 1992. Chromate and oxalate adsorption on goethite. 1. Calibration of surface complexation models. Environ. Sci. Technol. 26, 2357–2364. https://doi.org/10.1021/es00036a004

Penners, N.H.G., Koopal, L.K., Lyklema, J., 1986. Interfacial electrochemistry of haematite (α-Fe2O3): homodisperse and heterodisperse sols. Colloids Surf. 21, 457–468. https://doi.org/10.1016/0166-6622(86)80109-3

Sahai, N., Sverjensky, D.A., 1997. Evaluation of internally consistent parameters for the triple-layer model by the systematic analysis of oxide surface titration data. Geochim. Cosmochim. Acta 61, 2801–2826. https://doi.org/10.1016/S0016-7037(97)00128-2

Schwertmann, U., Cornell, R.M., 2000. The Iron Oxides, in: Iron Oxides in the Laboratory. Wiley-VCH Verlag GmbH, pp. 5–18.

Venema, P., Hiemstra, T., van Riemsdijk, W.H., 1996. Multisite Adsorption of Cadmium on Goethite. J. Colloid Interface Sci. 183, 515–527. https://doi.org/10.1006/jcis.1996.0575

Venema, P., Hiemstra, T., Weidler, P.G., van Riemsdijk, W.H., 1998. Intrinsic Proton Affinity of Reactive Surface Groups of Metal (Hydr)oxides: Application to Iron (Hydr)oxides. J. Colloid Interface Sci. 198, 282–295. https://doi.org/10.1006/jcis.1997.5245

Villacís-García, M., Ugalde-Arzate, M., Vaca-Escobar, K., Villalobos, M., Zanella, R., Martínez-Villegas, N., 2015. Laboratory synthesis of goethite and ferrihydrite of controlled particle sizes. Bol. Soc. Geológica Mex. 67, 433.

Villalobos, M., Leckie, J.O., 2001. Surface Complexation Modeling and FTIR Study of Carbonate Adsorption to Goethite. J. Colloid Interface Sci. 235, 15–32. https://doi.org/10.1006/jcis.2000.7341

Villalobos, M., Pérez-Gallegos, A., 2008. Goethite surface reactivity: A macroscopic investigation unifying proton, chromate, carbonate, and lead(II) adsorption. J. Colloid Interface Sci. 326, 307–323. https://doi.org/10.1016/j.jcis.2008.06.026

Weerasooriya, R., Tobschall, H.J., 2000. Mechanistic modeling of chromate adsorption onto goethite. Colloids Surf. Physicochem. Eng. Asp. 162, 167–175. https://doi.org/10.1016/S0927-7757(99)00229-0

Xie, J., Gu, X., Tong, F., Zhao, Y., Tan, Y., 2015. Surface complexation modeling of Cr(VI) adsorption at the goethite–water interface. J. Colloid Interface Sci. 455, 55–62. https://doi.org/10.1016/j.jcis.2015.05.041

Zachara, J., Girvln, D., Schmidt, R., Resch, C., 1987. Chromate Adsorption on Amorphous Iron Oxyhydroxide in the Presence of Major Groundwater Ions. US Dep. Energy Publ.

CHAPTER 5 Conclusions

Overall, the main objective of this research was to develop a unified framework for the reactivity of iron oxides (ferrihydrite, hematite, and goethite) towards ions, and specifically protons and one ligand (chromate). The approach focused on developing a consistent database for surface complexation parameters and validating its applicability on all available datasets reported in the literature. That attempt, ambitious as it was, resulted in important relationships that retain the predictive capability of surface complexation models (SCMs), and important physical insights were revealed as well. With potential field applications always in mind, this is an engineering perspective with respect to modeling adsorption processes ultimately within reactive transport modeling.

First, a unified model for surface charge of FH was developed. The model faced two main challenges: differences in charging values and the differences in PZNPC values. Both aspects appear to be dependent upon the size and shape of FH crystals, which are in turn related to precipitation methods, handling of the suspension, i.e. freeze drying, and presumably aging during and after preparation. The experimental information for each of these factors is currently lacking in order to be able to confirm their influence on particle sizes. We observed that the "fresh" FH suspensions had smaller crystals with higher SSAs and lower PZNPC values, while "aged" suspensions had smaller SSAs and higher PZNPCs. The model was based on the proposed surface structure of Hiemstra (2013) that includes 11 different sites along with their corresponding site densities and protonation constants. However, to accommodate large differences in PZNPC values, it was necessary to change the contribution of different crystal faces. A simplified model was proposed that involved three sites, with one singly and two triply coordinated oxygens, one of

which was placed on the basal planes and one on the more reactive faces of the FH crystal. This approach described all eight datasets quite well, but had two drawbacks: there is no experimental evidence to support the variable contributions of crystal faces, and perhaps more importantly, the relative contribution of singly and triply coordinated groups to the overall charge is substantially different compared to the full 11-site model.

The advancement of the optimization algorithm (MUSE algorithm) was a necessary step to optimize multiple thermodynamic parameters for surface complexation modeling. The transferability of mineral-specific SCMs to reactive transport modeling is constrained by several lingering problems, including the fact that SCMs have a large number of interdependent parameters. This limits their usefulness and transferability in, for example, reactive transport models. With this in mind, a hybridized optimization approach, based on a multi – start algorithm combined with a local optimizer, was developed to allow the simultaneous optimization of SCM parameters. This offers two innovative advances to the inverse SCM modeling approach: a) determination of the true global optimum based on the minimization of the mean squared error between the simulated and observed data, and b) quantitative simulation of spectroscopic pH – dependent profiles for two chromate surface complexes. The thermodynamic constants are dependent on surface parameters, a fact that end users of geochemical modeling software cannot easily account for. The MUSE algorithm addresses this problem by allowing the simultaneous optimization of several parameters and enabling the determination of a global minimum that is not constrained by the initial guesses for the parameter values which invariably leads to local rather global minima. We demonstrate that when MUSE is implemented to determine chromate log Ks, their dependence on other adjustable parameters such as specific surface area (SSA) and capacitance is relatively small (i.e., one unit change for chromate log Ks on ferrihydrite) and can

be accounted by mathematical functions determined with the aid of the MUSE algorithm. The robustness of the algorithm is demonstrated in the absence of spectroscopy data as well, with traditional batch tests yielding similar thermodynamic constants as the spectroscopic data. Accommodating any type of SCM and choice of parameters, including equilibrium constants, capacitance values and sorbent properties, the MUSE algorithm can be used for optimizing parameters necessary for reactive transport modeling.

Finally, the MUSE was applied to a large and diverse chromate adsorption data sets for three iron oxides (ferrihydrite, hematite, and goethite). Data from different studies with different experimental conditions (ionic strength, solid: liquid ratio, surface area) and techniques were utilized to extract optimal equilibrium constants for chromate adsorption. With a unified approach in mind, the description of the available datasets with one set of equilibrium constants was not possible. We concluded that, besides the heterogeneity and experimental error, there are two main effects that drive the variability of the fitted binding constants. The first is the dependency of the parameters on the surface area, which the model can easily account for. The second reflects the energetics of adsorption at different adsorption densities, or surface coverages. This effect is, however, more difficult to account for, but it can be handled by approximating the surface coverage effect and incorporating it into the model. This outcome can be useful in the field reactive transport modeling in two ways: a) by adopting the appropriate predictive relationship for each surface coverage, in case the latter is estimated (by measuring solid: solution ratios, chromate in the solution, and surface area), and b) by performing modeling scenarios for different conditions in the field, i.e. different adsorption densities.